TAMPEREEN TEKNILLINEN YLIOPISTO
TAMPERE UNIVERSITY OF TECHNOLOGY

Florentino Luciano Caetano dos Santos

Automatic Evaluation of Carotid Stenosis Based on Computed Tomography Angiography

Julkaisu 1573 • Publication 1573

Tampere 2018

Tampereen teknillinen yliopisto. Julkaisu 1573
Tampere University of Technology. Publication 1573

Florentino Luciano Caetano dos Santos

Automatic Evaluation of Carotid Stenosis Based on Computed Tomography Angiography

Thesis for the degree of Doctor of Science in Technology to be presented with due permission for public examination and criticism in Sähkötalo Building, Auditorium S2, at Tampere University of Technology, on the 26th of October 2018, at 12 noon.

Tampereen teknillinen yliopisto - Tampere University of Technology
Tampere 2018

Doctoral candidate: Florentino Luciano Caetano dos Santos, M.Sc.
Quantitative Medical Image Analysis, BioMediTech
Faculty of Biomedical Sciences and Engineering
Tampere University of Technology
Finland

Supervisor: Professor Hannu Eskola
Quantitative Medical Image Analysis, BioMediTech
Faculty of Biomedical Sciences and Engineering
Tampere University of Technology
Finland

Instructors: Professor Juha-Pekka Salenius
Division of Vascular Surgery
Department of Surgery
Tampere University Hospital and Medical School
Finland

Michelangelo Paci, Ph.D.
Computational Biophysics and Imaging Group, BioMediTech
Faculty of Biomedical Sciences and Engineering
Tampere University of Technology
Finland

Pre-examiners: Professor Vicente Grau
Institute of Biomedical Engineering, Department of Engineering Science
University of Oxford
UK

Adjunct Professor Mika Kortesniemi
HUS Medical Imaging Center
University of Helsinki
Finland

Opponent: Associate Professor Cristiana Corsi
Department of Electrical, Electronic, and Information Engineering “Guglielmo Marconi”
University of Bologna
Italy

ISBN 978-952-15-4196-4 (printed)
ISBN 978-952-15-4238-1 (PDF)
ISSN 1459-2045

Abstract

Atherosclerosis is a systemic disease, affecting individuals of all ages. It is characterized by the deposition of foreign elements in the arterial intima-media layer, leading to a gradual narrowing of the vascular lumen, impeding the blood flow. One of the possible consequences of atherosclerosis is transient ischemia or infarction of internal organs, including heart and brain.

In the clinical practice, the diagnosis and evaluation of the progression of carotid atherosclerosis are usually performed by ultrasound imaging or computed tomography angiography. In both techniques, a large dependence on hand-operated assessment is present. To evaluate the stage of stenosis, a clinician has to take two measurements manually - the average lumen diameter, and the narrowest lumen diameter, i.e., where the plaque is located. The manual assessment of the carotid diameters does not guarantee reproducibility and repeatability of the results. It is also far from optimal due to the large chance of human error. An alternative approach is necessary.

The thesis focuses on the development of a tool capable of reducing or even eliminating human dependency and possible errors that can occur during the manual assessment. A fully automatic tool - VASIM (Vascular Imaging) was developed. It uses reliable, fast, and simple methods, such as morphological operators both in 2D and in 3D, to segment the lumen volume and areas for stenosis calculation but also for the examination of vascular walls, plaque, and vessel-surrounding tissues. The section analyzed by VASIM encompasses the carotid arteries, one of the most common locations of atherosclerotic plaques in the arterial system. VASIM presents to the user not only the routinely used metrics but also new parameters. They are based on different tissues' volumes, areas and progression throughout the arterial tree. Furthermore, VASIM creates 3D models, which could be used for surgery planning, plaque morphology and composition evaluation, and 2D linearization of all the components of the plaque.

To validate VASIM, a clinical material of fifty-nine individuals, both healthy and suffering from atherosclerosis of the carotid arteries, was tested and analyzed. For cases with stenosis over 50%, VASIM had a clinical accuracy of 71%. The software prototype results suggest that this approach has potential in areas such as analysis of the atherosclerosis of carotid arteries and it could be applied in a clinical environment.

Preface

This thesis is a result of a research project conducted at the Faculty of Biomedical Sciences and Engineering at the Tampere University of Technology.

I wish to express my gratitude to my thesis supervisor Professor Hannu Eskola for the guidance and motivational support during the course of the study. My wishes extend to my instructors, Professor Juha-Pekka Salenius (Division of Vascular Surgery, Department of Surgery, Tampere University Hospital and Medical School, Finland) for all the clinical insight and support throughout the years. I also want to thank my instructor and friend Doctor Michelangelo Paci (BioMediTech Institute and Faculty of Biomedical Sciences and Engineering, Tampere University of Technology, Finland), who was always guiding me through my doctoral process and presented me with new challenges and topics that allowed me to develop. If there is someone patient, it is him. We both know how long it took me to improve my writing skills.

I wish to thank Professor Vicente Grau (Institute of Biomedical Engineering, Department of Engineering Science, University of Oxford, Oxford, United Kingdom) and Adjunct Professor Mika Kortesniemi (Medical Imaging Center, Helsinki University Hospital, Helsinki, Finland) for their constructive criticism and advice as examiners of this thesis. Also, I am thankful to Assistant Professor Stefano Severi (Department of Electrical, Electronic, and Information Engineering "Guglielmo Marconi", University of Bologna, Bologna, Italy), member of my doctoral follow-up group, for his insights in the last stages of the dissertation.

I would like to thank my co-authors Mitsugu Terada and Marcin Kolasa, with whom I had the pleasure of exchanging ideas and who have helped me with the articles presented in this thesis. A special thank you goes to Atte Joutsen, not only one of my co-authors but also the first person that I met after arriving in Finland, still during my internship. He helped me to integrate and start my journey here. This study could not have been possible without the help of Päivi Laarne. Thank you for all the help and guidance during data collection and all the imaging sessions.

I am grateful for the financial support provided by the CIMO Foundation, the iBioMEP, and my supervisor Professor Hannu Eskola. I would also like to thank Professor Jari Hyttinen and Docent Soile Nymark for trusting me and allowing me to work in their groups while developing my skills.

I also wish to give a special thanks to my colleagues Tomas Cervinka, Antti Aula, Alper Cömert, Baran Aydogan, Markus Hannula, Nathaniel Narra, Jarno Taskanen, Emre Kapucu, Narayan Subramaniyam, Kerstin Lenk, Edite Figueiras, Jari Hyttinen, Soile Nymark, Teemu Ihalainen, Julia Johansson, Toni Montonen and to all the amazing people that I have met both in TUT, UTA, and BioMediTech. Thank you for all the good laughs, comments and support that you gave me. A special thanks for Soile Lönnqvist, someone that the department and the research group defines as our mother, for being there for us, always willing to help, guide, and keep us in our toes for all the bureaucratic. It is impossible to forget the fantastic friends that I made during my time in Tampere. They have been my rock and some of the best advisers I ever got. A warm thank you for all the good times, help and experiences shared.

Finally, I would like to thank my family. I owe them more than I can ever return. They have been my support throughout my life showing an unyielding interest and being always there for me. Last but not least, I would like to thank my partner for her love and support, enduring my rants and crazy ideas in these last months. You have made me evolve and grow so much, thank you for standing by my side now and in the years to come.

Tampere 2018

Florentino Santos

List of original publications

This thesis is based on the following original publications, which are referred to in the text as I-IV. The publications are reproduced with kind permissions from the publishers.

I. **Santos, F.**, Joutsen, A., Terada, M., Salenius, J., Eskola, H., A Semi-Automatic Segmentation Method for the Structural Analysis of Carotid Atherosclerotic Plaques by Computed Tomography Angiography, Journal of Atherosclerosis and Thrombosis, 2014, 21:930-940

II. **Santos, F.**, Joutsen, A., Salenius, J., Eskola, H., Fusion of Edge Enhancing Algorithms for Atherosclerotic Carotid Wall Contour Detection in Computed Tomography Angiography, Computing in Cardiology, 2014; 41: 925-928

III. **Santos, F.**, Joutsen, A., Paci, M., Salenius, J., Eskola, H., Automatic detection of carotid arteries in computed tomography angiography: a proof of concept protocol, International Journal of Cardiovascular Imaging, 2016, 32:1299-1310

Unpublished manuscripts

IV. **Santos, F.**, Kolasa, M., Terada, M., Salenius, J., Eskola, H., Paci, M., VASIM: An Automated Tool for the Quantification of Carotid Atherosclerosis by Computed Tomography Angiography

Author's contributions

I. The author was responsible for defining the study objectives and design, development of the image processing and segmentation algorithms, analysis of the data, and statistical analysis. Atte Joutsen was responsible for data collection. The author also wrote the manuscript and the co-authors reviewed, commented and improved the text.

II. The author was responsible for defining the study objectives and design, development of the image processing and segmentation algorithms, analysis of the data, and statistical

analysis. Atte Joutsen was responsible for data collection. The author also wrote the manuscript and the co-authors reviewed, commented and improved the text.

III. The author was responsible for defining the study objectives and design, development of the image processing and segmentation algorithms, analysis of the data, and statistical analysis. Atte Joutsen was responsible for data collection. The author also wrote the manuscript and the co-authors reviewed, commented and improved the text.

IV. The author was responsible for defining the study objectives and design, data collection, development of the image processing and segmentation algorithms, analysis of the data, and statistical analysis. Marcin Kolasa was responsible for data collection from the patient files information. The author also wrote the manuscript and the co-authors reviewed, commented and improved the text.

Contents

List of Figures

List of Symbols and Abbreviations

CT	Computed tomography
CTA	Computed tomography angiography
DECT	Dual-energy CT
HU	Hounsfield units
IMT	Intima-media thickness
LDL	Low-density lipoprotein
MRI	Magnetic resonance imaging
NASCET	North American Symptomatic Carotid Endarterectomy Trial
NCD	Noncommunicable disease
PET	Positron emission tomography
US	Ultrasound
VASIM	Vascular Imaging
VOI	Volume of interest

1 Introduction

Cardiovascular diseases are the most common non-communicable diseases (NCDs), and they are the leading cause of mortality in this group globally (37% of all NCDs related deaths) (World Health Organization 2010; Kim & Johnston 2013). Annually this corresponds to 17.5 million deaths, of which 7.4 million due to myocardial infarction, and 6.7 million due to ischemic stroke (Beevers 2005; Strong et al. 2007).

Stroke is a medical condition that can be divided into ischemic stroke and hemorrhagic stroke. Ischemic stroke is a result of decreased blood supplies to the brain, leading to necrosis of nervous tissue (Virmani et al. 2005; Seevinck et al. 2010; Shuaib et al. 2011; Gupta et al. 2013; Winship et al. 2014; Price et al. 2018). This thesis focuses on atherosclerosis of the carotid arteries, which is the main cause of ischemic stroke. The blockage of the cerebral arterial vessel is caused by clots, that most often follow the rupture of the atherosclerotic plaque. The plaques are products of the inflammatory processes, initiated by the accumulation of low-density lipoproteins (LDL) in the inner layer of the arterial walls (Chambless et al. 1997; Achenbach 2002). The atheromatous plaque can be divided roughly into three components: lipid material, fibrotic tissue, and calcified tissue, in the order demonstrating the plaque structural evolution throughout time (Langer & Gawaz 2006; Weert et al. 2008). While calcified tissue provides stability, fibrotic tissue and lipids are critical factors of the plaque instability and susceptibility to becoming an embolic material (Shaalan et al. 2004; Nandalur et al. 2007; Medbury et al. 2013; Diab et al. 2017).

The standard imaging methods for assessing the stage of atherosclerosis are ultrasound (US) and computed tomography (CT) angiography (CTA). CTA is an imaging technique that enhances

the contrast of the carotid lumen against the surrounding tissues (Naim et al. 2014; Huibers et al. 2015). Using CTA, the radiologist can measure and calculate the degree of stenosis of a vessel (Feinstein 2006; Weert et al. 2008; Saba et al. 2012; Carnicelli et al. 2013; Akkus et al. 2015). The manual measurement is far from optimal as it is clinician-dependent, characterized by low reliability and repeatability, and is highly time-consuming (Silvennoinen et al. 2007; Marquering et al. 2012; Vukadinovic et al. 2012; Meiburger et al. 2016; Smits et al. 2016). There remains a need for an efficient automatic method that can segment, analyze and evaluate the degree of stenosis and stability of the plaque.

2 Literature review

2.1 Carotid atherosclerosis

2.1.1 Carotid arteries

The common carotid arteries, located bilaterally along the neck, are the primary supplier of blood to the cranial, facial and cervical regions.

They bifurcate into the internal and external carotid arteries, supplying the brain, and the neck and face, respectively (Dungan & Heiserman 1996; Schulz & Rothwell 2001; Phan et al. 2012; Prasad et al. 2015; Michalinos et al. 2016). The structure of the arterial wall is composed of three different layers: tunica intima, tunica media, and tunica adventitia. While tunica intima is composed of endothelial cells, the tunica media is a smooth muscle structure, responsible for adapting the vessel to the blood pressure. The tunica adventitia is a rigid external layer composed of collagen and fibroblasts (Feeley et al. 1991; Hayashi 2007; Tamakawa et al. 2007; Groen et al. 2010; Santos, F. et al. 2011).

The measurement of the two innermost tunicae, which is called intima-media thickness (IMT), is considered one of the most critical metrics in the evaluation of atherosclerosis (Simons et al. 1999; Zureik et al. 2000; Lorenz et al. 2007; Mathiesen et al. 2011). The accumulation of debris in the arterial wall (explained in more detail in the section “Atherogenesis”) increases the IMT and decreases the caliber of the arterial lumen (Lusis 2000; Rohani et al. 2005; Virmani et al. 2005; Weert et al. 2008). An increase in this indicator is reflected in the limited blood supply of the

supracervical regions (Enterline & Kapoor 2006; Han et al. 2007). Moreover, the gradual accumulation of debris, increase of the IMT and continual degeneration of the intima layer might lead to rupture of the arterial wall, the release of thrombi into the bloodstream, and finally transient ischemic attack or ischemic stroke (Arbustini et al. 1999; Hashimoto et al. 1999; Fisher et al. 2005; van der Hagen, P B et al. 2006; De Vasconcellos et al. 2009).

2.1.2 Atherogenesis

Atherogenesis is a process of thickening and loss of elasticity of the arterial wall with formation of atherosclerotic plaque, evolving gradually (Ross & Agius 1992; Brown et al. 2016). The most common location of the atherosclerotic lesions are arterial bifurcations and branching points, characterized by high wall-shear stress. In the system of carotid arteries, atheromatous plaques are usually found in the carotid bifurcation (Zarins et al. 1983; Augst & Ariff 2007; Giannoglou et al. 2010; Cantón et al. 2012). The constant strain of the blood flow in this location causes micro-ruptures of the intima layer, enabling the infiltration of LDLs to endothelium. The LDLs are considered to be the precursor of the atherosclerotic lesion (Chambless et al. 1997; Mora et al. 2007; Ridker et al. 2009; Mitra et al. 2011; Patel et al. 2015). Products synthesized during their oxidation stimulate cell-mediated immunity, i.e., the migration of macrophages to the region to engulf and digest LDLs. Unless they succeed, they start apoptosis, forming foam cells, the precursors of the lipidic core of the atherosclerotic plaque. The frail plaque, which is highly susceptible to become an embolic material, triggers the proliferation and migration of the adjacent smooth muscle cells to stabilize the core, forming the fibrous plaque. Subsequently, the fibrous cap of the plaque becomes calcified, due to continuous high wall shear stress. In mechanical terms, a calcified cap surrounding a lipidic/fibrotic core is more stable and less prone to rupture and consequently cause thrombosis, transient ischemic attacks, and strokes (Virmani et al. 2005; Nandalur et al. 2007; Saba et al. 2012; Trelles et al. 2013). With the development of the atherosclerotic plaque (lipid, fibrotic, and calcified) the IMT index increases and the arterial lumen is reduced (Stary et al. 1994; Lusis 2000; Groen et al. 2010). A summary of the atherogenesis is presented in Figure 1 (adapted from (Naim et al. 2014)).

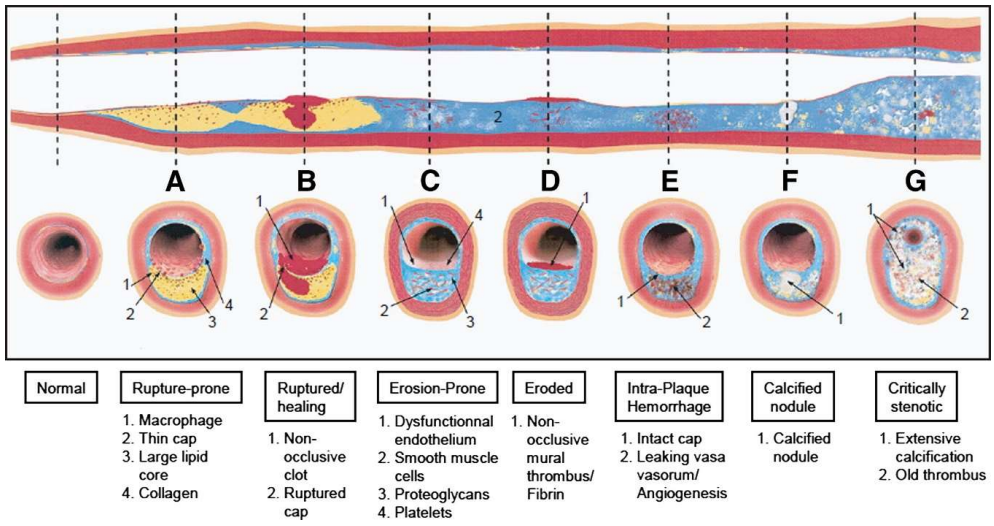

Figure 1. Atherogenesis evolution, stages, and components (Adapted from (Naim et al. 2014))

2.2 Imaging and diagnostic of atherosclerosis in the carotid arteries

Currently, the clinical evaluation of the atherosclerotic burden is based on two criteria: (i) degree of maximal luminal stenosis and (ii) atherosclerotic plaque composition (Carrascosa et al. 2006; Rozie et al. 2009; Cantón et al. 2012; Gils et al. 2012). The extent of carotid artery stenosis is the only widely accepted indicator describing and categorizing the urgency for pharmacological or surgical treatment, such as endarterectomy or stenting (Wiesmann et al. 2008; Liapis et al. 2009; Meier et al. 2010). The evaluation of the degree of stenosis is based on the North American Symptomatic Carotid Endarterectomy Trial criterion (NASCET). The stenosis percentage is computed by Formula 1:

$$Stenosis(\%) = \left(1 - \frac{N}{D}\right) x\ 100 \quad (1)$$

, where *N* represents the narrowest observable diameter in the residual lumen and *D* the diameter of the adjacent non-occluded lumen (Fox 1993; Ferguson et al. 1999; Santos, Florentino Luciano Caetano et al. 2016). Both diameters are currently manually measured (Silvennoinen et al. 2007;

Cheng, D. et al. 2011; Zhu et al. 2013). Furthermore, the analysis of the atherosclerotic plaque composition is also conducted with a manual, clinician-dependent segmentation of the tissues (Liu et al. 2006; Vukadinovic et al. 2012; Smits et al. 2016).

2.2.1 Ultrasound

Ultrasound (US) is a non-invasive diagnostic method, which enables the evaluation of the degree of stenosis, plaque formation, and evolution in the artery by assessing the IMT (Zureik et al. 2000; Molinari et al. 2012; Vaishali Naik et al. 2013). Moreover, it is optimal to evaluate the degree of stability of the plaque (Zureik et al. 2000; Carrascosa et al. 2006; Feinstein 2006; Akkus et al. 2015). Its additional, invasive expansion, called the intravascular US, is used to assess both the volume and component properties of the plaque (de Groot et al. 2004; Augst & Ariff 2007; Teramoto et al. 2014).

2.2.2 Computed Tomography

Computed tomography (CT) is one of the most common imaging techniques used to measure and analyze stenosis of the arteries directly. It usually employs a multidetector row CT, providing a reliable and fast examination (approximately 30 s for the cervical region), characterized by a spatial resolution superior to other imaging methods (Ergün et al. 2011; Vukadinovic 2012; Hemmati et al. 2015). The contrast between the arterial wall and surrounding tissues is enhanced by the technique called computed tomography angiography (CTA), due to the intravascular administration of contrast agents (Ergün et al. 2011; Trelles et al. 2013; Eller et al. 2014). Additionally, CTA allows differentiating the different components of the atherosclerotic plaque such as lipidic, fibrotic and calcified (Groen et al. 2010; Vukadinovic 2012; Engelen et al. 2014; Diab et al. 2017). As the contrast agent does not perfuse calcified tissues, they are characterized by a high attenuation, measured in Hounsfield units (HU) (Enterline & Kapoor 2006; Rozie et al. 2009; Teramoto et al. 2014).

Dual-energy CT (DECT), a variation of CT, applies two energy signatures to provide better contrast between tissues of higher and lower attenuation. DECT can also be enhanced by contrast agents, allowing to lower patient radiation dose (Coursey et al. 2010). Several studies confirmed that DECT has a high success in plaque composition analysis (Biermann et al. 2012; Shinohara et al. 2015), it facilitates plaque removal from the image (Thomas et al. 2010; Mannelli et al. 2015),

and has a high sensitivity for detection of relevant stenosis (Thomas et al. 2010; Shinohara et al. 2015).

2.2.3 Magnetic Resonance Imaging

Magnetic resonance imaging (MRI) is still an uncommon technique to diagnose atherosclerosis (Corti & Fuster 2011; van Hoof et al. 2017). Notwithstanding, it is one of the most promising ones as it excellently captures the contrast between soft tissues, enabling precise assessment of the plaque morphology and monitoring the evolution of the disease over time. Moreover, MRI does not expose the patient to radiation (Cai et al. 2005; Yuan et al. 2008). Its expansion - magnetic resonance angiography (MRA), allows to evaluate the intra-plaque hemorrhage and to assess the time of its onset (Yuan et al. 2008; Kwee et al. 2009; Teramoto et al. 2014). A relatively high imaging time remains a major limitation of this diagnostic technique (Thoeny et al. 2012).

2.2.4 Positron emission tomography

Positron emission tomography (PET) is one of the most promising upcoming imaging modalities applied in carotid atherosclerosis. Several studies confirmed that a relation exists between ^{18}F-FDG (fluorodeoxyglucose) uptake and the inflammatory status of an atherosclerotic lesion. These findings were subsequently validated by histopathology studies (Græbe et al 2010; Johnsrud et al. 2017).

Several specific variants of PET for the analysis of atherosclerosis or cardiovascular assessment exist. These include two hybrid imaging modalities - PET-CT and PET-MRI. While PET-CT improves the contrast between soft tissue intake of the fluorophore (PET) and the hard attenuation tissues (CT) (Kwee et al. 2009; Huibers et al. 2015), PET-MRI improves the soft tissues contrast only. By the increased soft tissues contrast, PET-MRI is capable of detecting and analyzing early stages of atherogenesis and intraplaque hemorrhage (Kwee et al. 2009; Rajiah et al. 2016).

2.2.5 Physiological tests

Physiological tests of the carotid arteries include flow-mediated vasodilation (Kobayashi et al. 2004; Bartoli et al. 2007; Irace et al. 2013) or bruit auscultation, i.e., listening to the sound produced by the blood passing through a sudden narrowing of the artery (Teramoto et al. 2014).

2.3 Segmentation techniques in atherosclerosis

2.3.1 Thresholding

Thresholding is the oldest and simplest of the segmentation methods (Arifin & Asano 2006). Usually, the result of thresholding is a binarization of the image into subparts. Sezgin et al. (Sezgin & Sankur 2004) divide the thresholding techniques into six categories: (i) histogram shape-based methods, e.g., (Arifin & Asano 2006; Bali & Singh 2015); (ii) clustering-based methods, e.g., (Wang, Z. & Yang 2010; Ma et al. 2010); (iii) entropy-based methods, e.g., (Li et al. 1995; Zimmer et al. 1996; Horng 2010); (iv) object similarity attribute-based methods, e.g., (Ling & Hurlbert 2004; Uijlings et al. 2013); (v) spatial methods, e.g., (Wong & Sahoo 1989; Hoover et al. 2000); and (vi) local methods, e.g., (Leedham et al. 2003; Burghardt et al. 2007).

They can be further divided into global and adaptive methods. The former one is used for segmenting the image or volume with the same threshold, and the latter one for adjusting the threshold to the processed sub-region of the image (Zimmer et al. 1996; Van Aarle et al. 2011; Hafiane et al. 2015; Wang, J. et al. 2015). The adaptive methods are frequently applied to 3D volumes, as tissue characteristics tend to change gradually regarding location: e.g., in the proximal cervical region there are large volumes of pulmonary air and muscle tissue, while in the distal part of this region there is more ambient air and the muscular tissue is more lean and compact.

Focusing on the segmentation of arteries, which are linear and tubular structures, the threshold methods present several assets. They are very fast, easy to implement, and computationally light. The limitations of these methods include the requirement of parametrization, histogram overlap for different objects, too harsh segmentation results (e.g., in partial-volume-effect pixels or whole regions might be misclassified because of the blurred edges), and the incorrect identification of segments in complex multi-tissue images (Pal & Pal 1993; Cheng, H. D. et al. 2001; Ma et al. 2010; Bali & Singh 2015).

Several thresholding methods have been applied to CTA images (Manniesing & Niessen 2005; Vukadinovic et al. 2012; Markiewicz et al. 2014). An example of automation of the threshold-based segmentation of the carotid arteries was proposed by Sanderse et al. (Sanderse et al. 2005). In this method, the Hough transform was applied after the detection of the shoulder blades

to detect circular objects in the proximal cervical region and expand thence distantly, with a detection rate of 88%. Cheng et al. have used the detection and segmentation of the carotid lumen and their external boundaries to images obtained using MRI (Cheng, D. et al. 2011). The study was divided into two stages. The first discriminated the actual arteries based on intensity threshold and area of the objects. The second was the segmentation of the outer vascular wall, which used the higher soft-tissue contrast provided by MRI. The developed protocol, using directional pixel gradients, circular Hough transform, and circle model guided dynamic programming, achieved an increase in segmentation accuracy of 2.56% compared with manual contour delineation.

2.3.2 Pixel clustering

Clustering methods define clusters and segments based on the assumption that similar pixels are part of the same structure or tissue, forming regions of interest, both locally or in different regions of the image (Pal & Pal 1993; Abrantes & Marques 1996; Cheng, H. D. et al. 2001; Yogamangalam & Karthikeyan 2013). The similarity indexes are based on lighting, color, and texture. Subsequent classification of such clusters into bigger ones is based on the characteristics of the tissues of interest, defined *a priori* (Pal & Pal 1993; Hafiane et al. 2008; Al-Kofahi et al. 2010; Naz et al. 2010; Hassan et al. 2014). These clustering methods require previous training to segment and classify tissues as part of the same cluster (Sanderse et al. 2005). After such training, a prototype of a segmentation mask starts to emerge. This procedure is connected with the deformable models, explained in detail in the next section. Clustering methods can be unsupervised, i.e., unprovided with *a priori* knowledge of the model of segmentation. However, over- or under-segmentation of the image may occur in such unsupervised clusters. Increasing the size of the dataset is one of the ways to cope with this problem, as it is normalizing the discrepancies and variability of the scans. On the other hand, due to detecting patterns and tissues unrecognizable for the human-trained mask, unsupervised clustering can provide unbiased analysis of the images (Duncan, J.S. James S. J.S. & Ayache 2000; Pham et al. 2000; Gamarra et al. 2017).

The implementation of the clustering methods in the medical field is increasing (Sanderse et al. 2005; Withey et al. 2009; Naz et al. 2010; Ma et al. 2010; Ghose et al. 2013; Hassan et al. 2014). As all medical images can be considered as a recurrent pattern between patients (Cruz-Roa et al. 2011), new techniques based on pattern or texture recognition tend to emerge. The main focus

is on machine learning methods, where a classifier is trained, tested and validated in classifying textures and segmenting images to specific predetermined (supervised) or not (unsupervised) classes of pixels and regions (Duncan, J.S. James S. J.S. & Ayache 2000; Pham et al. 2000; Comin et al. 2014). An example of a classifier is neural networks. They are classification techniques based on the biological functioning of neurons, with several inputs, passed to a decision matrix, classifying the signal as “go”/ “no-go”. A “go” signal is transmitted to the following neurons in the layer (Duncan, J.S. James S. J.S. & Ayache 2000; Wang, S. & Summers 2012; Sonka et al. 2015). The process is comprised of multiple decision layers. Each of the layers is composed of several neurons working in parallel. The final result of this process is a classification or segmentation of the original texture into one of the classes. This region and pixel classification process is used to segment images into its various components. Neural networks require training to integrate transformation matrixes and neuron path and to optimize the decision success rate and accuracy (Menchón-Lara & Sancho-Gómez 2015; Wang, Y. et al. 2017).

Most studies dealing with clustering-based segmentation and classification of carotid arteries, were based on neural networks (Hassan et al. 2014; Loizou 2014; Menchón-Lara & Sancho-Gómez 2015), fuzzy clustering (Adame et al. 2004; Hassan et al. 2014), Bayes clustering (Liu et al. 2006; Vukadinovic et al. 2010; Guan et al. 2012), and support vector machines (Guan et al. 2012). Menchón-Lara et al. used neural networks to classify intravascular US images for detection of the carotid wall by IMT (Menchón-Lara & Sancho-Gómez 2015). Their methodology employed region-of-interest detection and image cropping, followed by intensity patterns extraction, feature mapping, and classification. Hassan et al. expanded this approach by focusing on plaque detection and segmentation using neural networks and fuzzy clustering (Hassan et al. 2014).

Recently, deep-learning methodologies have been employed in the analysis and segmentation of medical images. To the knowledge of the author, no deep-learning methodology has ever been developed to assess, classify or segment CTA images of carotid arteries and possible atherosclerotic lesion. The most comparable approach is the methodology developed by Menchón-Lara et al., which applied extreme learning machine, based on single-layer feed-forward networks, to detect and segment the atherosclerotic lesion in carotid arteries. The developed method was applied in US images of early-stage lesions (Menchón-Lara et al. 2016). Another work done with US is by Lekadir et al., adopting convolutional neural networks for the automatic characterization of plaque composition (Lekadir et al. 2017). The research conducted by Avendi et al. focused in

the automatic segmentation of the left (Avendi, M. R. et al. 2016) and right (Avendi, Michael R. et al. 2017) ventricle in cardiac MRI. In both, the group used a three-step approach: (i) the ventricle is detected by a pre-trained convolutional network, (ii) the ventricle shape is inferred using stacked autoencoders, and (iii) the ventricle shape is used for initializing a deformable model for segmentation. Other examples of deep-learning approaches in medical image segmentation include semantic image segmentation based on deep convolutional nets (Badrinarayanan et al. 2017; Liang-Chieh Chen et al. 2018), U-net (Ronneberger et al. 2015), very deep residual networks (Simonyan & Zisserman 2015; Yu et al. 2017), or dropout convolutional neural networks (Jiang et al. 2017).

2.3.3 Deformable models

Deformable models are a growing field of research in the medical image and volume segmentation, as they present a higher degree of flexibility compared to the previous methods and they can process more complex datasets (Duncan, J.S. James S. J.S. & Ayache 2000; Pham et al. 2000). Their principle is the expansion and compression of a general model that changes its conformation and size to fit the desired 2D/3D shape. These transforms are based on minimization of entropy, i.e., the minimization of the internal and external energy. Internal energy correlates with the elasticity and rigidity of the shape and the external energy with the image/ volume characteristics (Sotiras et al. 2013; Nejati et al. 2016). Examples of deformable models applied to medical image segmentation are active contours (Hafiane et al. 2008; Stoitsis et al. 2008; Wang, X. & Zhang 2012; Cheng, Y. et al. 2015; Bonanno et al. 2017) and level-sets (Sethian 2006; Saba et al. 2012; Santos, André Miguel F. et al. 2013; Tang, Hui et al. 2013; Woźniak et al. 2017). One of the main disadvantages of deformable models is their inability of adapting to several regions simultaneously (Abrantes & Marques 1996). The usage of adaptive level-sets allows coping with this limitation by splitting and merging neighboring regions with similar properties during model evolution (Cebral et al. 2018; Xian Fan et al. Jun 2008; Erdt et al. Nov 2010).

Wang et al. applied deformable models for the segmentation of the carotid tree in the 3D US (Wang, X. & Zhang 2012). The preprocessing was done using a double threshold followed by a region growing algorithm (part of the thresholding methods). The final models were obtained by marching cubes followed by deformable models.

In 2010, Vukadinovic et al. proposed a methodology to segment semi-automatically the outer carotid wall from CTA images (Vukadinovic et al. 2010). The first step in the proposed methodology was a semi-automated level-set segmentation, followed by GentleBoost classification for the automatic detection of the calcium regions of the plaque. In the next step, the GentleBoost was used again, to classify the tissues inside the wall and plaque. Finally, the fitting of a 2D ellipse-shaped deformable model into the segmented wall and plaque area was performed.

2.3.4 Active shape models

Active shape models are similar to deformable models, sharing some operations also with clustering methods. As deformable models, they require a pre-defined prototype of segmentation mask, which is expanded adapting to the image to be segmented (Cootes et al. 2001). The equilibrium of the expanding and contracting forces of the mask is achieved by locating pre-determined landmarks in the image and correlating them to the correspondent feature in the mask (Cootes et al. 2001; Heimann & Meinzer 2009; Cerrolaza et al. 2015). An example of this method was presented by Stoitsis et al., who used Hough transform to initialize the active shape model for the segmentation of the carotid wall in B-mode US (Stoitsis et al. 2008). Additionally, active shape models have been used to segment the carotid arteries and their components in MRI (Tang, H. & Walsum 2012; Fasquel et al. 2015; van Engelen et al. 2015).

2.3.5 Synopsis of image processing bottlenecks in carotid segmentation

There are many bottlenecks in the methodology currently used to study carotid atherosclerosis. The crucial gap is clinician dependency for initial masks, points (referred in this thesis as seeds), and parameters. The next major problem is the need of datasets for training and testing of machine learning-based approaches. Finally, the overall time required to implement and run such methods in a clinical setting remains a significant limitation.

3 Aims of the study

The final goal of this thesis was to develop automatic, clinician- and parameter-independent image processing and segmentation algorithms for the assessment of the burden of atherosclerosis of the carotid arteries. Also, these developed tools are integrated into a single software system, VASIM, possible to deploy in a clinical or research environment in the future. The following aims were given for the study to reach these goals:

1) the development and implementation of an automatic detection system for carotid arteries in CTA;
2) the development of an automatic segmentation protocol for carotid artery lumen;
3) the development of automatic segmentation algorithms for the carotid artery outer wall;
4) the integration of the developed methods into a software system suitable for clinical applications.

4 Materials and Methods

The development of VASIM and the research completed within the scope of this thesis can be divided into four essential cornerstones required for a correct segmentation of the carotid tree and evaluation of the atherosclerosis burden. The cornerstones are:

1. Detection of the carotid arteries in CTA stack [III];
2. 3D segmentation of the carotid tree and lumen [I];
3. 3D segmentation of the carotid wall and plaques [II];
4. Calculation and presentation of quantitative and qualitative results of the analysis of atherosclerosis (IV and (Santos, F. et al. 2011))

An updated and improved version of the algorithms developed in the previous studies was presented in publication [IV]. The approach shown in this publication was more complex and time-consuming but provided better results and a better correlation between manual and automatic assessment of stenosis.

4.1 Patient data

The research was based on CTA exams taken at the Tampere University Hospital (Tampere, Finland). For all of the studies, the following inclusion criterion was defined *a priori*: the presence of the neck-and-head CTA in the hospital database. Both non-atherosclerotic

related exams, and pre- and post-endarterectomy examinations were included in the studies' datasets.

All of the patients were examined using one of the two different helical, 64-slice, multidetector CT scanners either Philips® Brilliance CT (slice thickness 1 mm; increment 0.5 mm; pixel size 0.42–0.49 mm; 120 kVp; 178–243 mAs) or General Electric® LightSpeed (slice thickness 1.25 mm; increment 0.5–0.7 mm; pixel size 0.6–0.7 mm; 120 kVp; 130–327 mAs). One of the following contrast media was administered intravascularly: either Iomeron (350mg/ml), General Electric Omnipaque® (350 mg/ml), or Guerbet Xenetix® (350 mg/ml), according to the manufacturers' recommendations. The average imaging time was 30 seconds. Each CTA slice was exported as a 512x512 matrix.

In Studies [I] and [III], fourteen patients' image sets were analyzed. In the publication [II], four image sets were used. Finally, in the publication [IV] image sets of fifty-nine individuals were included (thirty-eight diagnosed with atherosclerosis and twenty-one healthy). Their mean age was 64 years (range 37-83). More detailed data on the analyzed population were given in publication [IV].

All of the supra-aortic CTA slices were analyzed. Percentage of stenosis was calculated based on the NASCET criterion. Stenosis over 70% was considered clinically relevant. Patients with stenosis below 50% were classified as healthy. The research was approved by the Ethical Committee of the Pirkanmaa Hospital District (decision number R07210).

4.2 Atherosclerotic carotid artery detection, segmentation, and evaluation

As mentioned before, the algorithm applied by VASIM is divided into four steps: detection of the carotid artery, lumen segmentation, wall segmentation, and calculation of metrics and presentation of results. Figure 2 presents the overall VASIM process (explained further in the next subchapters).

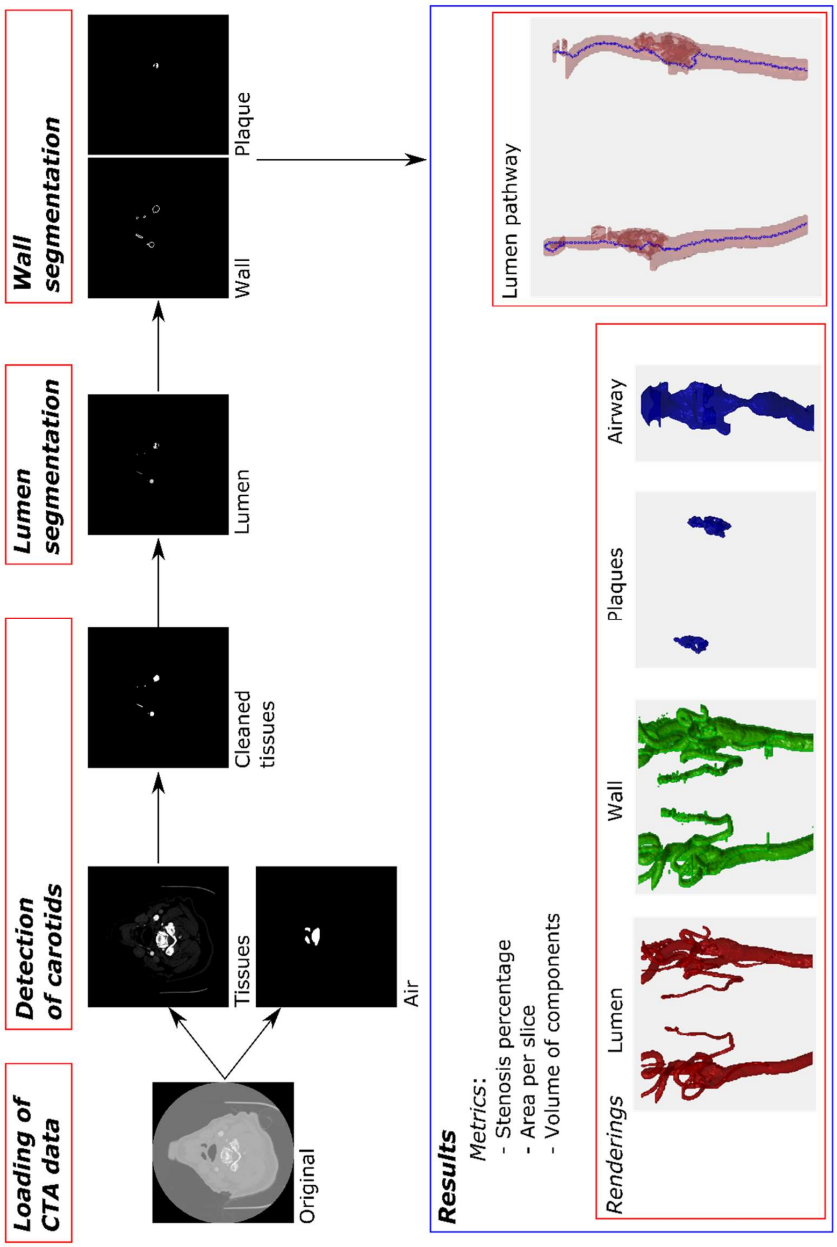

Figure 2. The modules of VASIM software

VASIM was developed and tested using Matlab® (version R2017a, Image Processing Toolbox version 10.0, Signal Processing Toolbox version 7.4, and Statistical Analysis and Machine Learning Toolbox version 11.1). The processing was executed with a Lenovo W541, Windows 7 Enterprise, 64-bits, Intel® Core i7 2.80 GHz, and 32.0 GB RAM with an NVIDIA Quadro K2100M graphics card.

4.2.1 Loading of the CTA data

Loading of the patient DICOM files into a single stack is the first stage in the analysis executed by VASIM. Different CTA machines use different rescale functions. VASIM divides the patient model into two datasets: one for the air volume (<-500 HU) and one for the tissues (>0 HU). Dividing the model allows to standardize the dataset and decrease the memory consumption of the analysis.

4.2.2 Detection and segmentation of the carotid arteries [I, III, and IV]

The method presented in this thesis allows locating the carotid arteries automatically. The diagram of this process is presented in Figure 3.

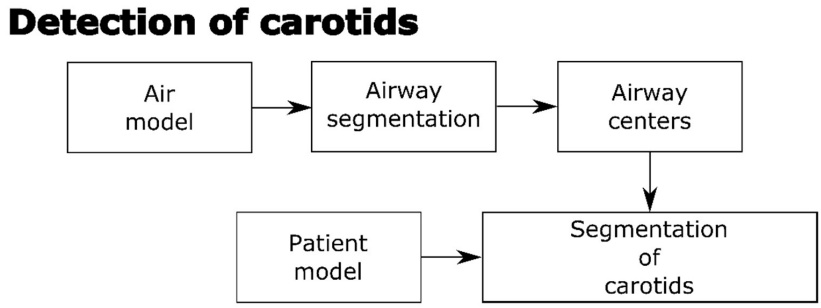

Figure 3. Process diagram for detection of carotids

Air model

Based on the patient stack, two different models are created. The first one represents tissues. The second one describes the total air volume inside and outside of the patient. The latter model is created by thresholding the volume below -500 HU. This low value restricts

the representation of tissues characterized by low attenuation values (e.g., lipid tissues) in the volume.

Airway segmentation

The upper airways play a crucial role in VASIM. They provide a 3D anatomical landmark that is easy to identify and segment in all patients. Airways are represented as a vertical hollow tube in the CTA scans, even in case of intubated patients. As the attenuation of the airways is lower than the attenuation of the adjacent tissues, they cannot be connected with the surrounding air. However, it is true only when the analysis of the scan is restrained to the slice most proximal to the nasal cavity. The final result of the modeling is a 3D object representing the patient' airway. It is usually located in the center of the volume. The coordinates of the center (for each slice) are stored for the next steps of the analysis.

Segmentation of carotid arteries

Publications [I] and [III] used a seed identification system that searched scans slice-by-slice for circular/ellipsoidal shapes, similarly to the Hough transform. However, the detection was relatively sensitive to noise and artifacts. Moreover, the speed and performance of the analysis were unsatisfying. For publication [III] a manual seeding tool (SeedsTool) was created, facilitating independent seeding of the initial and final points in several patients. These seeds were compared to the automatically determined seeds.

In publication [IV] the methodology of identification of carotid arteries was updated. It both identifies the carotid arteries and segments them. All tubular structures are determined based on the airway center points. In the beginning, a cylindrical VOI within the radius of 5 cm from the airways is created. It eliminates several structures and part of the vertebral column. Subsequently, using the Matlab® function *isovalue*, an automatic threshold is applied to segment the tissues based on their attenuation. The models of two carotid arteries are created in this process. In case of occlusion, VASIM checks for the possible distant objects that would fit better into a linear pathway upward of the vessel.

Afterward, all objects crossing the sagittal plane between carotid arteries are detected. The detection process is based on the airway centers again. Most common artifacts found during this process are the mandible, and the hyoid bone, characterized by lower density and attenuation than other bones. Five steps comprise the process of cleaning these foreign objects: (i) skeletonization of the model(s), (ii) cleaning of skeleton nodes, (iii) calculation of vertical degree of each sub-model, (iv) deletion of non-vertical objects, and (v) reconstruction of the arterial tree based on the original model and the previously extracted nodes. The vertical orientation of each object is defined as the ratio between the axes of the bounding box containing the object. In VASIM, the acceptance threshold for the vertical degree is 1.5. After the cleaning process, the model is readjusted to the original one. The area of the lumen is analyzed perpendicularly to the arterial pathway. The final model presents two carotid arteries, independently from region growing and initialization parameters.

Additionally, the presented method can cope with loops and twists in the arteries. The separation of the common, internal, and external carotid arteries and the carotid bifurcation is executed side-wisely. It is based on locating the slice where the number of the objects increases from one to two, and the distance between centroids is <1 cm.

4.2.3 Segmentation of the carotid wall [II]

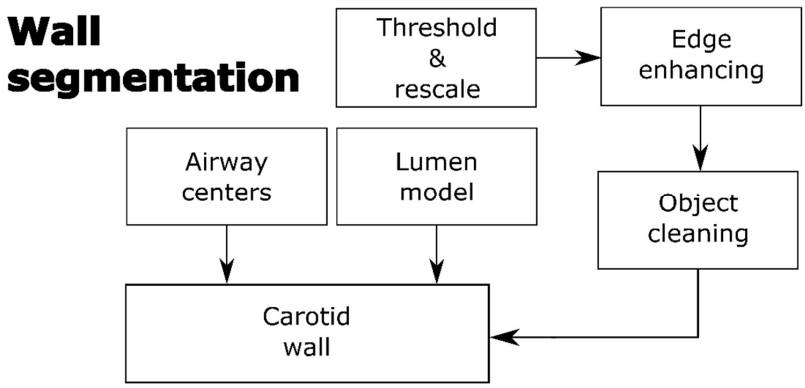

Figure 4. Carotid wall segmentation diagram

In the course of atherosclerosis progression, the IMT increases due to the accumulation of lipid, fibrotic, and calcified compounds in the vascular wall. The analysis of the morphology and distribution of the plaque components allows determining the stability of the atherosclerotic plaque (Nandalur et al. 2007). VASIM enables the segmentation of the vascular wall from the lumen and adjacent tissues, using the method (Figure 4) presented in detail in publication [II]. The algorithm is based on detection of the edge. It is capable of performing slice-wise segmentation in less than 0.05 seconds. The protocol has five steps: (i) hard thresholding of the intensities over 500 HU (all pixels over this value are assigned to 20 HU to prevent deletion of atherosclerotic calcified tissues), (ii) binarization of the image, (iii) enhancement of the carotid edge, based on five edge detectors (Sobel, Prewitt, Roberts, Laplacian of Gaussian, and Canny), and five filters/mapping functions (Laplacian filter, gradient map, Otsu threshold, local range map, and standard deviation map), (iv) filtering of objects, and (v) identification of the object closest to the luminal center in the final outer-inner wall map. The enhancement of the carotid edge was developed in publication [II]. Several edge detectors and filters/mapping functions were tested for the correlation with manually segmented outer vascular wall masks both individually and as ensembles. The highest achieving ensemble was used for outer carotid edge detection. The inner wall contours are based on the luminal outline obtained from the previous slice masks.

4.2.4 Detection and segmentation of the atherosclerotic plaque [IV]

Identification and segmentation of the healthy and the atherosclerotic vascular walls are the next step of the analysis (Figure 5). They can be conducted using calcified tissues as a marker. Attenuation of such tissues is higher than the attenuation of the non-calcified part of the plaque and vascular wall components. They are easy to segment with an automatic threshold (Otsu in VASIM) calculated in the three projections after a 3D maximum intensity projection in the sagittal, coronal and transverse plane. Unless a plaque is present, the histogram of the whole volume does not present a higher peak in its last bin (representing the >500 HU tissues), and the volume is not thresholded. In case of plaques, these thresholded projections are reassembled to three dimensions and create a 3D model of the plaque.

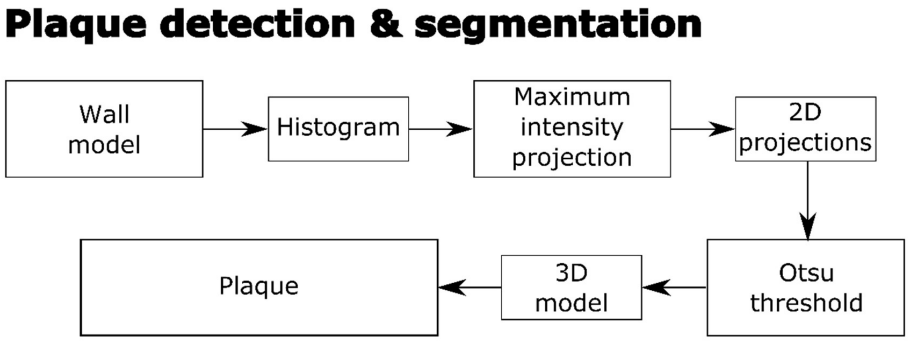

Figure 5. Plaque detection and segmentation diagram

4.2.5 User interface structure and operation [IV]

VASIM is a tool created for analysis of atherosclerosis and follow-up of its course in research and clinical practice. Hence, it requires an easy to use and intuitive interface. For purposes of research, using the source code is feasible. However, for clinical practice, the system should be packaged in a self-contained bundle. The analysis should be straightforward, and results should be obtained without proficiency in programming or parameterization. In publication [IV], a user-friendly interface was presented. After loading the patient data, one click is enough to start the analysis.

4.3 Statistical analysis

While the NASCET criterion for the evaluation of stenosis relies on the manual measurement of the lumen diameters, VASIM enables assessment of the degree of stenosis based on areas. For that reason, in publication [IV], diameters were additionally calculated to compare automatic and manual methods.

After analysis with VASIM, a clinician obtains several metrics based on the area or total volume. This is true for both lumens, carotid wall, and atherosclerotic plaque. Currently, no tool segmenting the carotid tree or extracting such metrics is available. The obtained metrics can correlate, e.g., the volume of the lumen and wall, or the percentage of the wall

occupied by atherosclerosis. The limits of the degree of clinically-relevant stenosis can be set for the clinical practice. Additionally, quantitative analysis is useful in follow-up, i.e., monitoring of the evolution of atherosclerosis.

Analysis of the components/tissues distribution is possible based on the segmentation of the plaque as a single element (i.e., separation from the vascular wall). The distribution of these components determines the stability of the plaque (as mentioned in the Introduction). If it is possible to distinguish its calcified cap, the plaque is classified as stable, and urgent endarterectomy is not required.

5 Results

5.1 Detection of the carotids [III]

The carotid detection method, which we presented in publication [III], had a detection rate of 75% and 71% for the assessment of morphological 2D features, and automatic lower and upper seed positioning, respectively. The mean coefficient of variation between the four sets of seeds manually determined by the user and the automatic method was 2% (0%-5% range).

Additionally, for publication [III], SeedsTool was developed (Figure 6). It is an interface that allows the user to load an image and hand-seed the proximal and distant carotid slice. It was used to pinpoint the aforementioned manual seeds.

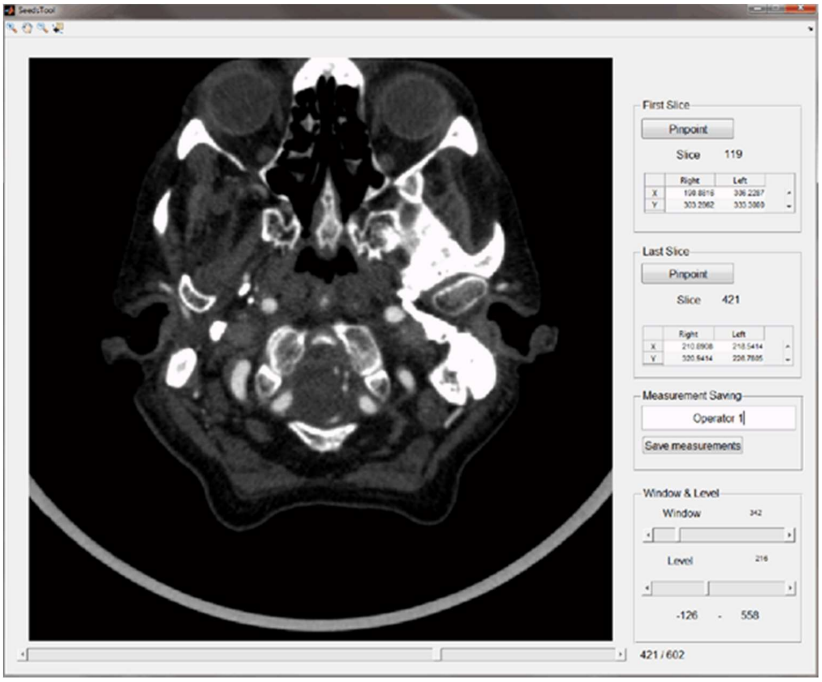

Figure 6. The SeedsTool: interface for semi-automatic carotid detection and segmentation based on user input of seeds (Adapted from publication [III])

5.2 Segmentation of the arterial lumen [I and IV]

A preliminary solution to the segmentation of the lumen was presented in publication [I], where manual and automatic segmentation of the lumen were compared in the population of eight patients. The difference between the manual and automatic measurement of the luminal cross-section area was 6% (P = 0.31). Additionally, following the segmentation of the arteries (both healthy and atherosclerotic), the linearization of the vessels and the adjacent tissues was performed (Figure 7). The segmentation of the lumen has been improved in publication [IV].

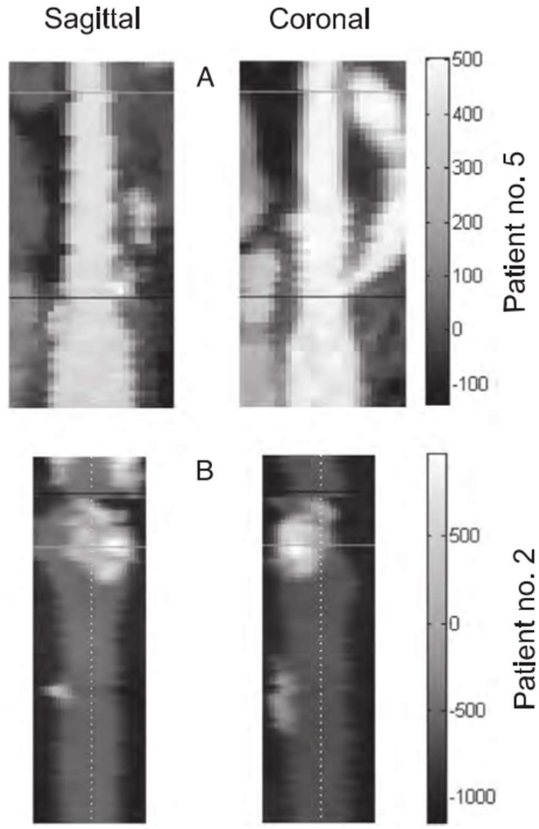

Figure 7. An example of vessel linearization (Adapted from publication [I])

5.3 Arterial wall segmentation [II]

In publication [II], the algorithm for segmentation of the outer vascular wall (example in Figure 8) was presented. The highest correlation between manual and automatic segmentation of the outline was achieved by using a set of edge-enhancing and mapping methods: local range maps, gradient mapping, and standard deviation mapping followed by edge enhancement and threshold. The correlation between the automatic and manual method was 58%.

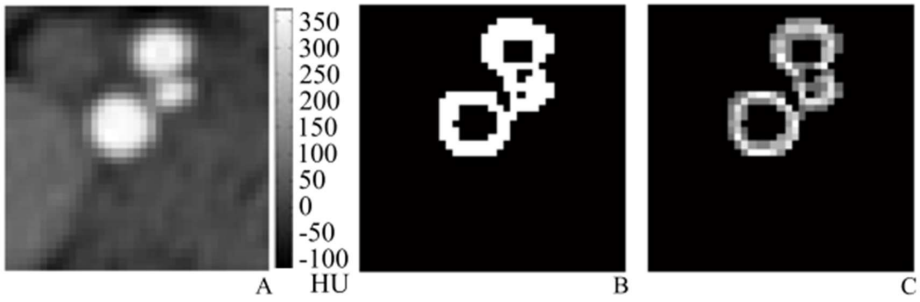

Figure 8. An example of the segmentation of the outer vascular wall

(Adapted from publication [II])

5.4 Detection of atherosclerosis [IV]

Image sets of 59 individuals were analyzed for the burden of atherosclerosis by VASIM, in publication [IV]. The carotid artery was correctly detected and segmented in 83% of the patients. For the stenosis higher than 50%, the specificity and the sensitivity of the detecting and classifying algorithm were 25% and 83%, respectively. The overall accuracy of the algorithm was 71%. The average absolute difference between the automatic and manual method was 33% (95% confidence interval 29% - 46%). The average time of the analysis of the data with VASIM software was 23 minutes per patient (1.62 seconds per slice).

5.5 VASIM interface [IV]

VASIM interface is comprised of a message board and six blocks (Figure 9). The message board shows information on what stage of the analysis VASIM is. Block A enables loading and modeling of the patient's dataset. The modeling function presents a 3D rendering of the current patient's dataset, thresholded by the user-determined level and window. In Block B personal data of the patient (name and social security number) and the characteristics of the imaging session (scanner, imaging and image parameters) are presented. Block C specifies the level of stenosis of the detected arteries. Block D arranges all the image results and their 2D representations (patient dataset and carotid linearizations). After

the analysis, the 2D patient slices and linearizations can be overlapped with the components' (lumen, wall, and plaque) masks. Additionally, the linearization sub-windows show the location of the maximum stenosis and carotid bifurcation as horizontal lines (purple and blue, respectively). The 3D renderings can be rotated to inspect specific locations in more detail. Block E gives the user control of the window and level of the 2D slices for the histogram and quantification. Block F allows for the selection of masks to overlap the 2D slices, both in the patient dataset, linearizations, and in the 3D renderings. Moreover, it contains the selection of the color map.

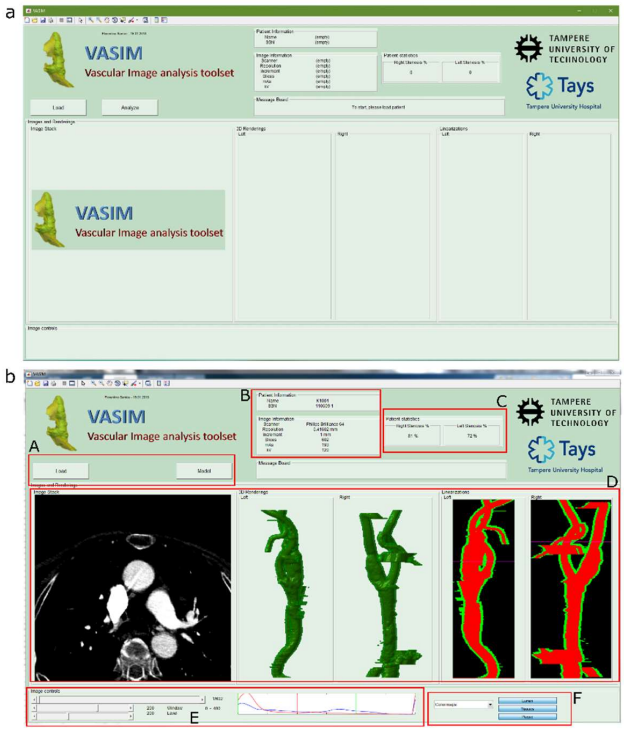

Figure 9. VASIM before (a) and after (b) analysis of the patient's data. Red boxes represent the different interface components. (Adapted from publication [IV])

6 Discussion

The outcome of this study - VASIM, provides a number of image processing and analysis tools for the evaluation of the presence and burden of carotid atherosclerosis, based on CTA images. The aim of this research was to develop a tool based on a simple and reliable set of algorithms, that can detect, segment, and analyze the carotid arteries, regarding both lumen, vascular wall, and possible atherosclerotic plaque.

In general, because of the limited CTA image quality and resolution, the analysis of the substructures of carotid arteries, such as lumen and plaque remains a challenging task (see Fig. 10A). Nevertheless, VASIM tool success rate of detection and segmentation of carotid arteries was 83%. The overall accuracy of the tool was 71% when compared to the manual analysis. The main strength of VASIM is its ability to segment and separate the different compartments of the carotid vessel. Although the average processing time was 23 minutes per patient, VASIM could be used as an automatic tool in everyday radiological practice. As usually the radiological analysis of images is not performed in real-time, VASIM can be run in advance.

The major weakness of the method was its low specificity - 25%. This represents a four-fold increase of false positives in the detection of stenosis levels over 50%. The usability of VASIM in a clinical setup is still limited, and the detection and segmentation methods need to be improved. Nonetheless, in a clinical setup, it is more advantageous to have a higher

level of false positives than false negatives. VASIM is not intended to replace expert evaluation but to provide a preliminary patient analysis. A clinician will always make the final decision on patient care.

The aforementioned results are encouraging and provide the framework for future studies on automatic detection and analysis of carotid arteries.

The methods presented in the introduction and in this thesis adopt several different imaging modalities (e.g., MRI and US), datasets (e.g., coronary, aorta, cerebral), and present the results with different metrics (e.g., Dice similarity, p-values, mean absolute surface distance, mask overlap percentage, performance). Therefore, it was not feasible to compare the results and metrics obtained by VASIM with the existing literature and methodologies published previously.

VASIM consists of algorithms for image enhancement, morphological operators, and segmentation in 3D volume image processing. Their application is a serial process, consisting of detection and segmentation of a plaque and carotid wall and lumen. Finally, the quantitative and qualitative results are output.

6.1 Carotid detection and segmentation

The first step of detection of carotid arteries by VASIM is creating a 3D landmark. The structure we have chosen is the upper respiratory tract, as relatively few anatomical variants are observed in its construction. In case of assisted breathing patients, even though the intubation tube changed the shape of the cylinder, the algorithm worked properly. A potential source of errors in this method may be the algorithm reading the air surrounding the patient as a further part of its airway, i.e., spreading detection of volume to the nasal cavity, and spilling through the nostrils. Limiting the airway volume detection to the ceiling of the mouth is a way of prevention of these errors.

Detection of carotid arteries by VASIM is dependent on a previous overall segmentation. Using the airway as an anatomical landmark gives the general direction for the cropping cylinder. It excludes most of the surrounding tissues and limits the VOI attenuation values to more constrained and vessel-representative scale. Even though a partial exclusion of

carotid tree branches or loops falling outside of the cylinder borders is a potential source of error, we did not observe it in our dataset. Such error would critically bias the vessel segmentation. Therefore, a segmentation independent from the directionality of the vessel, like the one implemented in VASIM, is crucial.

VASIM bilaterally checks for interconnectivity after thresholding. The first step of this process is to determine whether the carotid arteries are connected to other single objects like the hyoid bone or the mandibular artery. This step is crucial, as in the process of carotid artery detection many structures must be analyzed by VASIM. For example, if either of the carotid arteries is fully occluded, two candidate structures will appear on the respective side - a proximal and distant section of the common carotid artery, and internal carotid artery. Other examples are a fully occluded artery without the distant part and an excised artery. In case of a fully occluded carotid artery, VASIM creates an assumption of the vascular pathway, based on the linear approximations, connecting the proximal and distant section of the vessel. A possible source of error is connecting the common carotid artery to the external carotid artery, in case of insufficient or poor thresholding of the tissues. Finally, VASIM can also analyze healthy arteries.

One of the methods studied for the automatic detection and segmentation of the carotid tree is the vesselness, developed by Frangi et al. (Frangi et al. 1998). It is based on all eigenvalues of the image's Hessian. The method was discarded during the development of VASIM since it is highly sensitive to tissues characterized by high attenuation (Figure 10).

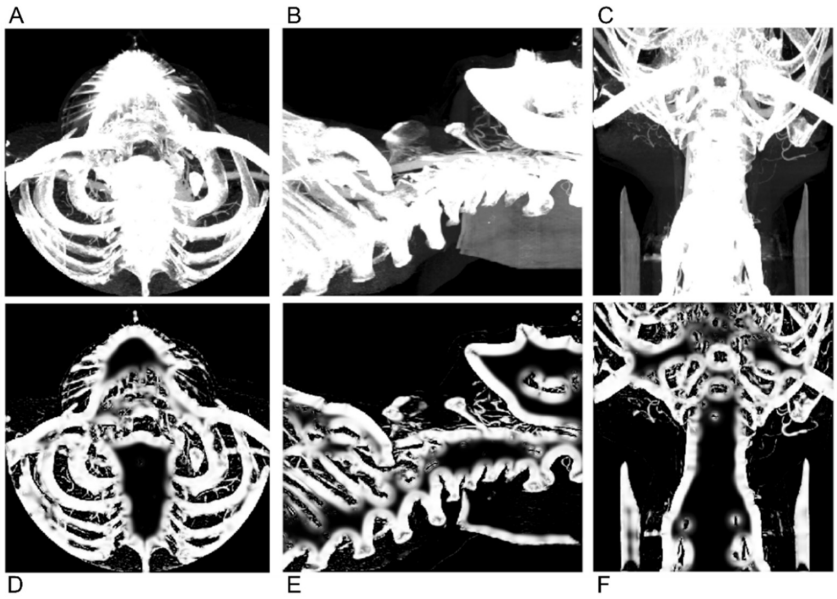

Figure 10. An example of Hessian-based Frangi vesselness filter applied to the three projections of the cylinder-cut VOI.[1]

6.2 Segmentation of the carotid wall and atherosclerotic plaque

In 2012, Saba et al. presented a method of semi-automatic segmentation of the carotid wall and atherosclerotic plaque (Saba et al. 2012). The method is comprised of two stages. The first step is manual inner and outer boundary delimitation. It is followed by an automatic tracking of these structures using level-sets. According to the authors, the correlation between manual and semi-automatic method was high (0.84). The manual initialization and duration of the shaping with the level-sets remain significant limitations of the method.

[1] Original implementation parameters: range: [1, 10], Scale ratio: 2, beta one: 0.5, beta two: 15. A-D Transverse MIP, B-E Sagittal MIP, C-F Coronal MIP. The spine and overall bone-based tissues lower contrast and detection of the carotid tree (with calcified plaque included).

In our Studies [I] and [III], we applied an adaptive region-growing algorithm, to segment and evolve the carotid tree after seeding. The method was quite sensitive to spillage of the tree (branching to neighboring structures).

Several studies, using both semi-automatic and automatic protocols, applied the same region growing methodology (e.g., (Yi & Ra 2003; Weert et al. 2008; Bozkurt et al. 2018)). It is frequently used in MRI, where arteries present a homogenous contrast. Such homogenous vessels are easier to segment. In the future, when MRI will be used in the evaluation of atherosclerosis more often, and CT technology will evolve in a contrast-free pathway, we might see a breakthrough in the examination of the carotid tree.

6.3 VASIM contribution to the clinical practice

The goal of the study was the development of VASIM - a tool for clinical usage and research, automatically evaluating carotid atherosclerosis.

Currently, few commercial software tools, approaching the aims of VASIM, are available on the market. An example is Autobone and VesselIQ Xpress (GE Healthcare®). It is a tool used for CTA analysis regarding vascular anatomy and pathology, specifically for coronary arteries. It provides a visualization and analysis tool, providing tissue distinction, vessel tortuosity, quantification of abnormal anatomical structures, and automatic segmentation of bones (Autobone and VesselIQ Xpress). The other solutions used for heart image analysis are suiteHeart® (suiteHEART), 3mensioWorkstation™ (3mensio Workstation), and Medis Suite CT (Medis Suite CT). For imaging of abdominal and thoracic vessels Vessel (Vessel) and 3mensio Vascular™ (3mensio Workstation) are used. All of the software mentioned above relies on manual operations and/or parameterization. Their common advantage is the visualization and optimization methodology that is somehow superior to VASIM. However, these features were not the primary aims of VASIM.

Both VASIM and the other tools (apart from the Autobone and VesselIQ Xpress), require installing additional third parties software. In the case of VASIM, it is necessary to install the Matlab® Compiler Runtime (MCR). Informatics safety, certification, and requirement of expert installer remain limitations of this approach.

VASIM can contribute to three specific subjects: 3D models, shift from diameter measurements to area-based, and vessel linearizations. It also provides a framework for the presurgical planning and future treatment.

6.3.1 3D models

The 3D models of the carotid tree created with VASIM, facilitate planning of the surgery, providing a clear and intuitive presentation of objects encountered during the procedure. Also, these models make a choice between removing the plaque or stenting easier. Moreover, the models of the structures such as carotid arteries and airways could be printed in 3D in the future. A 3D-printed, palpable physical object would be an extremely useful tool for the clinicians. The 3D physical models can also be used for medical training, e.g., as phantoms, or blood flow and behavior models of different atherosclerotic stages.

6.3.2 Area versus diameter

VASIM provides not only the full-automation of the carotid arteries' evaluation process but also measures areas (of lumen, wall, and plaque) instead of diameters. To the knowledge of the author, it is the first tool of its kind. Currently, the stenosis is evaluated manually based on diameters. As the hand segmentation of the arteries is highly time-consuming, measurements of areas are not conducted. VASIM overcomes this limitation by segmenting the total lumen area perpendicularly to the vascular pathway. By avoiding false sectioning of oval structures, it enables correct adaptability to the vessel, increasing the precision of the evaluation of the stage of atherosclerosis.

6.3.3 Carotid linearizations

VASIM presents linearizations of the carotid vessel (**Erro! A origem da referência não foi encontrada.**B). It linearizes (or flattens) the complete carotid tree into a single 2D image, based on the skeleton of the lumen path. This presentation helps to distinguish different structures, such as arterial lumen and wall, and structures of the plaque.

6.4 Future work

To the knowledge of the author, VASIM is the first fully automated tool for detecting and evaluating carotid arteries. The methodology of VASIM is promising and should be improved in the future. The work should focus on improvements in the luminal and wall segmentation, and implementation of the 3D detection algorithms. These two approaches would lead to an increase of the sensitivity and relatively low specificity presented currently by VASIM. Additionally, the duration of the analysis should be reduced. This could be achieved either by implementing different methods and algorithms or by using more computational power (e.g., parallelization or computer clusters).

6.4.1 New metrics

It is generally accepted that atherosclerotic plaque composition and component distribution depict the stage of the plaque and its stability (Nandalur et al. 2007). VASIM enables extraction of healthy and atherosclerotic areas and volumes, both for the lumen and wall components. Extracting areas from each slice perpendicularly to the vascular wall allows creating new metrics, e.g., the ratio between the lumen and vascular wall, and the ratios between wall and plaque. Future work should focus on the development of such metrics, that would be correlating with the vessel stenosis more accurately than the ones used nowadays.

6.4.2 Blood flow modeling

The blood flow in healthy and diseased patients can be modeled based on the carotid tree presented in 3D rendering. It shows the wall shear stress, stability of the plaque, and its risk of becoming an embolic material. Moreover, based on the modeling, the urgency for endarterectomy and evolution of the disease can be assessed.

According to Cerbal et al. (Cebral, Yim, Löhner, Soto, & Choyke, 2002) evaluation of the blood flow patterns using MRI techniques can be conducted, after segmenting the carotid tree. It serves as a supplement to the imaging studies and predictor of the treatments' efficacy.

6.4.3 Machine learning

Much research in recent years has focused on the development of image processing techniques. A multidisciplinary approach is crucial for algorithm development. The fusion of traditional image processing and advanced computer science is closer than ever before. Machine learning techniques have already been applied in the analysis of medical US images of carotid arteries (Santos, André Miguel F. et al. 2013; Menchón-Lara et al. 2014; Menchón-Lara & Sancho-Gómez 2015). Machine learning and deep learning methodologies could also be utilized in VASIM. It would increase VASIM's stability and adaptability. The program would learn from the images already analyzed. With the increase in the number of cases examined, it would improve the segmentation and detection of the carotid arteries.

Machine learning could also be applied to integrate an adaptive segmentation of the vascular wall and plaque, and to classify the structures/materials inside the wall. This would attenuate independent segmentation of the fibrotic, lipid, and calcified structures in CT-based imaging, to study plaque stability and risk of its rupture. Finally, machine learning could be used in personalized medicine, crossing results obtained with VASIM with the patient's laboratory exams. It would provide a multidisciplinary and multivariable analysis of the stage of the disease and risk of its progression. Van Engelen et al. (Van Engelen et al., 2015) reported an average of the inter-center accuracy of 90% for MRI imaging analysis, using same-center training, voxel-wise tissue classification, a non-linear feature normalization, and two transfer-learning algorithms.

6.4.4 VASIM in other imaging modalities

In principle, VASIM can be applied in the analysis of the carotid trees in both CTA, CT, and MRI. However, the methodology included in its algorithm requires a normalization between scanners by the rescaling factor. Standardization allows VASIM to adapt standard CTA attenuation range to the ones present in CT or MRI pixel range.

7 Conclusions

The outcomes for each goal can be expressed as follows:

1) an automatic detection system for carotid arteries in CTA has been developed,
2) an automatic segmentation protocol for carotid artery lumen was designed, resulting in a success rate of 83%,
3) automatic segmentation algorithms were developed for the carotid artery outer wall,
4) a software system was constructed with a clinical accuracy of 71%.

The results presented in this manuscript are a compilation of the several years' research on the development of image-processing tools for the analysis of carotid atherosclerosis. The qualitative and quantitative results of these studies corroborate the validity of VASIM as a potential tool for clinical use. It is capable of coping with various degrees of the disease, from non-occluded to fully occluded arteries, based on an ensemble of simple but fast image-processing methods. The analysis is divided into lumen, vascular wall outer and vascular wall segmentation, and presentation of both qualitative and quantitative results with an easy to use interface - VASIM.

VASIM had an overall clinical accuracy of 71% in the detection, segmentation, and analysis in the population of patients with stenosis over 50%. Even if the specificity was low - 25%, the sensitivity was high - 83%, which is likely to result in overestimation of the urgency of the patient condition. The average time required to use this software was 1.6 seconds per slice and 23 minutes per patient. It can be shortened to suit the clinical practice better.

References

3mensio Workstation, PIE Medical Imaging, web page. Available (accessed 09.05.2018): https://www.piemedicalimaging.com/product_category/ct/.

Abrantes, A.J. & Marques, J.S. (1996). A class of constrained clustering algorithms for object boundary extraction, IEEE Transactions on Image Processing, Vol. 5(11), pp. 1507-1521.

Achenbach, S. (2002). Influence of Lipid-Lowering Therapy on the Progression of Coronary Artery Calcification: A Prospective Evaluation, Circulation, Vol. 106(9), pp. 1077-1082.

Adame, I.M., van der Geest, R J, Wasserman, B.A., Mohamed, M.A., Reiber, J.H.C. & Lelieveldt, B.P.F. (2004). Automatic segmentation and plaque characterization in atherosclerotic carotid artery MR images, Magnetic Resonance Materials in Physics, Biology and Medicine, Vol. 16(5), pp. 227-234.

Akkus, Z., Carvalho, D.D.B., van den Oord, Stijn C H, Schinkel, A.F.L., Niessen, W.J., de Jong, N., van der Steen, Antonius F W, Klein, S. & Bosch, J.G. (2015). Fully Automated Carotid Plaque Segmentation in Combined Contrast-Enhanced and B-Mode Ultrasound, Ultrasound in Medicine & Biology, Vol. 41(2), pp. 517-531.

Al-Kofahi, Y., Lassoued, W., Lee, W. & Roysam, B. (2010). Improved automatic detection and segmentation of cell nuclei in histopathology images, IEEE Transactions on Biomedical Engineering, Vol. 57(4), pp. 841-852.

Arbustini, E., Dal Bello, B., Morbini, P., Burke, A.P., Bocciarelli, M., Specchia, G. & Virmani, R. (1999). Plaque erosion is a major substrate for coronary thrombosis in acute myocardial infarction, Heart, Vol. 82(3), pp. 269-272.

Arifin, A.Z. & Asano, A. (2006). Image segmentation by histogram thresholding using hierarchical cluster analysis, Pattern Recognition Letters, Vol. 27(13), pp. 1515-1521.

Augst, A. & Ariff, B. (2007). Analysis of complex flow and the relationship between blood pressure, wall shear stress, and intima-media thickness in the human carotid artery, Am J Physiol Heart Circ Physiol, Vol. 293(2), pp. 1031-1037.

Autobone and VesselIQ Xpress, GE Healthcare, web page. Available (accessed 09.05.2018): http://www3.gehealthcare.com/en/products/categories/advanced_visualization/applications/autobone_and_vesseliq_xpress#tabs/tabDED3FDCA0B904300B47A4CBBE2D011DB.

Avendi, M.R., Kheradvar, A. & Jafarkhani, H. (2016). A combined deep-learning and deformable-model approach to fully automatic segmentation of the left ventricle in cardiac MRI, Medical Image Analysis, Vol. 30 pp. 108-119.

Avendi, M.R., Kheradvar, A. & Jafarkhani, H. (2017). Automatic segmentation of the right ventricle from cardiac MRI using a learning-based approach, Magnetic Resonance in Medicine, Vol. 78(6), pp. 2439-2448.

Badrinarayanan, V., Kendall, A. & Cipolla, R. (2017). SegNet: A Deep Convolutional Encoder-Decoder Architecture for Image Segmentation, IEEE Transactions on Pattern Analysis and Machine Intelligence, Vol. 39(12), pp. 2481-2495.

Bali, A. & Singh, S.N. (2015). A Review on the Strategies and Techniques of Image Segmentation, 5th International Conference on Advanced Computing & Communication Technologies, IEEE, pp. 113-120.

Bartoli, F., Blagojevic, J., Bacci, M., Fiori, G., Tempestini, A., Conforti, M.L., Guiducci, S., Miniati, I., Di Chicco, M., Del Rosso, A., Perfetto, F., Castellani, S., Pignone, A. & Cerinic, M.M. (2007). Flow-mediated vasodilation and carotid intima-media thickness in systemic sclerosis, Annals of the New York Academy of Sciences, pp. 283-290.

Beevers, D.G. (2005). The atlas of heart disease and stroke, Journal of Human Hypertension, Vol. 19(6), pp. 505-617.

Biermann, C., Tsiflikas, I., Thomas, C., Kasperek, B., Heuschmid, M. & Claussen, C. (2012). Evaluation of Computer-Assisted Quantification of Carotid Artery Stenosis, Journal of Digital Imaging, Vol. 25(2), pp. 250-257.

Bonanno, L., Sottile, F., Ciurleo, R., Di Lorenzo, G., Bruschetta, D., Bramanti, A., Ascenti, G., Bramanti, P. & Marino, S. (2017). Automatic Algorithm for Segmentation of Atherosclerotic Carotid Plaque, Journal of Stroke and Cerebrovascular Diseases, Vol. 26(2), pp. 411-416.

Bozkurt, F., Köse, C. & Sarı, A. (2018). An inverse approach for automatic segmentation of carotid and vertebral arteries in CTA, Expert Systems With Applications, Vol. 93 pp. 358-375.

Brown, R.A., Shantsila, E., Varma, C. & Lip, G. (2016). Current Understanding of Atherogenesis, American Journal of Medicine, Vol. 130(3), pp. 268-282.

Burghardt, A., Kazakia, G. & Majumdar, S. (2007). A Local Adaptive Threshold Strategy for High Resolution Peripheral Quantitative Computed Tomography of Trabecular Bone, Annals of Biomedical Engineering, Vol. 35(10), pp. 1678-1686.

Cai, J., Hatsukami, T.S., Ferguson, M.S., Kerwin, W.S., Saam, T., Chu, B., Takaya, N., Polissar, N.L. & Yuan, C. (2005). In vivo quantitative measurement of intact fibrous cap and lipid-rich necrotic core size in atherosclerotic carotid plaque: Comparison of high-resolution, contrast-enhanced magnetic resonance imaging and histology, Circulation, Vol. 112(22), pp. 3437-3444.

Cantón, G., Hippe, D.S., Sun, J., Underhill, H.R., Kerwin, W.S., Tang, D. & Yuan, C. (2012). Characterization of distensibility, plaque burden, and composition of the atherosclerotic carotid artery using magnetic resonance imaging, Medical Physics, Vol. 39(10), pp. 6247-6253.

Carnicelli, A.P., Stone, J.J., Doyle, A., Chowdhry, A.K., Mix, D., Ellis, J., Gillespie, D.L. & Chandra, A. (2013). Cross-sectional area for the calculation of carotid artery stenosis on computed tomographic angiography, Journal of Vascular Surgery, pp. 659-665.

Carrascosa, J., Carrascosa, P.M., Capuñay, C.M., Garcia-Merletti, P. & Garcia, M.J. (2006). Characterization of Coronary Atherosclerotic Plaques by Multidetector Computed Tomography, The American Journal of Cardiology, Vol. 97(5), pp. 598-602.

Cebral, J.R., Mut, F., Gade, P., Cheng, F., Tobe, Y., Frosen, J. & Robertson, A.M. (2018). Combining Data from Multiple Sources to Study Mechanisms of Aneurysm Disease: Tools and Techniques, International journal for numerical methods in biomedical engineering, pp. e3133.

Cerrolaza, J.J., Reyes, M., Summers, R.M., González-Ballester, M.Á & Linguraru, M.G. (2015). Automatic Multi-Resolution Shape Modeling of Multi-Organ Structures, Medical Image Analysis, Vol. 25(1), pp. 11-21.

Chambless, L.E., Heiss, G., Folsom, A.R., Rosamond, W., Szklo, M., Sharrett, A.R. & Clegg, L.X. (1997). Association of coronary heart disease incidence with carotid arterial wall thickness and major risk factors: the Atherosclerosis Risk in Communities (ARIC) Study, 1987-1993, American journal of epidemiology, Vol. 146(6), pp. 483-494.

Cheng, D., Billich, C., Liu, S., Brunner, H., Qiu, Y., Shen, Y., Brambs, H.J., Schmidt-Trucksäss, A. & Schütz, U.H. (2011). Automatic detection of the carotid artery boundary on cross-sectional MR image sequences using a circle model guided dynamic programming, Biomedical engineering online, Vol. 10(1), pp. 26.

Cheng, H.D., Jiang, X.H., Sun, Y. & Wang, J. (2001). Color image segmentation: Advances and prospects, Pattern Recognition, Vol. 34(12), pp. 2259-2281.

Cheng, Y., Hu, X., Wang, J., Wang, Y. & Tamura, S. (2015). Accurate Vessel Segmentation With Constrained B-Snake, IEEE Transactions on Image Processing, Vol. 24(8), pp. 2440-2455.

Comin, C.H., Xu, X., Wang, Y., da Fontoura Costa, L. & Yang, Z. (2014). An image processing approach to analyze morphological features of microscopic images of muscle fibers. Computerized Medical Imaging and Graphics, Vol. 38(8), pp. 803-814.

Cootes, T.F., Edwards, G.J. & Taylor, C.J. (2001). Active appearance models, IEEE Transactions on Pattern Analysis and Machine Intelligence, Vol. 23(6), pp. 236-248.

Corti, R. & Fuster, V. (2011). Imaging of atherosclerosis: magnetic resonance imaging, European Heart Journal, Vol. 32(14), pp. 1709-1719.

Coursey, C.A., Nelson, R.C., Boll, D.T., Paulson, E.K., Ho, L.M., Neville, A.M., Marin, D., Gupta, R.T. & Schindera, S.T. (2010). Dual-energy multidetector CT: how does it work, what can it tell us, and when can we use it in abdominopelvic imaging? Radiographics, Vol. 30(4), pp. 1037-1055.

Cruz-Roa, A., Caicedo, J.C. & González, F.A. (2011). Visual pattern mining in histology image collections using bag of features, Artificial Intelligence in Medicine, Vol. 52(2), pp. 91-106.

de Groot, E., Hovingh, G.K., Wiegman, A., Duriez, P., Smit, A.J., Fruchart, J. & Kastelein, J.J.P. (2004). Measurement of Arterial Wall Thickness as a Surrogate Marker for Atherosclerosis, Circulation, Vol. 109(23), pp. 33-38.

De Vasconcellos, L.P., Flores, J.A.C., Conti, M.L.M., Veiga, J.C.E. & Lancellotti, C.L.P. (2009). Spontaneous thrombosis of internal carotid artery: A natural history of giant carotid cavernous aneurysms, Arquivos de Neuro-Psiquiatria, Vol. 67(2 A), pp. 278-283.

Diab, H.M.H., Rasmussen, L.M., Duvnjak, S., Diederichsen, A., Jensen, P.S. & Lindholt, J.S. (2017). Computed tomography scan based prediction of the vulnerable carotid plaque, BMC medical imaging, Vol. 17(1), pp. 61.

Duncan, J.S. James S. J.S. & Ayache, N. (2000). Medical image analysis: progress over two decades and the challenges ahead, IEEE Transactions on Pattern Analysis and Machine Intelligence, Vol. 22(1), pp. 85-106.

Dungan, D.H. & Heiserman, J.E. (1996). The carotid artery: embryology, normal anatomy, and physiology, Neuroimaging clinics of North America, Vol. 6(4), pp. 789-799.

Eller, A., Wuest, W., Kramer, M., May, M., Schmid, A., Uder, M. & Lell, M.M. (2014). Carotid CTA: radiation exposure and image quality with the use of attenuation-based, automated kilovolt selection. American journal of neuroradiology, Vol. 35(2), pp. 237-241.

Engelen, A., Niessen, W., Klein, S., Groen, H., Verhagen, H., Wentzel, J., Lugt, A. & Bruijne, M. (2014). Atherosclerotic plaque component segmentation in combined carotid MRI and CTA data incorporating class label uncertainty, PLoS ONE, Vol. 9(4), pp. 1-10.

Enterline, D.S. & Kapoor, G. (2006). A Practical Approach to CT Angiography of the Neck and Brain, Techniques in Vascular and Interventional Radiology, Vol. 9(4), pp. 192-204.

Erdt, M., Schlegel, P. & Wesarg, S. (Nov 2010). Multi-Layer Deformable Models for medical image segmentation, Proceedings of the 10th IEEE International Conference on Information Technology and Applications in Biomedicine, pp. 1-4.

Ergün, E., Koşar, P., Öztürk, C., Başbay, E., Koç, F. & Koşar, U. (2011). Prevalence and extent of coronary artery disease determined by 64-slice CTA in patients with zero coronary calcium score, International Journal of Cardiovascular Imaging, Vol. 27(3), pp. 451-458.

Fasquel, J., Lécluse, A., Cavaro-Ménard, C. & Willoteaux, S. (2015). A semi-automated method for measuring the evolution of both lumen area and blood flow in carotid from Phase Contrast MRI, Computers in Biology and Medicine, Vol. 66 pp. 269-277.

Feeley, T.M., Leen, E.J., Colgan, M., Moore, D.J., Hourihane, D.O. & Shanik, G.D. (1991). Histologic characteristics of carotid artery plaque, Journal of Vascular Surgery, Vol. 13(5), pp. 719-724.

Feinstein, S.B. (2006). Contrast Ultrasound Imaging of the Carotid Artery Vasa Vasorum and Atherosclerotic Plaque Neovascularization, Journal of the American College of Cardiology, Vol. 48(2), pp. 236-243.

Ferguson, G.G., Eliasziw, M., Barr, H.W.K., Clagett, G.P., Barnes, R.W., Wallace, M.C., Taylor, D.W., Haynes, R.B., Finan, J.W., Hachinski, V.C. & Barnett, H.J.M. (1999). The North American Symptomatic Carotid Endarterectomy Trial : Surgical Results in 1415 Patients, Stroke, Vol. 30(9), pp. 1751-1758.

Fisher, M., Paganini-Hill, A., Martin, A., Cosgrove, M., Toole, J.F., Barnett, H.J.M. & Norris, J. (2005). Carotid plaque pathology: Thrombosis, ulceration, and stroke pathogenesis, Stroke, Vol. 36(2), pp. 253-257.

Fox, A.J. (1993). How to measure carotid stenosis. Radiology, Vol. 186(2), pp. 316-318.

Frangi, A.F., Niessen, W.J., Vincken, K.L. & Viergever, M.A. (1998). Multiscale vessel enhancement filtering, Medical Image Computing and Computer-Assisted Intervention — MICCAI'98, pp. 130-137.

Gamarra, M., Zurek, E. & San-Juan, H. (2017). Study of Image Analysis Algorithms for Segmentation, Feature Extraction and Classification of Cells, Journal of Information Systems Engineering & Management, Vol. 2(4), pp. 20-24.

Ghose, S., Oliver, A., Mitra, J., Martí, R., Lladó, X., Freixenet, J., Sidibé, D., Vilanova, J.C., Comet, J. & Meriaudeau, F. (2013). A supervised learning framework of statistical shape and probability priors for automatic prostate segmentation in ultrasound images, Medical image analysis, Vol. 17(6), pp. 587-600.

Giannoglou, G.D., Antoniadis, A.P., Koskinas, K.C. & Chatzizisis, Y.S. (2010). Flow and atherosclerosis in coronary bifurcations, EuroIntervention, Vol. 6 pp. 16-23.

Gils, M., Vukadinovic, D., Nouwens- van Dijk, A., Dippel, D., Niessen, W. & Lugt, A. (2012). Carotid atherosclerotic plaque progression and change in plaque composition over time: A 5-year follow-up study using serial ct angiography, American Journal of Neuroradiology, Vol. 33(7), pp. 1267-1273.

Groen, H.C.H., van Walsum, T., Rozie, S., Klein, S., van Gaalen, K., Gijsen, F.J.H., Wielopolski, P.A., van Beusekom, Heleen M M, de Crom, R., Verhagen, H.J.M., van der Steen, Antonius F W, van der Lugt, A., Wentzel, J.J., Niessen, W.J., Walsum, T.v. & Rozie, S. (2010). Three-dimensional registration of histology of human atherosclerotic carotid plaques to in-vivo imaging, Journal of Biomechanics, Vol. 43(11), pp. 2087-2092.

Græbe, M., Pedersen, S. F., Højgaard, L., Kjær, A., Sillesen, H. (2010). 18 FDG PET and Ultrasound Echolucency in Carotid Artery Plaques, JACC: Cardiovascular Imaging, Vol. 3(3), pp. 289-295.

Guan, Q., Du, B., Teng, Z., Gillard, J. & Chen, S. (2012). Bayes clustering and structural support vector machines for segmentation of carotid artery plaques in multicontrast MRI, Computational and mathematical methods in medicine, Vol. 2012 pp. 1-12.

Gupta, A., Baradaran, H., Schweitzer, A.D., Kamel, H., Pandya, A., Delgado, D., Dunning, A., Mushlin, A.I. & Sanelli, P.C. (2013). Carotid Plaque MRI and Stroke Risk: A Systematic Review and Meta-analysis, Stroke, Vol. 44(11), pp. 3071-3077.

Hafiane, A., Bunyak, F. & Palaniappan, K. (2008). Fuzzy Clustering and Active Contours for Histopathology Image Segmentation and Nuclei Detection, Advanced Concepts for Intelligent Vision Systems, Vol. 5259 pp. 903-914.

Hafiane, A., Palaniappan, K. & Seetharaman, G. (2015). Joint Adaptive Median Binary Patterns for texture classification, Pattern Recognition, Vol. 48(8), pp. 2609-2620.

Han, J.H., Ho, S.S.Y., Lam, W.W.M. & Wong, K.S. (2007). Total cerebral blood flow estimated by color velocity imaging quantification ultrasound: A predictor for recurrent stroke? Journal of Cerebral Blood Flow and Metabolism, Vol. 27(4), pp. 850-856.

Hashimoto, M., Eto, M., Akishita, M., Kozaki, K., Ako, J., Iijima, K., Kim, S., Toba, K., Yoshizumi, M. & Ouchi, Y. (1999). Correlation Between Flow-Mediated Vasodilatation of the Brachial Artery and Intima-Media Thickness in the Carotid Artery in Men, Arteriosclerosis, Thrombosis, and Vascular Biology, Vol. 19(11), pp. 2795-2800.

Hassan, M., Chaudhry, A., Khan, A. & Iftikhar, M.A. (2014). Robust information gain based fuzzy c-means clustering and classification of carotid artery ultrasound images, Computer methods and programs in biomedicine, Vol. 113(2), pp. 593-609.

Hayashi, S. (2007). Histology of the Human Carotid Sheath Revisited, Okajimas Folia Anat. Jpn, Vol. 84(2), pp. 49-60.

Heimann, T. & Meinzer, H. (2009). Statistical shape models for 3D medical image segmentation: A review, Medical Image Analysis, Vol. 13(4), pp. 543-563.

Hemmati, H., Kamli-Asl, A., Talebpour, A. & Shirani, S. (2015). Semi-automatic 3D segmentation of carotid lumen in contrast-enhanced computed tomography angiography images, Physica Medica, Vol. 31(8), pp. 1098-1104.

Hoover, A.D., Kouznetsova, V. & Goldbaum, M. (2000). Locating blood vessels in retinal images by piecewise threshold probing of a matched filter response, IEEE Transactions on Medical Imaging, Vol. 19(3), pp. 203-210.

Horng, M. (2010). Multilevel minimum cross entropy threshold selection based on the honey bee mating optimization, Expert Systems With Applications, Vol. 37(6), pp. 4580-4592.

Huibers, A., de Borst, G.J., Wan, S., Kennedy, F., Giannopoulos, A., Moll, F.L. & Richards, T. (2015). Non-invasive Carotid Artery Imaging to Identify the Vulnerable Plaque: Current Status and Future Goals, European Journal of Vascular & Endovascular Surgery, Vol. 50(5), pp. 563-572.

Irace, C., Carallo, C., Loprete, A., Tripolino, C., Scavelli, F. & Gnasso, A. (2013). Delayed flow-mediated vasodilation and carotid atherosclerosis, European Journal of Clinical Investigation, Vol. 43(1), pp. 49-55.

Jiang, B., He, Q. & Wang, P. (2017). Deep Learning for Computer-aided Diagnosis of Brain Diseases Through MRI Multi-classification, International Conference on Medicine Sciences and Bioengineering, Vol. 1(1), pp. 185-196.

Johnsrud, K., Skagen, K., Seierstad, T., Skjelland, M., Russell, D. & Revheim, M. (2017). 18F-FDG PET/CT for the quantification of inflammation in large carotid artery plaques, Journal of Nuclear Cardiology, pp. 1-11.

Kim, A.S. & Johnston, S.C. (2013). Temporal and geographic trends in the global stroke epidemic, Stroke, Vol. 44(6), pp. 123-125.

Kobayashi, K., Akishita, M., Yu, W., Hashimoto, M., Ohni, M. & Toba, K. (2004). Interrelationship between non-invasive measurements of atherosclerosis: flow-mediated dilation of brachial artery, carotid intima-media thickness and pulse wave velocity, Atherosclerosis, Vol. 173(1), pp. 13-18.

Kwee, R.M., Teule, G.J.J., van Oostenbrugge, R.J., Mess, W.H., Prins, M.H., van der Geest, R. J., ter Berg, J.W.M., Franke, C.L., Korten, A.G.G.C., Meems, B.J., Hofman, P.A.M., van Engelshoven, J.M.A., Wildberger, J.E. & Kooi, M.E. (2009). Multimodality Imaging of Carotid Artery Plaques: 18F-Fluoro-2-Deoxyglucose Positron Emission Tomography, Computed Tomography, and Magnetic Resonance Imaging, Stroke, Vol. 40(12), pp. 3718-3724.

Langer, H. & Gawaz, M. (2006). Molecular imaging of vulnerable atherosclerotic plaques, Future cardiology, Vol. 2(1), pp. 113-122.

Leedham, G., Chen Yan, Takru, K., Joie Hadi Nata Tan & Li Mian (2003). Comparison of some thresholding algorithms for text/background segmentation in difficult document images, 7th International Conference on Document Analysis and Recognition, IEEE, pp. 859-864.

Lekadir, K., Galimzianova, A., À. Betriu, del Mar Vila, M., Igual, L., Rubin, D.L., Fernández, E., Radeva, P. & Napel, S. (2017). A Convolutional Neural Network for Automatic Characterization of Plaque Composition in Carotid Ultrasound, IEEE Journal of Biomedical and Health Informatics, Vol. 21(1), pp. 48-55.

Li, X., Zhao, Z. & Cheng, H.D. (1995). Fuzzy entropy threshold approach to breast cancer detection, Information Sciences - Applications, Vol. 4(1), pp. 49-56.

Liang-Chieh Chen, Papandreou, G., Kokkinos, I., Murphy, K. & Yuille, A.L. (2018). DeepLab: Semantic Image Segmentation with Deep Convolutional Nets, Atrous Convolution, and Fully Connected CRFs, IEEE Transactions on Pattern Analysis and Machine Intelligence, Vol. 40(4), pp. 834-848.

Liapis, C.D., Bell, Sir P R F, Mikhailidis, D., Sivenius, J., Nicolaides, A., Fernandes e Fernandes, J., Biasi, G., Norgren, L., Avgerinos, E.D., Becker, F., Benedetti Valentini, F., Becquemin, J.P., Diener, H.C., Froio, A., Gaines, P.A., Gensini, G., Gerotziafas, G., Griffin, M., Hacke, W., Heikkinen, M.A., Norrving, B., Powell, J., Kakisis, J., Karkos, C., Konstantinidis, K., Kotsis, T., Lavitrano, M., Matzsch, T., Parsson, H., Pedro, L.M., Salenius, J.P., Schachter, M., Sillesen, H. & Thomas, D.J. (2009). ESVS Guidelines. Invasive Treatment for Carotid Stenosis: Indications, Techniques, European Journal of Vascular and Endovascular Surgery, Vol. 37(4), pp. 1-19.

Ling, Y. & Hurlbert, A. (2004). Color and size interactions in a real 3D object similarity task, Journal of vision, Vol. 4(9), pp. 721-734.

Liu, F., Xu, D., Ferguson, M.S., Chu, B., Saam, T., Takaya, N., Hatsukami, T.S., Yuan, C. & Kerwin, W.S. (2006). Automated in vivo segmentation of carotid plaque MRI with Morphology-Enhanced probability maps, Magnetic Resonance in Medicine, Vol. 55(3), pp. 659-668.

Loizou, C. (2014). A review of ultrasound common carotid artery image and video segmentation techniques, Medical & Biological Engineering & Computing, Vol. 52(12), pp. 1073-1093.

Lorenz, M.W., Markus, H.S., Bots, M.L., Rosvall, M. & Sitzer, M. (2007). Prediction of Clinical Cardiovascular Events With Carotid Intima-Media Thickness: A Systematic Review and Meta-Analysis, Circulation, Vol. 115(4), pp. 459-467.

Lusis, A.J. (2000). Atherosclerosis, Nature, Vol. 407 pp. 233–241.

Ma, Z., Tavares, João Manuel R. S, Jorge, R.N. & Mascarenhas, T. (2010). A review of algorithms for medical image segmentation and their applications to the female pelvic cavity, Computer Methods in Biomechanics and Biomedical Engineering, Vol. 13(2), pp. 235-246.

Mannelli, L., MacDonald, L., Mancini, M., Ferguson, M., Shuman, W.P., Ragucci, M., Monti, S., Xu, D., Yuan, C. & Mitsumori, L.M. (2015). Dual energy computed tomography quantification of carotid plaques calcification: comparison between monochromatic and polychromatic energies with pathology correlation, European radiology, Vol. 25(5), pp. 1238-1246.

Manniesing, R. & Niessen, W. (2005). Multiscale vessel enhancing diffusion in CT angiography noise filtering, Information processing in medical imaging, Vol. 19 pp. 138-149.

Markiewicz, T., Dziekiewicz, M., Maruszyński, M., Bogusławska-Walecka, R. & Kozłowski, W. (2014). Recognition of atherosclerotic plaques and their extended dimensioning with computerized tomography angiography imaging, International Journal of Applied Mathematics and Computer Science, Vol. 24(1), pp. 33-47.

Marquering, H.A., Nederkoorn, P.J., Smagge, L., Gratama Van Andel, H. A., Van Den Berg, R. & Majoie, C.B. (2012). Performance of semiautomatic assessment of carotid artery stenosis on CT angiography: Clarification of differences with manual assessment, American Journal of Neuroradiology, Vol. 33(4), pp. 747-754.

Mathiesen, E.B., Johnsen, S.H., Wilsgaard, T., Bonaa, K.H., Lochen, M.-. & Njolstad, I. (2011). Carotid Plaque Area and Intima-Media Thickness in Prediction of First-Ever Ischemic Stroke: A 10-Year Follow-Up of 6584 Men and Women: The Tromso Study, Stroke, Vol. 42(4), pp. 972-978.

Medbury, H.J., James, V., Ngo, J., Hitos, K., Wang, Y., Harris, D.C. & Fletcher, J.P. (2013). Differing association of macrophage subsets with atherosclerotic plaque stability, International angiology, Vol. 32(1), pp. 74-84.

Medis Suite CT, Medis, web page. Available (accessed 09.05.2018): https://www.medis.nl/Products/MedisSuiteCT.

Meiburger, K.M., Molinari, F., Wong, J., Aguilar, L., Gallo, D., Steinman, D.A. & Morbiducci, U. (2016). Validation of the carotid intima-media thickness variability: Can manual segmentations be trusted as ground truth? Ultrasound in Medicine and Biology, Vol. 42(7), pp. 1598-1611.

Meier, P., Knapp, G., Tamhane, U., Chaturvedi, S. & Gurm, H.S. (2010). Short term and intermediate term comparison of endarterectomy versus stenting for carotid artery stenosis: systematic review and meta-analysis of randomised controlled clinical trials, BMJ, Vol. 340(12), pp. 467-476.

Menchón-Lara, R., Bastida-Jumilla, M., Morales-Sánchez, J. & Sancho-Gómez, J. (2014). Automatic detection of the intima-media thickness in ultrasound images of the common carotid artery using neural networks, Medical & Biological Engineering & Computing, Vol. 52(2), pp. 169-181.

Menchón-Lara, R. & Sancho-Gómez, J. (2015). Fully automatic segmentation of ultrasound common carotid artery images based on machine learning, Neurocomputing, Vol. 151 pp. 161-167.

Menchón-Lara, R., Sancho-Gómez, J. & Bueno-Crespo, A. (2016). Early-stage atherosclerosis detection using deep learning over carotid ultrasound images, Applied Soft Computing, Vol. 49 pp. 616-628.

Michalinos, A., Chatzimarkos, M., Arkadopoulos, N., Safioleas, M. & Troupis, T. (2016). Anatomical Considerations on Surgical Anatomy of the Carotid Bifurcation, Anatomy Research International, Vol. 2016 pp. 1-8.

Mitra, S., Goyal, T. & Mehta, J.L. (2011). Oxidized LDL, LOX-1 and atherosclerosis, Cardiovascular Drugs and Therapy, Vol. 25(5), pp. 419-429.

Molinari, F., Pattichis, C.S., Zeng, G., Saba, L., Acharya, U.R., Sanfilippo, R., Nicolaides, A. & Suri, J.S. (2012). Completely automated multiresolution edge snapper-A new technique for an accurate carotid ultrasound IMT measurement: Clinical validation and benchmarking on a multiinstitutional database, IEEE Transactions on Image Processing, Vol. 21(3), pp. 1211-1222.

Mora, S., Szklo, M., Otvos, J.D., Greenland, P., Psaty, B.M., Goff, D.C., O'Leary, D.H., Saad, M.F., Tsai, M.Y. & Sharrett, A.R. (2007). LDL particle subclasses, LDL particle size, and carotid atherosclerosis in the Multi-Ethnic Study of Atherosclerosis (MESA), Atherosclerosis, Vol. 192(1), pp. 211-217.

Naim, C., Douziech, M., Therasse, E., Robillard, P., Giroux, M.F., Arsenault, F., Cloutier, G. & Soulez, G. (2014). Vulnerable atherosclerotic carotid plaque evaluation by ultrasound, computed tomography angiography, and magnetic resonance imaging: an overview, Journal of the Canadian Association of Radiologists, Vol. 65(3), pp. 275-286.

Nandalur, K.R., Hardie, A.D., Raghavan, P., Schipper, M.J., Baskurt, E. & Kramer, C.M. (2007). Composition of the Stable Carotid Plaque: Insights From a Multidetector Computed Tomography Study of Plaque Volume, Stroke, Vol. 38(3), pp. 935-940.

Naz, S., Majeed, H. & Irshad, H. (2010). Image segmentation using fuzzy clustering: A survey, 6th International Conference on Emerging Technologies, IEEE, pp. 181-186.

Nejati, A., Kabaliuk, N., Jermy, M.C. & Cater, J.E. (2016). A deformable template method for describing and averaging the anatomical variation of the human nasal cavity, BMC medical imaging, Vol. 16(1), pp. 55-67.

Pal, N.R. & Pal, S.K. (1993). A review on image segmentation techniques, Pattern Recognition, Vol. 26(9), pp. 1277-1294.

Patel, K.M., Strong, A., Tohyama, J., Jin, X., Morales, C.R., Billheimer, J., Millar, J., Kruth, H. & Rader, D.J. (2015). Macrophage sortilin promotes LDL uptake, foam cell formation, and atherosclerosis, Circulation Research, Vol. 116(5), pp. 789-796.

Pham, D.L., Xu, C. & Prince, J.L. (2000). Current methods in medical image segmentation, Annual review of biomedical engineering, Vol. 2(1), pp. 315-337.

Phan, T.G., Beare, R.J., Jolley, D., Das, G., Ren, M., Wong, K., Chong, W., Sinnott, M.D., Hilton, J.E. & Srikanth, V. (2012). Carotid artery anatomy and geometry as risk factors for carotid atherosclerotic disease, Stroke, Vol. 43(6), pp. 1596-1601.

Prasad, M., Lerman, L.O. & Lerman, A. (2015). Carotid Stiffness and Cerebrovascular Disease: The Physiology Beyond the Anatomy, Journal of the American College of Cardiology, Vol. 66(19), pp. 2126-2128.

Price, A., Wright, F., Green, J., Balkwill, A., Kan, S., Yang, T., Floud, S., Kroll, M., Simpson, R., Sudlow, C., Beral, V. & Reeves, G. (2018). Differences in risk factors for 3 types of stroke: UK prospective study and meta-analyses, Neurology, Vol. 90(4), pp. 298-306.

Rajiah, P., Hojjati, M., Lu, Z., Kosaraju, V., Partovi, S., O'Donnell, J.K., Longenecker, C., McComsey, G.A., Golden, J.B., Muakkassa, F., Santilli, S., McCormick, T.S., Cooper, K.D. & Korman, N.J. (2016). Feasibility of carotid artery PET/MRI in psoriasis patients, American journal of nuclear medicine and molecular imaging, Vol. 6(4), pp. 223-233.

Ridker, P.M., Danielson, E., Fonseca, F.A., Genest, J., Gotto, A.M., Kastelein, J.J., Koenig, W., Libby, P., Lorenzatti, A.J., MacFadyen, J.G., Nordestgaard, B.G., Shepherd, J., Willerson, J.T. & Glynn, R.J. (2009). Reduction in C-reactive protein and LDL cholesterol and cardiovascular event rates after initiation of rosuvastatin: a prospective study of the JUPITER trial, The Lancet, Vol. 373(9670), pp. 1175-1182.

Rohani, M., Jogestrand, T., Ekberg, M., van der Linden, J., Källner, G., Jussila, R. & Agewall, S. (2005). Interrelation between the extent of atherosclerosis in the thoracic aorta, carotid intima-media thickness and the extent of coronary artery disease, Atherosclerosis, Vol. 179(2), pp. 311-316.

Ronneberger, O., Fischer, P. & Brox, T. (2015). U-Net: Convolutional Networks for Biomedical Image Segmentation, Medical Image Computing and Computer-Assisted Intervention – MICCAI 2015, Vol. 9351(1), pp. 234-241.

Ross, R. & Agius, L. (1992). The process of atherogenesis — cellular and molecular interaction: from experimental animal models to humans, Diabetologia, Vol. 35(2), pp. 34-40.

Rozie, S., Monyé, C., Homburg, P., Tanghe, H., Dippel, D., Lugt, A. & Weert, T. (2009). Atherosclerotic plaque volume and composition in symptomatic carotid arteries assessed with multidetector CT angiography; relationship with severity of stenosis and cardiovascular risk factors, European Radiology, Vol. 19(9), pp. 2294-2301.

Saba, L., Gao, H., Acharya, U.R., Sannia, S., Ledda, G. & Suri, J.S. (2012). Analysis of carotid artery plaque and wall boundaries on CT images by using a semi-automatic method based on level set model, Neuroradiology, Vol. 54(11), pp. 1207-1214.

Sanderse, M., Marquering, H.A., Heniks, E.A., van der Lugt, A. & Reiber, J.H.C. (2005). Automatic initialization algorithm for carotid artery segmentation in CTA images, Medical image computing and computer-assisted intervention, Vol. 8(2), pp. 846-853.

Santos, A.M.F., Dos Santos, R.M., Castro, P.M.A.C., Azevedo, E., Sousa, L. & Tavares, J.M.R.S. (2013). A novel automatic algorithm for the segmentation of the lumen of the carotid artery in ultrasound B-mode images, Expert Systems with Applications, Vol. 40(16), pp. 6570-6579.

Santos, F.L.C., Joutsen, A., Paci, M., Salenius, J. & Eskola, H. (2016). Automatic detection of carotid arteries in computed tomography angiography: a proof of concept protocol, The International Journal of Cardiovascular Imaging, Vol. 32(8), pp. 1299-1310.

Santos, F., Joutsen, A., Salenius, J. & Eskola, H. (2011). Carotid Artery Atherosclerosis Plaque Analysis Using CT and Histology, Computational Vision on Medical Image Processing - VIPImage 2011, pp. 82-86.

Schulz, U.G.R. & Rothwell, P.M. (2001). Sex differences in carotid bifurcation anatomy and the distribution of atherosclerotic plaque, Stroke, Vol. 32(7), pp. 1525-1531.

Seevinck, P.R., Deddens, L.H. & Dijkhuizen, R.M. (2010). Magnetic resonance imaging of brain angiogenesis after stroke, Angiogenesis, Vol. 13(2), pp. 101-111.

Sethian, J.A. (2006). Level set methods and fast marching methods, 2nd ed. Cambridge Univ. Press, 239-248 p.

Sezgin, M. & Sankur, B. (2004). Survey over image thresholding techniques and quantitative performance evaluation, Journal of Electronic Imaging, Vol. 13(1), pp. 146-168.

Shaalan, W.E., Cheng, H., Gewertz, B., McKinsey, J.F., Schwartz, L.B., Katz, D., Cao, D., Desai, T., Glagov, S. & Bassiouny, H.S. (2004). Degree of carotid plaque calcification in relation to symptomatic outcome and plaque inflammation, Journal of Vascular Surgery, Vol. 40(2), pp. 262-269.

Shinohara, Y., Sakamoto, M., Kuya, K., Kishimoto, J., Iwata, N., Ohta, Y., Fujii, S., Watanabe, T. & Ogawa, T. (2015). Assessment of carotid plaque composition using fast-kV switching dual-energy CT with gemstone detector: comparison with extracorporeal and virtual histology-intravascular ultrasound, Neuroradiology, Vol. 57(9), pp. 889-895.

Shuaib, A., Saqqur, M., Liebeskind, D.S., Butcher, K. & Mohammad, A.A. (2011). Collateral blood vessels in acute ischaemic stroke: a potential therapeutic target, Lancet Neurology, Vol. 10(10), pp. 909-921.

Silvennoinen, H.M., Ikonen, S., Soinne, L., Railo, M. & Valanne, L. (2007). CT Angiographic Analysis of Carotid Artery Stenosis: Comparison of Manual Assessment, Semiautomatic Vessel Analysis, and Digital Subtraction Angiography, American Journal of Neuroradiology, Vol. 28(1), pp. 97-103.

Simons, P., Algra, A., Bots, M.L., Grobbee, D.E. & van der Graaf, Y. (1999). Common carotid intima-media thickness and arterial stiffness - Indicators of cardiovascular risk in high-risk patients - The SMART study (Second Manifestations of ARTerial disease), Circulation, Vol. 100(9), pp. 951-957.

Simonyan, K. & Zisserman, A. (2015). Very Deep Convolutional Networks for Large-Scale Image Recognition, International Conference on Learning Representations, pp. 24-28.

Smits, L.P., van Wijk, D.F., Duivenvoorden, R., Xu, D., Yuan, C., Stroes, E.S. & Nederveen, A.J. (2016). Manual versus Automated Carotid Artery Plaque Component Segmentation in High and Lower Quality 3.0 Tesla MRI Scans, PLoS ONE, Vol. 11(12), pp. 1-12.

Sonka, M., Hlavac, V. & Boyle, R. (2015). Image processing, analysis, and machine vision, 4th International Edition ed. Cengage Learning, Australia, 255-315 p.

Sotiras, A., Davatzikos, C. & Paragios, N. (2013). Deformable medical image registration: A survey, IEEE Transactions on Medical Imaging, Vol. 32(7), pp. 1153-1190.

Stary, H.C., Chandler, A.B., Glagov, S., Guyton, J.R., Insull, W., Jr, Rosenfeld, M.E., Schaffer, S.A., Schwartz, C.J., Wagner, W.D. & Wissler, R.W. (1994). A definition of initial, fatty streak, and

intermediate lesions of atherosclerosis. A report from the Committee on Vascular Lesions of the Council on Arteriosclerosis, American Heart Association, Circulation, Vol. 89(5), pp. 2462-2478.

Stoitsis, J., Golemati, S., Kendros, S. & Nikita, K.S. (2008). Automated detection of the carotid artery wall in B-mode ultrasound images using active contours initialized by the Hough Transform. Conference proceedings IEEE Engineering in Medicine and Biology Society, Vol. 2008 pp. 3146-3149.

Strong, K., Mathers, C. & Bonita, R. (2007). Preventing stroke: saving lives around the world, The Lancet Neurology, Vol. 6(2), pp. 182-187.

suiteHEART, NeoSoft, web page. Available (accessed 09.05.2018): http://neosoftllc.com/neosoft/186/.

Tamakawa, N., Sakai, H. & Nishimura, Y. (2007). Evaluation of carotid artery plaque using IVUS virtual histology, Interventional Neuroradiology, Vol. 13(S1), pp. 100-105.

Tang, H., van Walsum, T., Hameeteman, R., Shahzad, R., van Vliet, L.J. & Niessen, W.J. (2013). Lumen segmentation and stenosis quantification of atherosclerotic carotid arteries in CTA utilizing a centerline intensity prior, Medical Physics, Vol. 40(5), pp. 1-13.

Tang, H. & Walsum, T.V. (2012). Lumen segmentation of atherosclerotic carotid arteries in CTA, Biomedical Imaging (ISBI), pp. 274-277.

Teramoto, T., Sasaki, J., Ishibashi, S., Birou, S., Daida, H., Dohi, S., Egusa, G., Hiro, T., Hirobe, K., Iida, M., Kihara, S., Kinoshita, M., Maruyama, C., Ohta, T., Okamura, T., Yamashita, S., Yokode, M. & Yokote, K. (2014). Diagnosis of Atherosclerosis, Journal of Atherosclerosis and Thrombosis, Vol. 21(4), pp. 296-298.

Thoeny, H.C., De Keyzer, F. & King, A.D. (2012). Diffusion-weighted MR Imaging in the Head and Neck, Radiology, Vol. 263(1), pp. 19-32.

Thomas, C., Korn, A., Ketelsen, D., Danz, S., Tsifikas, I., Claussen, C.D., Ernemann, U. & Heuschmid, M. (2010). Automatic lumen segmentation in calcified plaques: dual-energy CT versus standard reconstructions in comparison with digital subtraction angiography, American journal of roentgenology, Vol. 194(6), pp. 1590-1595.

Trelles, M., Eberhardt, K.M., Buchholz, M., Schindler, A., Bayer-Karpinska, A., Dichgans, M., Reiser, M.F., Nikolaou, K. & Saam, T. (2013). CTA for screening of complicated atherosclerotic carotid plaque--American Heart Association type VI lesions as defined by MRI, American journal of neuroradiology, Vol. 34(12), pp. 2331-2337.

Uijlings, J.R., van de Sande, K. E. A, Gevers, T. & Smeulders, A.W.M. (2013). Selective Search for Object Recognition, International Journal of Computer Vision, Vol. 104(2), pp. 154-171.

Vaishali Naik, R. S. Gamad & P. P. Bansod (2013). Carotid Artery Segmentation in Ultrasound Images and Measurement of Intima-Media Thickness, BioMed Research International, Vol. 2013 pp. 1-10.

Van Aarle, W., Batenburg, K.J. & Sijbers, J. (2011). Optimal threshold selection for segmentation of dense homogeneous objects in tomographic reconstructions, IEEE Transactions on Medical Imaging, Vol. 30(4), pp. 980-989.

van der Hagen, P B, Folsom, a.R., Jenny, N.S., Heckbert, S.R., O'Meara, E.S., Reich, L.M., Rosendaal, F.R. & Cushman, M. (2006). Subclinical atherosclerosis and the risk of future venous thrombosis in the Cardiovascular Health Study, Journal of thrombosis and haemostasis, Vol. 4(9), pp. 1903-1908.

van Engelen, A., van Dijk, A.C., Truijman, M.T.B., van't Klooster, R., van Opbroek, A., van der Lugt, A., Niessen, W.J., Kooi, M.E. & de Bruijne, M. (2015). Multi-Center MRI Carotid Plaque Component Segmentation Using Feature Normalization and Transfer Learning, IEEE Transactions on Medical Imaging, Vol. 34(6), pp. 1294-1305.

van Hoof, R.H.M., Vöö, S.A., Sluimer, J.C., Wijnen, N.J.A., Hermeling, E., Schreuder, F.H.B.M., Truijman, M.T.B., Cleutjens, J.P.M., Daemen, M.J.A.P., Daemen, J.H., van Oostenbrugge, R.J., Mess, W.H., Wildberger, J.E., Heeneman, S. & Kooi, M.E. (2017). Vessel wall and adventitial DCE-MRI parameters demonstrate similar correlations with carotid plaque microvasculature on histology, Journal of Magnetic Resonance Imaging, Vol. 46(4), pp. 1053-1059.

Vessel, Circle Cardiovascular Imaging, web page. Available (accessed 09.05.2018): https://www.circlecvi.com/features/vessel.php.

Virmani, R., Kolodgie, F.D., Burke, A.P., Finn, A.V., Gold, H.K., Tulenko, T.N., Wrenn, S.P. & Narula, J. (2005). Atherosclerotic Plaque Progression and Vulnerability to Rupture: Angiogenesis as a Source of Intraplaque Hemorrhage, Arteriosclerosis, Thrombosis, and Vascular Biology, Vol. 25(10), pp. 2054-2061.

Vukadinovic, D. (2012). Automated Quantification of Atherosclerosis in CTA of Carotid Arteries, Erasmus University Rotterdam, Available: http://www.narcis.nl/publication/RecordID/oai:repub.eur.nl:32465.

Vukadinovic, D., Rozie, S., van Gils, M., van Walsum, T., Manniesing, R., van der Lugt, A. & Niessen, W.J. (2012). Automated versus manual segmentation of atherosclerotic carotid plaque volume and components in CTA: associations with cardiovascular risk factors, The International Journal of Cardiovascular Imaging, Vol. 28(4), pp. 877-887.

Vukadinovic, D., van Walsum, T., Manniesing, R., Rozie, S., Hameeteman, R., de Weert, T.T., van der Lugt, A. & Niessen, W.J. (2010). Segmentation of the outer vessel wall of the common carotid artery in CTA. IEEE transactions on medical imaging, Vol. 29(1), pp. 65-76.

Wang, J., Wang, R., Li, C., Li, Y., Wei, X., Zhu, Y. & Zhang, S. (2015). Threshold segmentation algorithm for automatic extraction of cerebral vessels from brain magnetic resonance angiography images, Journal of Neuroscience Methods, Vol. 241(1), pp. 30-36.

Wang, S. & Summers, R.M. (2012). Machine learning and radiology, Medical Image Analysis, Vol. 16(5), pp. 933-951.

Wang, X. & Zhang, Y. (2012). Carotid artery segmentation in 3D ultrasound images using a hybrid framework, IEEE International Conference on Information and Automation, IEEE, pp. 698-703.

Wang, Y., Qiu, Y., Thai, T., Moore, K., Liu, H. & Zheng, B. (2017). A two-step convolutional neural network based computer-aided detection scheme for automatically segmenting adipose tissue volume depicting on CT images, Computer Methods and Programs in Biomedicine, Vol. 144 pp. 97-104.

Wang, Z. & Yang, M. (2010). A fast clustering algorithm in image segmentation, 2nd International Conference on Computer Engineering and Technology, IEEE, pp. 592-594.

Weert, T.T., Monyé, C., Meijering, E., Booij, R., Niessen, W.J., Dippel, D.W.J. & Lugt, A. (2008). Assessment of atherosclerotic carotid plaque volume with multidetector computed tomography angiography, International Journal of Cardiovascular Imaging, Vol. 24(7), pp. 751-759.

Wiesmann, M., Schöpf, V., Jansen, O. & Brückmann, H. (2008). Stent-protected angioplasty versus carotid endarterectomy in patients with carotid artery stenosis: Meta-analysis of randomized trial data, European Radiology, Vol. 18(12), pp. 2956-2966.

Winship, I.R., Armitage, G.A., Ramakrishnan, G., Dong, B., Todd, K.G. & Shuaib, A. (2014). Augmenting Collateral Blood Flow during Ischemic Stroke via Transient Aortic Occlusion, Journal of Cerebral Blood Flow & Metabolism, Vol. 34(1), pp. 61-71.

Withey, D.J., Pedrycz, W. & Koles, Z.J. (2009). Dynamic edge tracing: Boundary identification in medical images, Computer Vision and Image Understanding, Vol. 113(10), pp. 1039-1052.

Wong, A.K.C. & Sahoo, P.K. (1989). A gray-level threshold selection method based on maximum entropy principle, IEEE Transactions on Systems, Man, and Cybernetics, Vol. 19(4), pp. 866-871.

World Health Organization (2010). WHO | The Atlas of Heart Disease and Stroke, World Health Organization, Available: http://www.who.int/cardiovascular_diseases/resources/atlas/en/.

Woźniak, T., Strzelecki, M., Majos, A. & Stefańczyk, L. (2017). 3D vascular tree segmentation using a multiscale vesselness function and a level set approach, Biocybernetics and Biomedical Engineering, Vol. 37(1), pp. 66-77.

Xian Fan, Bazin, P.L., Bogovic, J., Ying Bai & Prince, J.L. (Jun 2008). A multiple geometric deformable model framework for homeomorphic 3D medical image segmentation, IEEE Computer Society Conference on Computer Vision and Pattern Recognition Workshops, pp. 1-7.

Yi, J. & Ra, J.B. (2003). A locally adaptive region growing algorithm for vascular segmentation, International Journal of Imaging Systems and Technology, Vol. 13(4), pp. 208-214.

Yogamangalam, R. & Karthikeyan, B. (2013). Segmentation Techniques Comparison in Image Processing, International Journal of Engineering and Technology (IJET), Vol. 5(1), pp. 307-313.

Yu, L., Chen, H., Dou, Q., Qin, J. & Heng, P. (2017). Automated Melanoma Recognition in Dermoscopy Images via Very Deep Residual Networks, IEEE Transactions on Medical Imaging, Vol. 36(4), pp. 994-1004.

Yuan, C., Oikawa, M., Miller, Z. & Hatsukami, T. (2008). MRI of carotid atherosclerosis, Journal of Nuclear Cardiology, Vol. 15(2), pp. 266-275.

Zarins, C.K., Giddens, D.P., Bharadvaj, B.K., Sottiurai, V.S., Mabon, R.F. & Glagov, S. (1983). Carotid bifurcation atherosclerosis. Quantitative correlation of plaque localization with flow velocity profiles and wall shear stress, Circulation Research, Vol. 53(4), pp. 502-514.

Zhu, C., Patterson, A.J., Thomas, O.M., Sadat, U., Graves, M.J. & Gillard, J.H. (2013). Carotid stenosis assessment with multi-detector CT angiography: comparison between manual and automatic segmentation methods, The International Journal of Cardiovascular Imaging, Vol. 29(4), pp. 899-905.

Zimmer, Y., Tepper, R. & Akselrod, S. (1996). A two-dimensional extension of minimum cross entropy thresholding for the segmentation of ultrasound images, Ultrasound in Medicine and Biology, Vol. 22(9), pp. 1183-1190.

Zureik, M., Ducimetiere, P., Touboul, P., Courbon, D., Bonithon-Kopp, C., Berr, C. & Magne, C. (2000). Common Carotid Intima-Media Thickness Predicts Occurrence of Carotid Atherosclerotic Plaques : Longitudinal Results From the Aging Vascular Study (EVA) Study, Arteriosclerosis, Thrombosis, and Vascular Biology, Vol. 20(6), pp. 1622-1629.

ORIGINAL PAPERS

I

A SEMI-AUTOMATIC SEGMENTATION METHOD FOR THE STRUCTURAL ANALYSIS OF CAROTID ATHEROSCLEROTIC PLAQUE BY COMPUTED TOMOGRAPHY ANGIOGRAPHY

by

Santos, F., Joutsen, A., Terada, M., Salenius, J. & Eskola, H., May 2014

Journal of Atherosclerosis and Thrombosis, vol 21, 9

Original Article

A Semi-Automatic Segmentation Method for the Structural Analysis of Carotid Atherosclerotic Plaques by Computed Tomography Angiography

Florentino Santos[1], Atte Joutsen[1], Mitsugu Terada[2], Juha Salenius[3] and Hannu Eskola[1, 4]

[1]Department of Electronics and Communications Engineering, Tampere University of Technology, Tampere, Finland
[2]Department of Applied Physics, Faculty of Science, Fukuoka University, Fukuoka, Japan
[3]Division of Vascular Surgery, Department of Surgery, Tampere University Hospital and Medical School, Tampere, Finland
[4]Department of Radiology, Regional Imaging Centre, Tampere University Hospital

***Background*: Computed tomography angiography (CTA) is currently the most reliable imaging technique for evaluating and planning the treatment of atherosclerosis. The drawbacks of the technique are its low spatial resolution and challenging manual measurements. The purpose of this study was to develop a semi-automatic method to segment vessel walls, surrounding tissue, and the carotid artery lumen to measure the severity of stenosis.**

***Methods*: *In vivo* contrast CTA images from eight patients undergoing endarterectomy were analyzed using a tailored five-step process involving an adaptive segmentation algorithm and region growing to measure the maximum percent stenosis in the cross-sectional area of the carotid artery. The accuracy of this method was compared with that of manual measurements made by physicians.**

***Results*: There were no significant differences between the maximum percent stenosis value obtained using the semi-automatic tool and that obtained using manual measurements (6%; $p=0.31$). The data acquisition and analysis required an average of 145 seconds.**

***Conclusion*: This new semi-automatic segmentation method for CTA provides a fast and reliable tool to quantify the severity of carotid artery stenosis.**

J Atheroscler Thromb, 2014; 21:000-000.

Key words: Atherosclerosis, Computed tomography angiography, Carotid, Stenosis, Segmentation

Introduction

Atherosclerosis is the most common vascular disorder and constitutes the greatest risk of mortality and morbidity. In 2005, strokes were responsible for 35% of all deaths, and 30% were related to extracranial carotid atherosclerosis. The cost of stroke management reached 62.7 billion dollars in 2007 in the USA[1-4]. The first signs of atherosclerosis as a systemic disease appear early in life and develop over time[5]. The risk of stroke is evaluated by the degree of stenosis and plaque composition and the plaque morphology[1, 6, 7]. Surgical extraction of an atherosclerotic plaque (endarterectomy) dramatically decreases the risk of stroke or related death to $<6\%$ within the first 30 days after surgery[8] and 10%-17% in the long-term[2]. Early symptom detection is essential to follow the evolution of atherosclerosis and initiate preemptive measures to prevent stroke onset[2, 4].

The carotid artery atherosclerotic burden, stenosis and plaque components are analyzed by the manual segmentation of diagnostic images acquired by magnetic resonance imaging (MRI), ultrasound (US) or computed tomography angiography (CTA)[9, 10]. For this purpose, CTA is deemed superior to MRI and US, because the vascular components produce different Hounsfield units (HU), making them easier to differentiate by CTA. Previous atherosclerosis imaging studies on symptomatic and asymptomatic atheroscle-

Address for correspondence: Florentino Santos, Department of Electronics and Communications Engineering, Tampere University of Technology, Finn-Medi 1 4-208, Biokatu 6, FI-33520, Tampere, Finland
E-mail: florentino.caetanodossantos@tut.fi
Received: September 3, 2013
Accepted for publication: March 27, 2014

Table 1. The clinical characteristics of the patients

Patient no.	Time interval between CTA and surgery (days)	Age	Sex	Medical history
1	23	56	M	No information available
2	14	84	M	Prostate Cancer, aphasia, atrial fibrillation
3	17	75	M	Hypertension
4	10	70	M	Hypertension, hypercholesterolemia, hypothyreosis, diabetes mellitus type II, amaurosis fugax
5	7	54	M	Hypertension, hypercholesterolemia, cerebral infarction
6	31	72	F	Pulmonary embolism
7	16	79	M	Hypertension, glaucoma
8	7	72	M	Hypertension, hypothyreosis, prostate cancer

rotic patients primarily focused on the wall characteristics (i.e., plaque stability), because this information is critical for the clinical diagnosis[11]. In 1998, Heinonen *et al*. introduced a semi-automatic segmentation system named IARD (image enhancement, amplitude segmentation, region growing, and decision trees)[12]. This protocol showed promising results for the segmentation and classification of different tissues by MRI and CT[13, 14]. The de Weert group recently developed an ImageJ[15] plugin that could semi-automatically analyze atherosclerotic plaques[16] on the basis of the definition of two regions of interest (ROI; the lumen and vessel outline) and the different HU components. However, manual segmentation is time-consuming for the operator and is prone to human errors. Accordingly, the inter-operator and intra-operator coefficients of variation (COV) were 19% and 58%, respectively[16]. On the other hand, automated measurements are objective, more reproducible and faster; however, they are very sensitive to noise.

Image segmentation techniques fall into three categories: thresholding, clustering and deformable models. The choice of an optimal method depends on the specific requirements of the application. The main challenge associated with the segmentation of CTA images of carotid plaques is the limited spatial resolution and the short processing time. Our preliminary studies support a correlation between CTA image segmentation and histological data[17]. The goal of this study was to develop a semi-automatic toolset capable of segmenting the lumen and vessel wall in CTA images to characterize the morphology of atherosclerotic carotid arteries. The results were compared with manual measurements of arterial stenosis obtained on the basis of the North American Symptomatic Carotid Endarterectomy Trial (NASCET) criteria[18]. This new clinical toolset provides an in-depth analysis of the atherosclerotic carotid arteries and considerably decreases the time required for patient evaluation.

Methods

Patients and Clinical Data

Eight elderly patients (mean age, 70 years; one woman and seven men) undergoing carotid artery endarterectomy were recruited at Tampere University Hospital (Tampere, Finland). Preoperative CTA examinations were performed for the region between the aortic arch and the vertex of the skull. Endarterectomy of the internal carotid artery was performed for eight carotid arteries to extract plaque. More specific clinical data and the patient background are referred to in **Table 1**, with the time lapse between CTA and endarterectomy presented in days. This study was approved by the ethics committee of the Pirkanmaa hospital district (decision number R07210).

Imaging Conditions

Because this study aimed to validate a new clinical toolset that could completely analyze carotid atherosclerotic plaques, we tested the applicability using two imaging systems from different manufacturers. The CTA examinations were conducted with two helical, 64-slice, multidetector computed tomography (MDCT) scanners: the General Electric (GE) LightSpeed (slice thickness, 1.25 mm; increment, 0.5-0.7 mm; pixel size, 0.6-0.7 mm; 120 kVp; 5-10 mAs) and the Philips Brilliance (slice thickness, 1 mm; increment, 0.5 mm; pixel size, 0.42-0.49 pixels; 120 kVp; 193-287 mAs). The average scanning time was 40 s, and each image was generated as a 512×512 matrix.

The contrast media, Omnipaque® (350 mg/mL) and Xenetic® (350 mg/mL), were used to perform CTA examinations. The injection dose, speed and

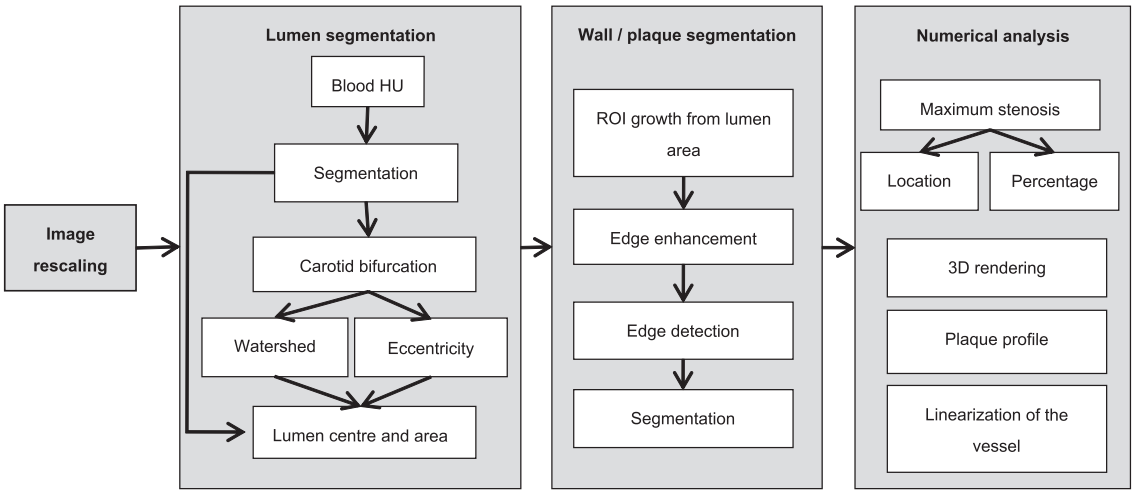

Fig. 1. The segmentation protocol.

time were patient-dependent and were selected according to the recommendations of the manufacturers of the contrast media. The contrast agent was injected into the antecubital fossa or in a vein of the hand if venous access could not be established.

Image Analysis

The IARD protocol[12] was modified to optimize the image segmentation of the lumen, vessel wall and surrounding tissues. The clustering and deformable models were not used because they require reference images for their implementation. The clinical data were used to validate the algorithm under different conditions (scanner type, attenuation, morphology, atherosclerosis stage, component distribution and image quality). Because the human anatomy (i.e., vessel position and path) varies among patients, it was not possible to develop a general reference image. In addition, the analysis was not conducted for the full length of the carotid arteries, but only from the aortic branch to the circle of Willis. Images were obtained in the plaque vicinity, with the slice interval defined by the operator. Therefore, the first slice did not correspond to a common anatomical position. Therefore, we used a thresholding model.

The CTA images were analyzed with a personal computer (HP dv3560ep, Windows 7 Ultimate, 32 bits, 2.40GHz, 4.0 GB RAM, with an NVIDIA GeForce 9300M GS graphics card) equipped with the Matlab version R2010a, Image Processing Toolbox version 7.0, Signal Processing Toolbox version 6.13, Curve Fitting Toolset version 2.2 and Statistical Toolbox version 7.3 software programs. Various stages of the sclerosis were chosen to test the efficiency of the segmentation algorithm in geometrically different cases. The algorithm comprised the five stages described below (**Fig. 1**). Because the two MDCT scanners had different rescale intersects and representation intervals, the data were rescaled and shifted to comply with the standard scale[19].

The Five-Step Process

The CTA images were analyzed to measure the maximum percent stenosis using a tailored five-step process involving an adaptive segmentation algorithm and region growing. First, the initial segmentation interval (first slice of the image stack) for the lumen was selected using the first three steps:

1) The slice interval is determined for the segmentation and analysis process.

2) The initial seed point in the lumen is set manually in the first slice to specify the artery side to be segmented and the exact position of the vessel.

3) A typical diameter of 6 mm is used to create a region of interest (ROI) around the lumen and to generate a histogram. Gaussian fitting is executed, and 90% of the area under the curve is chosen as the initial blood attenuation HU interval (**Fig. 2A**).

4) The next step is the segmentation of the lumen using the initial seed and the attenuation interval, with a region-growing algorithm[20]. The use of an adaptive attenuation interval in each slice prevents the

common problem of dilution during region growing. By fitting the attenuation value histogram onto a Gaussian curve, it is possible to decrease the influence of the less frequent attenuation values representing surrounding tissues.

5) After the initial slice is obtained, segmentation proceeds automatically along the vessel and throughout the entire CT image stack. If the stenosis is so severe that no pixel identifies the lumen, the same initial seed position is used for the next slice. If successful, the lumen area is used to calculate the diameter for ROI extraction in the following slice. If the algorithm is not able to detect the lumen in an interval of fives slices, it stops the segmentation to calculate and present the final results.

Gaussian fitting is conducted to determine the luminal attenuation interval and to determine whether tissue is present in the normal lumen area. The presence of tissue surrounding the lumen affects the Gaussian fitting. For example, **Fig. 2A** and **2B** show HU histograms of the lumen, with less or more tissue adhering to the artery wall, respectively. The HU interval that corresponds to the lumen was found at the edges of the curve fitting 90% of the area (**Fig. 2A**). In contrast, excess tissue generates two peaks in the histogram (**Fig. 2B**), and the correct peak was identified by comparison with the histogram of the previous slice. The different layers of the artery wall were detected in both cases (intima, media, and adventitia). The HU scale was adapted to fit between the minimum and maximum nonzero values present in the image.

Identification of the Carotid Bifurcation

To evaluate the atherosclerotic plaque burden in the common carotid artery (CCA) and the internal carotid artery (ICA), it is necessary to identify the slice separating the ICA from the external carotid artery (ECA), which is the carotid bifurcation (CB). This is accomplished using a region property called eccentricity, which corresponds to the ratio of the maximal to minimal artery wall diameter. If the image has an eccentricity higher than 0.85 (0 for a circular shape and 1 for a line segment), it is necessary to divide the image into the ICA and ECA. For this purpose, we used a watershed algorithm with 4-pixel neighborhood connectivity. The criteria used to identify the ICA level was the position of the two structures obtained in the watershed: the lowest anatomical image and the one nearer to the trachea easily identified by the air attenuation. After correct lumen segmentation, the center of the lumen was identified for use as the next slice seed point for the region growth algorithm and for tracking the vessel path.

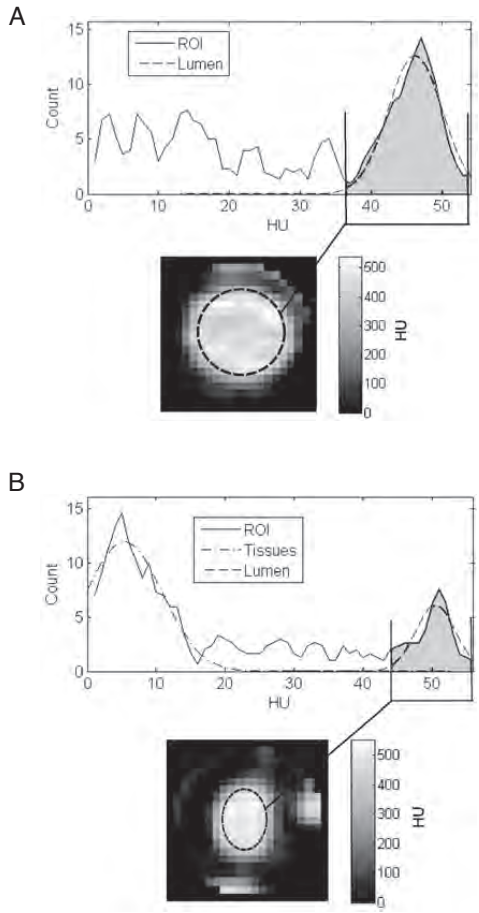

Fig. 2. Region of interest (ROI) histograms (60 bins) and segmentation intervals for Patient 5.

A. The lack of tissue inside the carotid artery (Slice 1, radius: 10 pixels)

B. The presence of tissue inside the carotid artery (atherosclerotic plaque; Slice 30, radius: 10 pixels)

Vessel Wall and Plaque Determination

The tissues around the lumen were classified as a single entity representing both the artery wall and the atherosclerotic plaque (lipidic, fibrotic and calcified tissue). Thereafter, two circular ROIs were automatically created, one from the original CTA image using a radius of 20 pixels around the lumen, and the other from the results of the lumen segmentation. Using this radius, all the surrounding tissue and plaque com-

$$S = \left(1 - \frac{A_{min}}{A_{ave}}\right) \times 100$$

Equation 1. The modified NASCET criteria (area).

$$D\,(\%) = \frac{E_{alg} - E_{phys}}{E_{phys}} \times 100$$

Equation 2. The relative difference.

ponents were included.

A Laplacian of the Gaussian filter (size: 5×5 pixels; standard deviation: 0.5) was used to enhance the contrast between the surrounding tissue and the outer and inner borders of the vessel wall. The minor structures (with areas smaller than twice the lumen area) in the artery wall vicinity were ignored. In the next step, the resulting image was merged with the lumen ROI to restore the lumen segmentation area. Finally, the area eccentricity was measured again. If the eccentricity was >0.30, a watershed algorithm was applied using an 8-pixel neighborhood connectivity. A circular ROI was defined using the prewatershed ROI area to calculate the radius.

Modifications to the NASCET Criteria

The unmodified NASCET criteria are based on the diameter of the carotid artery, with and without the atherosclerotic plaque[18]. However, the use of an area generates more precise data than the use of a diameter[21]. Most importantly, an area is not sensitive to the positioning of the measuring vector, which is the diameter of the lumen defined by the user applying the NASCET criteria. Therefore, we developed a modified NASCET criterion to determine the maximum percent stenosis (S; **Equation 1**), where A_{min} is the minimum area occupied by the lumen and A_{ave} is the average area occupied by the lumen (calculated at the CB site with maximum stenosis; pre-CB or post-CB).

Because the area of the lumen decreases drastically in the ICA after the CB (natural narrowing of the vessel), it is necessary to divide the pre-plaque and post-plaque data and compare them to determine the maximum percent stenosis and the position in the vessel. Another criterion used for the detection of the CB was the sudden shift in the center of the segmented lumen at the CB. The relative difference (*D*) between the evaluation by a physician (E_{phys}) and that by the algorithm (E_{alg}) was calculated as shown in **Equation 2**.

Vessel Visualization

The outputs of the algorithm are not only presented in numerical form, but also in two- (2D) and three-dimensional (3D) image format. The outputted images show the profile of each component (lumen and wall/plaque) throughout the slices, and the vessel linearity (sagittal and coronal planes). This longitudinal segmentation allows for a visual inspection of the lumen path, vessel wall, the presence of plaque and the plaque components (lipidic, fibrotic and calcified tissues). These images allow a visual analysis of the plaque status with regard to positive remodeling, vessel occlusion and the recurrence of downstream plaque lesions.

Manual Segmentation and Evaluation

The manual segmentation was derived from the clinical data, manual measurement of the stenosis, plaque profile and the analysis found in the medical transcript made by the radiologist. The data consisted of manual measurements of the lumen diameter in two distinct locations: below the plaque (native lumen diameter) and in the maximum occlusion site (minimum diameter). Both values were inserted in the NASCET stenosis calculation formula (Eq. 1) to obtain the final percent stenosis. If the maximum percent stenosis was located on the ICA, instead of the CCA or CB, the native measurement was made in the ICA.

Statistical Analysis

The parameters derived from the manual and algorithm-based disease evaluations were compared using the two-sided Wilcoxon rank sum test. The *p*-values were calculated using the Matlab® Statistics Toolbox function "ranksum" (MathWorks, USA). Because the function needs two linear datasets, we transformed the manual and algorithm stenosis values into single row arrays, disregarding the carotid side and maintaining the side correspondence in the arrays. All p values <0.05 were considered to be statistically significant.

Results

The patients' clinical data and medical background are presented in **Table 1**. Of the 16 carotid arteries examined, eight were atherosclerotic (>70% stenosis), four had mild stenosis (<70%) and four were open carotids.

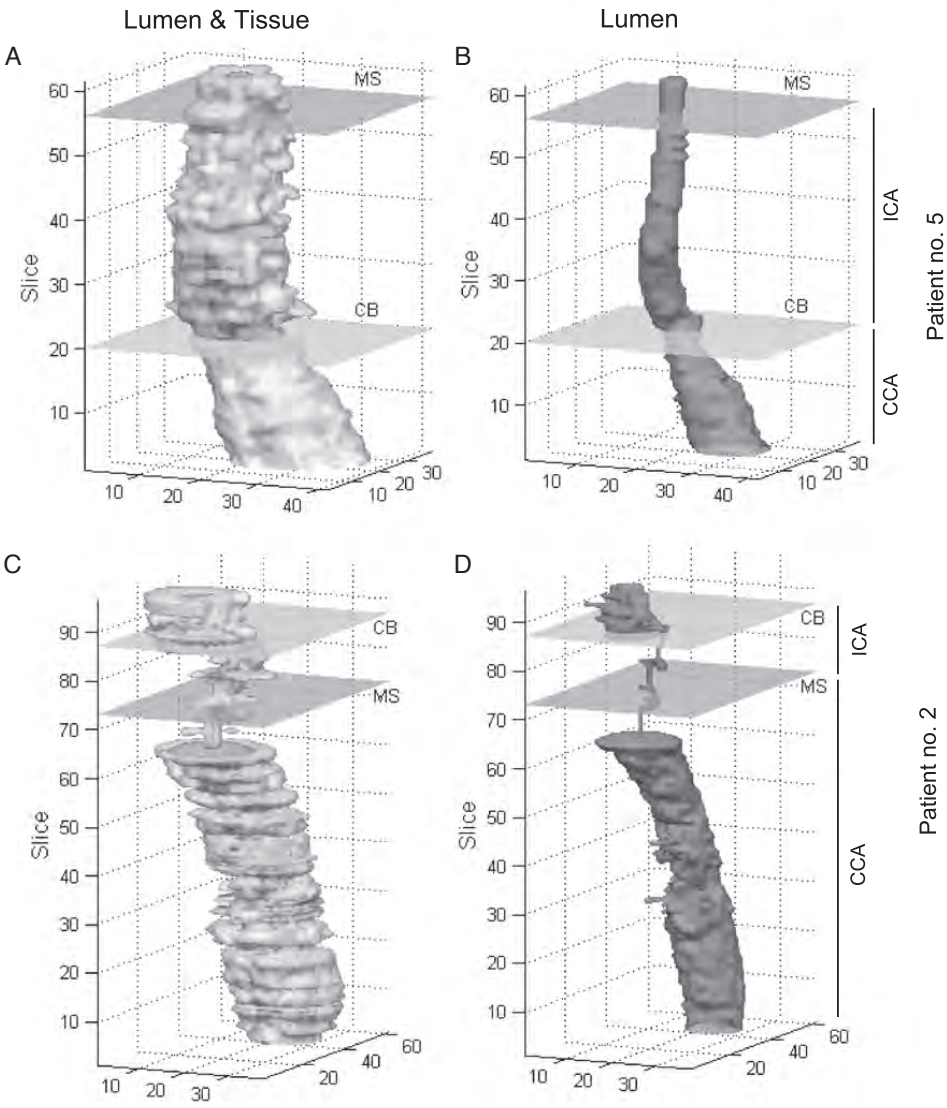

Fig. 3. An example of successful (Patient 5) and unsuccessful (Patient 2) 3D imaging results.

A and C: Vessel tissue, plaque components and lumen
B and D: Lumen
The position of the structures is indicated.
CB, carotid bifurcation; CCA, common carotid artery; ECA, external carotid artery; ICA, internal carotid artery

The carotid arteries were characterized in terms of the maximum percent stenosis and the location in the vessel, path of the vessel and linearity of the vessel with the area (mm^2) occupied by each vessel component (lumen and wall/plaque area). Also, a 3D image of the segmented vessel was generated. In five of the eight patients, the CCA and ICA were correctly segmented with the selected slice interval. The average

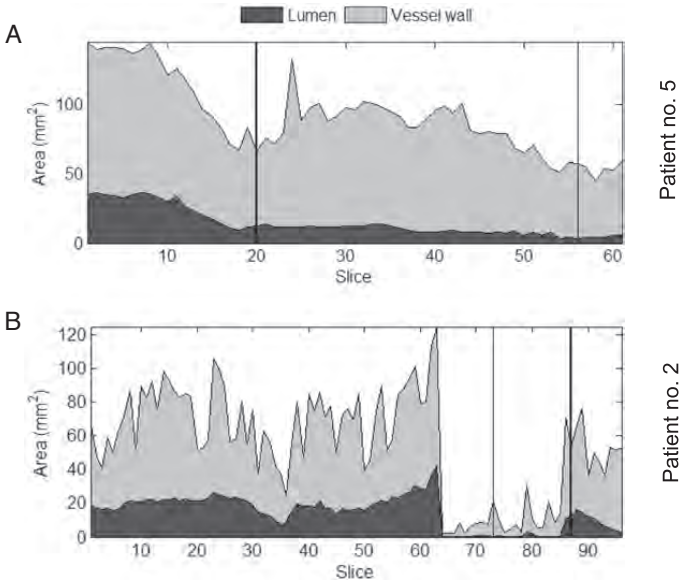

Fig. 4. The carotid lumen area and vessel wall for Patient 5 (A) and Patient 2 (B).

The sites of carotid bifurcation (thick line) and maximum stenosis (thin line) are indicated.

number of segmented slices was 76, which corresponded to a total length of 9.5 cm with the GE LightSpeed scan and 7.6 cm with the Philips CT scan.

Most patients exhibited positive remodeling of the vessel wall due to severe stenosis, detected by outward bulging of the artery wall in the linearization of the vessels. Two patients exhibited severe unilateral stenosis in the CB. In those cases, the algorithm could not find the path of the ICA because of the lack of lumen pixels. The algorithm was programmed to stop if the lumen was not found after 20 slices. We have described the carotid analysis of these two patients in detail below to provide examples of favorable (Patient 5) and challenging (Patient 2) cases.

Impact of the Severity of Stenosis on the Image Analysis

The two patients were first compared by examining the 3D images for the vessel shape, including the structures of the CCA, CB and ICA (**Fig. 3**). For Patient 5, the point of maximum stenosis was not easy to detect by visual inspection. **Fig. 3A** shows the lumen and vessel wall (fibrotic, lipidic, and calcified tissue), whereas **Fig. 3B** shows only the lumen. In contrast, the carotid of Patient 2 exhibited highly calcified stenosis that nearly occluded the lumen, causing the algorithm to lose the segmentation path (**Fig. 3C** and **D**). When the algorithm cannot determine the maximum stenosis, it miscalculates the position of the bifurcation and stenosis.

The Percent Stenosis and Location

For Patient 5, the area of the maximum percent stenosis was located at slice 56 (**Fig. 4A**), while the carotid bifurcation was located at slice 21 (**Fig. 4A**). The maximum percent stenosis defined by our algorithm (74%) was 18% lower than that defined by manual measurement (90%). The maximum percent stenosis values for all 16 carotids are presented in **Table 2**. In Patient 5, the lumen occupied a maximum of approximately 40% of the total segmented area (**Fig. 4A**). For Patient 2, who had severe stenosis, the vessel tracking was lost, and the position of components was not established because the analysis was not successful (**Fig. 4B**). The average and median differences between the manual measurements and algorithmic data were only 6% (Wilcoxon rank sum test; $p=0.31$), suggesting that our new semi-automatic toolset is as reliable as the physicians' manual measurements.

Table 2. The parameters of carotid stenosis for each patient

Patient no.	Affected artery	Manual evaluation		Algorithm evaluation		Relative difference (Eq. 2)	
		Left	Right	Left	Right	Left	Right
1	ICA	95%		73%		−23%	
2	ICA	70%	70%	80%	83%	14%	19%
3	ICA		75%		90%		20%
4	ICA	70%	80%	96%	74%	37%	−8%
5	ICA	90%	60%	74%	63%	−18%	5%
6	ICA		70%		75%		7%
7	ICA	85%	73%	89%	79%	5%	8%
8	CCA		60%		63%		5%

Evaluation of the Atherosclerotic Burden by Vessel Linearization

To obtain a better understanding of the plaque burden, we linearized the segmented vessels. **Fig. 5** shows where the CCA divides into the ICA and ECA, as well as the site of maximum stenosis for Patient 5 with mild disease. In **Fig. 5A**, the atherosclerotic burden could not be estimated because of the smoothness of the carotid walls and the nonexistent narrowing of the lumen. Wall calcification was only detected in a small patch at the CB, which was evidence of the initial stage of the disease. In **Fig. 5B**, calcifications are visible as white structures surrounding the lumen. Patient 2 had severe calcified stenosis that nearly occluded the lumen, which caused the algorithm to lose the segmentation path and miscalculate the position of the CB, thus invalidating the stenosis calculation. When the algorithm cannot determine the path of the vessel, it cannot calculate the maximum percent stenosis and the location of the CB accurately, which are critical steps in the analysis.

The Shorter Analysis Time of the Semi-Automatic Process

We generated a dataset of 62 slices for Patient 5, with a total analysis time of 95 s. The average processing speed was 1.2 s per slice, which was limited by the processing power of the personal computer. For the 16 carotid arteries, the average total time for booting, acquiring, analyzing and displaying the data was 145 s.

Discussion

The recent development of CTA imaging was a major technical breakthrough for the analysis of carotid artery stenosis, because it provides tissue attenuation data that allows efficient classification of the vessel wall and plaque components[9, 10]. While MRI was initially adopted as the gold standard because of its higher resolution and the availability of reference data, this imaging technique does not provide tissue attenuation data. Therefore, an MRI analysis requires models and training sets developed by the operator to classify the vascular tissue types[7, 22, 16]. Furthermore, CTA is currently available in most hospitals and constitutes the main imaging diagnostic method after US. Therefore, it is understandable that CTA should be selected to build the next generation of image segmentation toolsets for the characterization of the severity of atherosclerosis.

Our goal was to decrease the operator intervention in the CTA image analysis to improve the data accuracy and accelerate patient evaluation. This semi-automatic method is a considerable improvement over the current manual methods. Once the operator enters the initial seed into the algorithm, all other operations are automated. From a single seed in the initial slide, it can follow the vessel path, segment the lumen from the surrounding tissues and separate the outer vessel wall from the neighboring tissues. A segmentation protocol in which an operator does not manually predefine the areas containing the vessel for each image of the stack is considered automatic[16, 21]. Da-Chuan Cheng presented a fully automated process in which it was possible to segment the carotid arteries by MRI using image characteristics (intensity, area size and shape), and the data only differed from the manual measurement data by 2.6%[22]. However, MRI information does not separate the lumen from the vessel wall because it does not provide tissue attenuation data. Therefore, a semi-automatic CTA-based system would be more reliable than an automated MRI-based system for differentiating the vascular structures surrounding the plaque and for monitoring the patients.

The accurate measurement of the maximum percent stenosis is critical for the adequate management

of patients with atherosclerosis. The NASCET criteria are based on the measurement of the vessel diameter[18], which is less accurate than area measurements[21]. Therefore, our algorithm was designed to use carotid artery area measurements. In addition, we measured the lumen eccentricity as an early marker of the morphological changes caused by atherosclerosis. These modifications considerably improved the rendering of the blood vessels, wall and plaque, which is crucial to the correct positioning of the structures according to the anatomy of each patient.

The following considerations were essential to our modifications of the IARD semi-automatic segmentation system protocol:[12]. First, native CTA images were used without any enhancement. Smoothing diminishes the contrast between tissues, thereby interfering with the tissue classification and localization. The main disadvantage is the higher noise level, which implies lower region growth and irregular structure outlines. Second, although amplitude segmentation and region growing can be applied manually, they could be automated using predefined values (HU interval, lumen segmentation center from the previous slice and surrounding tissue determination). Third, the segmentation interval used in the region growth was adapted along the vessel because of the bolus effect of the contrast agent. When we analyzed the contrast of the lumen, the HU value of the lumen increased to a maximum value and then decreased, following a bell- or wave-shaped function. One disadvantage of this approach is that when the stenosis is severe, lumen narrowing makes it impossible to replicate and predict the necessary HU interval for lumen segmentation in this slice. Finally, the decision tree adaptive classifier specifies the classifier criteria (HU interval) not only for each slice, but also for each patient and CT device.

The length of the analysis was relatively long (1.2 s per slice) because we used a personal computer instead of a medical workstation. In a full-slice analysis (approximately 400 to 500 slices), the total time would be over 6 min under our conditions. When applied using a clinical workstation, this time would be drastically decreased. In addition, the virtual memory of the hardware limited the total number of slices to 96 (the maximum number per patient dataset that could be inputted). A workstation with sufficient memory would be able to analyze the entire vessel path, from the branching of the aortic arch to the circle of Willis.

The accuracy of our semi-automatic CTA-based segmentation system was tested against manual measurements of the maximum percent stenosis of the

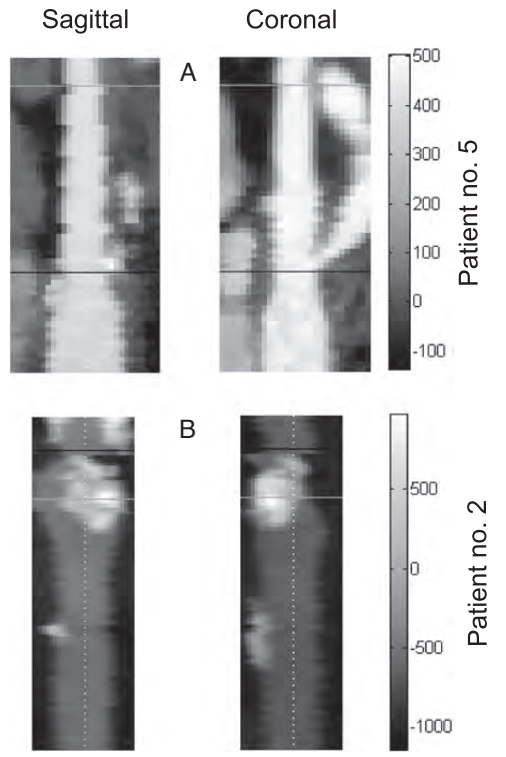

Fig. 5. The 2D linearization of the vessel.

Black line: carotid bifurcation
Gray line: site of maximum stenosis
White dots: lumen path

carotid artery as conducted by a physician. For Patient 5, the physician calculated a maximum percent stenosis of 90%, which was 18% higher than that determined by our algorithm. As de Weert reported an interoperator COV of 19%[16], this discrepancy could be a reasonable value owing to the possible variability in manual measurements. This discrepancy may also be due to the fact that the physician measured the vessel diameter according to the NASCET criteria[18], which is less accurate than the area measurements[21] obtained by using our algorithm. With area measurement, the lumen analysis becomes independent of the measuring vectors required to calculate the percent stenosis from the vessel diameter. In addition, area measurements allow the operator to follow the evolution of the lumen throughout the plaque, a parameter called the surface roughness of the plaque[21].

With regard to the statistical comparison between the manually and algorithm-derived stenosis values

($p=0.3105$), the methods seem to agree in most cases. **Table 2** shows a total of 12 measurements obtained in the eight patients (two datasets). There were too few data points for any statistical comparison. While our algorithm is able to calculate two stenosis values (for each carotid side), we did not have all of the manually obtained counterpart values for comparison.

The next step in algorithm development will be the design of a completely automatic system. For this purpose, reliable segmentation algorithms must be developed for the lumen and the surrounding tissues. This system will provide a full classification of the plaque components, with appropriate tissue attenuation intervals[17]. Rather than dealing with slices, the segmentation should be applied to a 3D model of the vessel. This will allow slicing that is perpendicular to the vessel path to avoid elliptical and incorrect slice outlines of the tissues. It will also allow the processing of complicated vessel geometries with sinusoidal directions in the vertical axis. Lumen eccentricity remains one of the major problems associated with the analysis of the carotid artery[23]. The error induced by incorrect measurement of the luminal eccentricity increases with the degree of stenosis and imaging slice thickness. This error also increases along vessels orientated perpendicular to the z-axis (vertical slicing). Nonetheless, the percent stenosis measured in our patient group was consistent with that measured in the NASCET study[18] (median, 6%; minimum, −23%; maximum, 37%). This slight overestimation may have been caused by the use of area measurements instead of diameter measurements. Another possible explanation is the different measurement locations used by the physician and the algorithm. It is better to slightly overestimate than underestimate stenosis, because an underestimation can lead to a depreciation of lesion urgency.

There are some limitations to this model with regard to patients in an advanced stage of atherosclerosis. First, the analysis is not able to follow the lumen path if the stenosis is too severe in a large interval of slices, i.e., if the plaque narrows the lumen in such a way that the MDCT resolution is inadequate. If the lumen has a nonlinear relationship with the last slice segmented correctly, the algorithm loses track of the vessel. In addition, the low resolution would decrease the ability of the algorithm to distinguish low-contrast and overlapping attenuation intervals between the surrounding tissues and the vessel wall, between the lumen and vessel wall components and between the plaque and the vessel wall.

Conclusions

This study demonstrated that a semi-automatic CTA-based image segmentation system can be used to identify, locate, characterize and measure atherosclerotic lesions in the carotid artery.

Acknowledgements

FS was supported by the CIMO Foundation (Centre for International Mobility; KM-12-8107) and AJ was supported by the Tampere City Science Fund. The authors would like to thank Raija Paalavuo, Anna-Kaisa Parkkila and Ullamari Hakulinen for patient recruitment and management and Professor Jari Viik from the Department of Electronics and Communications Engineering of the Tampere University of Technology for his advice on the statistical analyses.

Conflicts of Interest

None.

References

1) De Weert TT, Cretier S, Groen HC, Homburg P, Cakir H, Wentzel JJ, Dippel DWJ, van der Lugt A: Atherosclerotic plaque surface morphology in the carotid bifurcation assessed with multidetector computed tomography angiography. Stroke, 2009; 40: 1334-1340
2) Enterline DDS, Kapoor G: A practical approach to CT angiography of the neck and brain. Tech Vasc Interv Radiol, 2006; 9: 192-204
3) McKinney AM, Casey SO, Teksam M, Lucato LT, Smith M, Truwit CL, Kieffer S: Carotid bifurcation calcium and correlation with percent stenosis of the internal carotid artery on CT angiography. Neuroradiology, 2005; 47: 1-9
4) Vukadinovic D, van Walsum T, Manniesing R, Rozie S, Hameeteman R, de Weert TT, van der Lugt A, Niessen WJ: Segmentation of the outer vessel wall of the common carotid artery in CTA. IEEE Trans Med Imaging, 2010; 29: 65-76
5) Shinohara M, Yamashita T, Tawa H, Takeda M, Sasaki N, Takaya T, Toh R, Takeuchi A, Ohigashi T, Shinohara K, Kawashima S, Yokoyama M, Hirata K, Momose A: Atherosclerotic plaque imaging using phase-contrast X-ray computed tomography. Am J Physiol Heart Circ Physiol, 2008; 294: 1094-1100
6) Kwee RM, Teule GJJ, van Oostenbrugge RJ, Mess WH, Prins MH, van der Geest RJ, Ter Berg JWM, Franke CL, Korten AGGC, Meems BJ, Hofman P a M, van Engelshoven JM a, Wildberger JE, Kooi ME: Multimodality imaging of carotid artery plaques: 18F-fluoro-2-deoxyglucose positron emission tomography, computed tomography, and magnetic resonance imaging. Stroke,

2009; 40: 3718-3724
7) Wintermark M, Jawadi SS, Rapp JH, Tihan T, Tong E, Glidden D V, Abedin S, Schaeffer S, Acevedo-Bolton G, Boudignon B, Orwoll B, Pan X, Saloner D: High-resolution CT imaging of carotid artery atherosclerotic plaques. AJR Am J Roentgenol, 2008; 29: 875-882
8) Wiesmann M, Schöpf V, Jansen O, Brückmann H: Stent-protected angioplasty versus carotid endarterectomy in patients with carotid artery stenosis: meta-analysis of randomized trial data. Eur Radiol, 2008; 18: 2956-2966
9) Bartlett E: Quantification of carotid stenosis on CT angiography. AJR Am J Roentgenol, 2006; 27: 13-19
10) Renard F: Image analysis for detection of coronary artery soft plaques in MDCT images. 2008 5th IEEE International Symposium on Biomedical Imaging: From Nano to Macro. IEEE, 2008; 25-28
11) Takaya N, Yuan C, Chu B, Saam T, Underhill H, Cai J, Tran N, Polissar NL, Isaac C, Ferguson MS, Garden G a, Cramer SC, Maravilla KR, Hashimoto B, Hatsukami TS: Association between carotid plaque characteristics and subsequent ischemic cerebrovascular events: a prospective assessment with MRI--initial results. Stroke, 2006; 37: 818-823
12) Heinonen T, Dastidar P, Eskola H, Frey H, Ryymin P, Laasonen E: Applicability of semi-automatic segmentation for volumetric analysis of brain lesions. J Med Eng Technol, 1998; 22: 173-178
13) Numminen J, Dastidar P, Heinonen T, Karhuketo T, Rautiainen M: Reliability of acoustic rhinometry. Respir Med, 2003; 97: 421-427
14) Rossi M, Pertovaara H, Dastidar P, Järvenpää R, Luukkaala T, Rautakunnas S, Heinonen T, Eskola H, Soimakallio S, Kellokumpu-Lehtinen P-L: Computed tomography-based tumor volume in non-Hodgkin lymphoma: clinical correlation and comparison with magnetic resonance imaging. J Comput Assist Tomogr, 2009; 33: 641-649
15) Schneider CA, Rasband WS, Eliceiri KW: NIH Image to ImageJ: 25 years of image analysis. Nat Methods, Nature Publishing Group; 2012; 9: 671-675
16) De Weert TT, de Monyé C, Meijering E, Booij R, Niessen WJ, Dippel DWJ, van der Lugt A: Assessment of atherosclerotic carotid plaque volume with multidetector computed tomography angiography. Int J Cardiovasc Imaging, 2008; 24: 751-759
17) Santos F, Joutsen A, Salenius J, Eskola H: Carotid artery atherosclerosis plaque analysis using CT and histology. In: Computational Vision on Medical Image Processing - VIPImage 2011, ed by Tavares JM and Natal J, pp82-86, Olhão, Portugal, CRC Press, 2011
18) Ferguson GG, Eliasziw M, Barr HWK, Clagett GP, Barnes RW, Wallace MC, Taylor DW, Haynes RB, Finan JW, Hachinski VC, Barnett HJM: The North American Symptomatic Carotid Endarterectomy Trial: Surgical Results in 1415 Patients. Stroke, 1999; 30: 1751-1758
19) Hounsfield GN: Computed medical imaging. Computed Medical Imaging. Science, 1980; 210: 22-28
20) Koon D-J: Region Growing. Available: http://www.mathworks.com/matlabcentral/fileexchange/19084-region-growing.
21) Teng Z, Degnan AAJ, Sadat U, Wang F, Young VE, Graves MJ, Chen S, Gillard JH: Characterization of healing following atherosclerotic carotid plaque rupture in acutely symptomatic patients: an exploratory study using in vivo cardiovascular magnetic resonance. J Cardiovasc Magn Reson Off J Soc Cardiovasc Magn Reson, 2011; 13: 64
22) Cheng D-C, Billich C, Liu S-H, Brunner H, Qiu Y-C, Shen Y-L, Brambs HJ, Schmidt-Trucksäss A, Schütz UH: Automatic detection of the carotid artery boundary on cross-sectional MR image sequences using a circle model guided dynamic programming. Biomed Eng Online. BioMed Central Ltd, 2011; 10: 26
23) Wise S, Hopper K: Measuring carotid artery stenosis using CT angiography: the dilemma of artifactual lumen eccentricity. AJR Am J Roentgenol, 1998; 919-923

II

FUSION OF EDGE ENHANCING ALGORITHMS FOR ATHEROSCLEROTIC CAROTID WALL CONTOUR DETECTION IN COMPUTED TOMOGRAPHY ANGIOGRAPHY

by

Santos, F., Joutsen, A., Salenius, J. & Eskola, H., September 2014

Computing in Cardiology Conference (CinC). 41:925–928

Fusion of Edge Enhancing Algorithms for Atherosclerotic Carotid Wall Contour Detection in Computed Tomography Angiography

Florentino Luciano Caetano dos Santos[1], Atte Joutsen[1], Juha Salenius[2], Hannu Eskola[1,3]

[1]Department of Electronics and Communications Engineering, Tampere University of Technology, Tampere, Finland
[2]Division of Vascular Surgery, Department of Surgery, Tampere University Hospital and Medical School, Tampere, Finland
[3]Department of Radiology, Regional Imaging Centre, Tampere University Hospital, Tampere, Finland

Abstract

The aim of this study is to assess the feasibility and performances of the fusion of edge enhancers in in vivo computed tomography angiography (CTA) images for automatic segmentation of outer and inner vessel walls, in presence of atherosclerotic plaques.

From 4 patients' CTA exams (stenosis degrees 70% – 95%) the slices representing plaques were extracted (223 images) and hand segmented by a trained operator for the vessel walls. The analyzed slices depict the common and internal carotid arteries and the carotid bifurcation.

The automatic protocol exploits two different categories of image edge enhancers: 5 edge detectors (Sobel, Prewitt, Roberts, laplacian of gaussian (LOG) and Canny) and 5 filters/mapping functions (laplacian filter, gradient map (GM), Otsu thresholding (OT), local range map (LRM) and standard deviation (STD) map).

The mean correlation coefficient between the manual and the automatic masks is 48% [17%, 64%]. By selecting the GM, LRM and STD algorithms only, the mean performance is improved up to 58%.

This methodology was proven to be comparable to the manual one. The correct selection of the edge enhancers is critical for the performance optimization: GM, LRM and STD showed to be the most suitable for our purpose.

1. Introduction

Atherosclerosis is a systemic disease, defined by the American Heart Association as the accumulation of atherosclerotic plaque inside arteries. The atherosclerotic plaque develops with the buildup of cholesterol (low-density lipoproteins - LDL - as a precursor to the disease), fatty substances, various metabolites from surrounding cells, calcified and fibrotic tissues [1–3]. Diagnostic and characterization of the disease in arteries, more specifically in the carotid arteries, may lead to the prevention of future strokes [4,5]. The atherosclerotic plaque is usually located in or around the carotid bifurcation since this location presents the highest variance of wall-shear stress and artery wall stiffness. The former is one of the precursors of the development of the disease [6], the latter is associated with plaque composition [7] and both linked with plaque stability. To be able to study the impact and presence of arterial stiffness there is the need to separate in the CTA image the outer vessel from the surrounding tissues and the inner border from the lumen.

There are algorithms that allow to segment the carotid artery wall but the need for human intervention prevails for the initialization, parameterization or validation of results [8]. Manual segmentation is done by trained operators, by using two regions of interest (ROI) representing the carotid outer contour and the lumen contour, with the carotid wall defined as the difference between them. Moreover, the time factor has to be considered, since both state-of-the-art automatic procedures and the manual method are usually slow. A fully automated procedure will provide more consistent results and less prone to human errors. In [9] de Weert *et al.* showed that human (inter- and intra-operator) coefficients of variation are 19% and 58%, respectively. A disadvantage of automating such an analysis is that it becomes sensitive to image noise. In the classification of tissues in noisy images, humans are more proficient than machines.

In this work we propose a novel software-based protocol for the automatic detection of the carotid artery wall contour, using edge enhancing algorithms with the final aim of overcome the weaknesses of manual inspection of CTA images. Our approach is operator independent, fast and repeatable. This work is part of the wider VASIM project carried on at Tampere University

of Technology, Tampere, Finland.

2. Methods

2.1. Dataset and manual segmentation

Four patients undergoing carotid artery endarterectomy were recruited at the Tampere University Hospital (Tampere, Finland). Preoperative CTA examination was performed between the aortic arch and the vertex of the skull. In this dataset the stenosis range was [70%, 95%]. A total of 223 images were acquired depicting the plaque region present in the common and internal carotid arteries and the carotid bifurcation.

Each image meant for comparison with the automatic protocol was manually segmented by a trained operator for the outer vessel and lumen contours.

All the methodology was developed using a Dell workstation (Dell OptiPlex 9020, Windows 7 Enterprise, 64 bits, 3.10 GHz, 8.0 GB RAM) with Matlab® R2012b, Image Processing Toolbox 8.1, Signal Processing Toolbox 6.18, and Statistical Toolbox 8.1.

2.2. Automatic edge detection

Automatic segmentation was performed by processing each image using the edge enhancing protocol proposed in this article. Our approach can be summarized as follows:

(i) tissues characterized by a higher attenuation than 500 HU are assigned a new attenuation of 20 HU, intended to prevent the loss of the atherosclerotic calcified tissue. Subsequent thresholding of the image to the range [-100, 500] HU [8] allows cleaning artifacts and surrounding tissues (air, lipidic and calcified tissue);
(ii) grayscale rescaling to [0, 1] interval;
(iii) edge enhancing by the ensemble, explained in more detail below;
(iv) separating nearby objects by connected components (4 neighborhood);
(v) computing of the distance for each object to the center of the image by the *pdist2* function;
(vi) classifying the object with the smallest distance as the final outline.

In detail, the edge enhancers used in this automatic approach belong to two different categories: 5 edge detectors (Sobel, Prewitt, Roberts, laplacian of gaussian (LOG) and Canny) and 5 filters/mapping functions (laplacian filter, gradient map (GM), Otsu thresholding (OT), local range map (LRM) and standard deviation (STD) map).

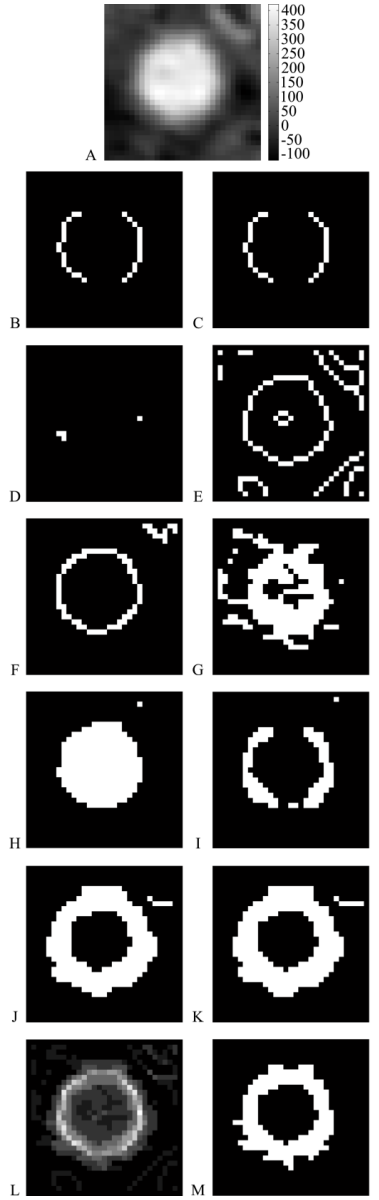

Figure 1. Edge enhancers applied to a carotid artery. A. Initial image, B. Sobel, C. Prewitt, D. Roberts, E. LOG, F. Canny, G. Laplacian, H. Otsu, I. LRM, J. GM, K. STD, L. Final contour (intersection of the initial image with the mask, M. Contour mask without lumen.

Each one of these edge enhancers was tested using a 3-pixel square window to produce an intermediate image INT_IM for each slice as follows: (i) the OT INT_IM was directly used; (ii) in LOG INT_IM a threshold of 0 was used for closed contours; (iii) LRM INT_IM was binarized using the inclusion range [0, 200]; and (iv) the 7 remaining INT_IMs were thresholded using OT. A single binary image (FUSION) was produced by fusing the 10 binary masks and thresholding using OT. An example of the application of these algorithms to a slice is represented in Fig. 1.

2.3. Comparison between manual and automatic contours

The comparison between manual and automatic segmentation of the carotid contours was done resorting to 2-dimensional correlation function *corr2* (with the manual contour as the ground truth). Each edge enhancer was also correlated individually with the manual mask. The three highest performing edge enhancers (GM, LRM and STD) were used to create a new ensemble (3M).

3. Results and discussion

The average time per image for FUSION was 0.034 s and for 3M 0.015 s. For manual segmentation the processing time for the outer contour and lumen was, in average, 5 s/slice.

Fig. 2 illustrates the three stages of the carotid contour protocol: the initial image fed to the edge enhancer algorithm (Fig. 2.A), the binary mask obtained with FUSION (Fig. 2.B) and the final segmented carotid contour (Fig. 2.C) as a result of the algorithm. The slice in Fig. 2 represents a section above the carotid bifurcation where the vessel walls haven't been separated enough to be segmented into three independent objects.

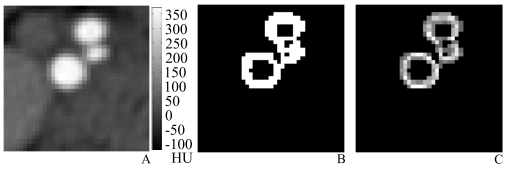

Figure 2. Carotid artery contour enhancing protocol step images. (internal carotid, lower element; external carotid, higher element; branching from the external carotid, middle element). A. Initial image; B. Contour mask without lumen; C. Final contour (intersection of the initial image with the mask).

Table 1. Performance (correlation) of the edge enhancers ensemble FUSION and 3M.

Patient	FUSION	3M	Increase
1	0.64	0.73	14%
2	0.17	0.24	47%
3	0.62	0.74	19%
4	0.51	0.60	17%
Mean	0.48	0.58	24%

The final performances (correlation between automatic and manual segmentation mask) for the four patients, using FUSION and 3M, as well as the increase of performance with 3M, are represented in Table 1.

The mean correlation coefficient between the manual and the automatic masks is 48% [17%, 64%]. By using the 3M algorithm, which presented the highest performances in the edge detection, the mean correlation is improved to 58%. This simpler (and faster) ensemble allowed obtaining a mean increase in correlation of 24%. This increase is dependent on the patient with a very wide interval ranging from 14% to 47%. This demonstrates that an approach effective for a specific patient can be non-optimal for another one.

The usage of OT for thresholding didn't provide good results, since it tends to over-threshold the objects in the image; this is clear by comparing Fig. 2 and 3 (both thresholded for 0.21 in the [0, 1] interval). This can be by the fact that the slice in Fig. 3 depicts an initial (non-homogenous) stage of atherosclerosis, as evident by the central and right bright spots (high attenuation) inside the carotid wall, that bias the optimal threshold calculation. This phenomenon didn't occur in case of a homogeneous level of atherosclerosis, advanced stage of atherosclerosis or healthy arteries.

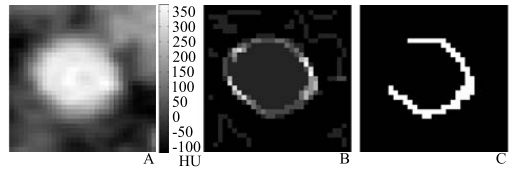

Figure 3. Extreme thresholding of the contour outline using OT. A. Initial image; B. Contour outline by FUSION; C. Final contour mask thresholded with 0.21 in the [0, 1] interval.

4. Conclusion

In this work we provide an efficient and fast method for the automatic detection of the contours of carotid arteries both in normal and atherosclerotic arteries. Our results are comparable with the manual segmented contour, as quantified by a correlation index of 58%.

Further work has to be done to improve the performance in inhomogeneous atherosclerotic plaques, such as filtering to clean abrupt changes in tissues and to select the optimal edge enhancers. GM, LRM and STD showed to be the most suitable for our purpose. Future improvements will lead to the usage of this methodology in plaque component characterization in atherosclerotic arteries.

Acknowledgements

The work presented in this paper has been partially supported by the iBioMEP national doctoral program, by the Tampere City Science Fund and by the Tampere University Hospital.

We would also like to thank iBioMEP for the travel grant given to participate in Computing in Cardiology 2014.

References

[1] Shaalan WWE, Cheng H, Gewertz B, McKinsey JF, Schwartz LB, Katz D, Cao D, Desai T, Glagov S, Bassiouny HS. Degree of carotid plaque calcification in relation to symptomatic outcome and plaque inflammation. J Vasc Surg 2004;40:262–9.

[2] Boudi FB, Ahsan CH, Ali YS. Coronary Artery Atherosclerosis 2013:1–20.

[3] Lusis AJ. Atherosclerosis. Nature 2000;407(6801):233–41.

[4] Enterline DDS, Kapoor G. A practical approach to CT angiography of the neck and brain. Tech Vasc Interv Radiol 2006;9:192–204.

[5] Vukadinovic D, van Walsum T, Manniesing R, Rozie S, Hameeteman R, de Weert TT, van der Lugt A, Niessen WJ. Segmentation of the outer vessel wall of the common carotid artery in CTA. IEEE Trans Med Imaging 2010;29:65–76.

[6] Augst AD, Ariff B, McG Thom SAG, Xu XY, Hughes AD. Analysis of complex flow and the relationship between blood pressure, wall shear stress, and intima-media thickness in the human carotid artery. Am J Physiol Heart Circ Physiol 2007;293:H1031–7.

[7] Canton G, Hippe DS, Sun J, Underhill HR, Kerwin WS, Tang D, Yuan C. Characterization of distensibility, plaque burden, and composition of the atherosclerotic carotid artery using magnetic resonance imaging. Med Phys 2012;39:6247–53.

[8] Santos FLC, Joutsen A, Terada M, Salenius J, Eskola H. A semi-automatic segmentation method for the structural analysis of carotid atherosclerotic plaques by computed tomography angiography. J Atheroscler Thromb 2014.

[9] De Weert TT, de Monyé C, Meijering E, Booij R, Niessen WJ, Dippel DWJ, van der Lugt A. Assessment of atherosclerotic carotid plaque volume with multidetector computed tomography angiography. Int J Cardiovasc Imaging 2008;24:751–9.

Address for correspondence.

Florentino Santos
Biokatu 6, Finn-Medi 1 4-208, FI-33520, Tampere, Finland
florentino.caetanodossantos@tut.fi

III

AUTOMATIC DETECTION OF CAROTID ARTERIES IN COMPUTED TOMOGRAPHY ANGIOGRAPHY: A PROOF OF CONCEPT PROTOCOL

by

Santos, F., Joutsen, A., Paci, M., Salenius, J. & Eskola, H., May 2016

The International Journal of Cardiovascular Imaging, vol 32:8, 1299-1310

Int J Cardiovasc Imaging (2016) 32:1299–1310
DOI 10.1007/s10554-016-0880-6

ORIGINAL PAPER

Automatic detection of carotid arteries in computed tomography angiography: a proof of concept protocol

Florentino Luciano Caetano dos Santos[1] · **Atte Joutsen**[1] · **Michelangelo Paci**[1,2] · **Juha Salenius**[3] · **Hannu Eskola**[1,4]

Received: 14 December 2015 / Accepted: 18 March 2016 / Published online: 3 May 2016

Abstract Atherosclerosis is one of the leading causes of mortality in the western world. Computed tomography angiography (CTA) is the conventional imaging method used for pre-surgery assessment of the blood flow within the carotid vessel. In this paper, we present a proof of concept of a novel, fast and operator independent protocol for the automatic detection (seeding) of the carotid arteries in CTA in the thorax and upper neck region. The dataset is composed of 14 patients' CTA images of the neck region. The performance of this method is compared with manual seeding by four trained operators. Inter-operator variation is also assessed based on the dataset. The minimum, average and maximum coefficient of variation among the operators was (0, 2, 5%), respectively. The performance of our method is comparable with the state of the art alternative, presenting a detection rate of 75 and 71% for the lowest and uppermost image levels, respectively. The mean processing time is 167 s per patient versus 386 s for manual seeding. There are no significant differences between the manual and automatic seed positions in the volumes ($p=0.29$). A fast, operator independent protocol was developed for the automatic detection of carotid arteries in CTA. The results are encouraging and provide the basis for the creation of automatic detection and analysis tools for carotid arteries.

Keywords Carotid angiography · Automatic image analysis · Atherosclerosis · Machine vision

Abbreviations

A	Area
BD^{var}	Border distance (variance)
CB	Carotid bifurcation
CCA	Common carotid artery
CTA	Computed tomography angiography
CV	Coefficient of variation
DCV	Distance to center of volume
DT	Distance to the center of the trachea
ECC	Eccentricity
HU	Hounsfield units
ICA	Internal carotid artery
MRI	Magnetic resonance imaging
Op	Operator
ROI	Region of interest
SF	Shape factor
TP	Trachea/pharynx volume
Var	Variance
w_p	Weight of descriptor P
τ_P	Threshold of descriptor P

Introduction

Stroke is the second largest cause of mortality worldwide, representing 10.6% of all deaths that occurred in 2011 [1]. Economically, the stroke related costs in the USA alone in

✉ Florentino Luciano Caetano dos Santos
florentino.caetanodossantos@tut.fi

[1] Department of Electronics and Communications Engineering, Tampere University of Technology, Finn-Medi 1 4-208, Biokatu 6, 33520 Tampere, Finland

[2] BioMediTech, Tampere, Finland

[3] Division of Vascular Surgery, Department of Surgery, Tampere University Hospital and Medical School, Tampere, Finland

[4] Department of Radiology, Regional Imaging Centre, Tampere University Hospital, Tampere, Finland

2009 reached 38.6 billion dollars, with a death rate of 40.6 % [2]. Atherosclerosis, as a systemic disease, can be observed from childhood and is usually progressive. Therefore, the detection of premature symptoms is vital in initiating pre-emptive measures to prevent strokes [3, 4].

The atherosclerotic plaque is commonly located in the carotid bifurcation (CB) as it presents the highest variation of wall-shear stress, one of the main precursors of the diseases' development [5]. The risk of stroke is assessed via two main characteristics of the carotid artery: (i) degree of luminal stenosis and (ii) plaque composition and morphology [6–8]. Both parameters are analyzed by manual segmentation of diagnostic images obtained by imaging techniques, such as magnetic resonance imaging (MRI), ultrasound and computed tomography angiography (CTA) [9, 10]. CTA is routinely used for pre-surgical assessment of endarterectomy.

Manual segmentation methods for the separation of the carotid artery lumen from the vessel wall and from the surrounding tissue involves several drawbacks, such as long computational time and operator-dependent parameters [6]. Indeed, de Weert et al. reported inter-operator and intra-operator coefficients of variation of 19 and 8 %, respectively for plaque area measurements [11]. Such operator dependency also affects the correct seeding (i.e. the correct identification of carotid arteries in an image). Automatic tools should therefore lead to higher reproducibility and shorter processing time.

Based on the work by Atherton et al. [12] and Yuen et al. [13] Matlab® (MathWorks®, USA) already has a circle finding function integrated in the Image Processing Toolbox. These approaches are based on a circular Hough transform, with a pre-specified radius range to decrease the number of false positives. Such false positive structures are typically bones and muscle as well as other blood vessels (e.g. the external carotid artery, jugular and subclavian arteries).

Further, Adame et al. used circle fitting in MRI images, although this approach requires the (manual) initial positioning of a circular mask over the carotid artery [14]. Bogunović et al. developed a completely automatic protocol in three-dimensional (3D) rotational angiography composed of three stages: (i) vessel centerline detection, (ii) vascular tree topology and bifurcations characterization, and (iii) internal carotid artery (ICA) identification by means of a support vector machine classifier [15]. Sanderse et al. [16] presented the *AnitA* method, consisting of two steps: (i) volume of interest estimation based on the shoulder plates as landmarks and (ii) axial detection of the carotid arteries by Hough transform and clustering [17]. The detection rate reported was 88 % for a dataset involving 31 patients.

Texture analysis and machine learning have also been suggested for the detection of the carotid artery in both ultrasound [18–20] and CTA [8, 21]. Although effective, these protocols require a reliable training set and a considerable amount of time for training the classifier. As atherosclerosis is a multi-factorial and widely variable disease, it presents high diversity in morphology, shape, size and location. Therefore, creating a solid and complete training set is not only very time-consuming but is also dependent on the size and representativeness of the training images.

In summary, the main weaknesses of the aforementioned state of the art methods are: (i) operator dependency, both in the initial seed placement and parameters identification, (ii) long computational time and (iii) the need of specialized training datasets for machine learning approaches.

Our previous work focused in the semi-automatic segmentation of the carotid vessel based on a manual seeding [6] (145 s/patient) and in a fully automatic segmentation of the carotid vessel wall [22] (0.015 s/slice). In the present paper we propose an operator independent software protocol to automatically detect the carotid arteries in CTA images in order to (i) efficiently overcome the fragilities of operator inspection, (ii) shorten the patient evaluation time, and (iii) allow the automatic segmentation of the carotid arteries.

Methods

Patient dataset

Fourteen patients (35–85 years old) undergoing general carotid artery, pre- and post-endarterectomy examination were recruited at the Tampere University Hospital (Tampere, Finland). CTA examinations were performed for the region between the aortic arch and the vertex of the skull. Of the 28 carotid arteries examined, seven were atherosclerotic (≥70 % stenosis), seven had mild stenosis (50 % ≤ stenosis < 70 %), while fourteen were open carotids (<50 %) or no information was present in the patient data sheets (Table 1). The percentage of stenosis was computed by radiologists at the Tampere University Hospital, according to the NASCET criterion [23, 24]. The percentage of stenosis was computed as

$$Stenosis\ (\%) = \left(1 - \frac{N}{D}\right) \times 100,$$

where N represents the narrowest diameter of the residual lumen and D the luminal diameter of the internal carotid after the occlusion. The images of patient 11 had particular influence of beam-hardening artifact. Patients 10 and 11 had a reconstruction error which thresholded all pixels with attenuation over 1000 HU as the rescale intersect value. In spite of the reconstruction errors, Patients 10 and 11 were not removed from the dataset, in order not to bias the results and to stress our protocol also in the more demanding and non-optimal cases such as in the presence of noise and

Table 1 Patient dataset characteristics (empty fields are from non-existent information)

	Age	Sex	Stenosis (%)	
			Left	Right
1	56	F	95	
2	85	M	70	70
3	76	F		75
4	71	M	70	80
5	55	M	90	60
6	73	F		70
7	80	M	85	73
8	73	M		60
9	73	M	0	0
10	59	M	<50	
11	67	M	50	<50
12	35	M	100	
13	49	M	0	0
14	57	M	0	0

human errors during acquisition. No other image preprocessing was conducted. This research was approved by the Ethics Committee of the Pirkanmaa Hospital District (decision number R07210).

Imaging

CTA examinations were conducted using two different helical, 64-slice, multidetector computed tomography scanners: General Electric LightSpeed (slice thickness 1.25 mm; increment 0.5–0.7 mm; pixel size 0.6–0.7 mm; 120 kVp; 130–327 mAs) and Philips Brilliance (slice thickness 1 mm; increment 0.5 mm; pixel size 0.42–0.49 mm; 120 kVp; 178–243 mAs). The average scanning time was 30 s for both scanners and each DICOM image was exported as a 512×512 matrix [6].

For CTA contrasts, the General Electric Omnipaque® (350 mg/ml) and the Guerbet Xenetix® (350 mg/ml) were used. If possible, venous access for injection was established in the antecubital fossa; otherwise, it was established in the hand. Dose, speed and injection time were all patient dependent and determined according to the recommendations of the manufacturer of the contrast media.

Image analysis

Due to the different image rescale intersects in the scanners, we performed normalization of the attenuations to the same scale, ranging from −1024 (air) to a variable upper attenuation limit. No other preprocessing was carried out on the initial images.

The methodology applied is sketched in Fig. 1. The purpose of the airway detection step (Fig. 1C, D) is to create a general landmark throughout the patient's volume. For each slice, the coordinates of the airway are used as an initial approximation of the location of the carotids.

The CTA images were analyzed with a Dell workstation (Dell OptiPlex 9020, Windows 7 Enterprise, 64 bits, 3.10 GHz, 8.0 GB RAM) equipped with Matlab version R2012b, Image Processing Toolbox version 8.1, Signal Processing Toolbox version 6.18, and Statistical Toolbox version 8.1. All the patients' data was exported from the hospital servers without any preprocessing or filtering.

Airway detection

During the detection of the carotid arteries in 2D images, multiple potential candidates occur. If circles are adopted as templates of the carotid arteries in each slice, other candidates are also found such as jugulars or fusiform muscles. A 3D anatomical landmark allows a more efficient localization of the vessels. The landmark chosen is the trachea/pharynx (TP) (also referred to as the airway in this manuscript), which is quite easy to segment from the CTA since (i) it displays low attenuation due to the air content, (ii) it is surrounded by much higher attenuations due to denser tissues and (iii) it cannot be mixed with the air around the patient. To guarantee this last point, the model is constrained to the uppermost slice where the nasal cavity is detected. The TP enables an adaptation to patient geometry, with variations in the neck thickness and airway volume. A summary of the substeps necessary for the airway detection is represented in Fig. 2. By using amplitude segmentation with the threshold value −500 HU, a 3D air volume is obtained (Fig. 2A). This threshold was chosen as some tissues, e.g. lipids, have a negative HU and therefore a higher limit would include these tissues as air.

The next substep consists of removing the air structures that surround the patient's CTA volume (Fig. 2A, B). Using a 6-faced cube edge connectivity as a discarding factor, the airway volume is attained and the holes filled.

After the suppression of the border connected components, several possible TP objects are attained, such as the real airway, lungs, probes and feeding tubes. Performing a slice-by-slice area-based filter with the area range of 150–600 mm^2 allows for clearing these foreign and unwanted objects[1] (Fig. 2B, C). The area ranges are adapted from Griscom and Wohl [25] and Hoffstein and Fredberg [26]: for the central airway ≈600 mm^2, for the trachea ≈300 mm^2, and for the glottis ≈150 mm^2. A margin of ±10 % is adopted to keep the allowed area flexible so as not to lose potential TP structures. The lower

[1] Matlab function: *bwareaopen* (image, minimum area value).

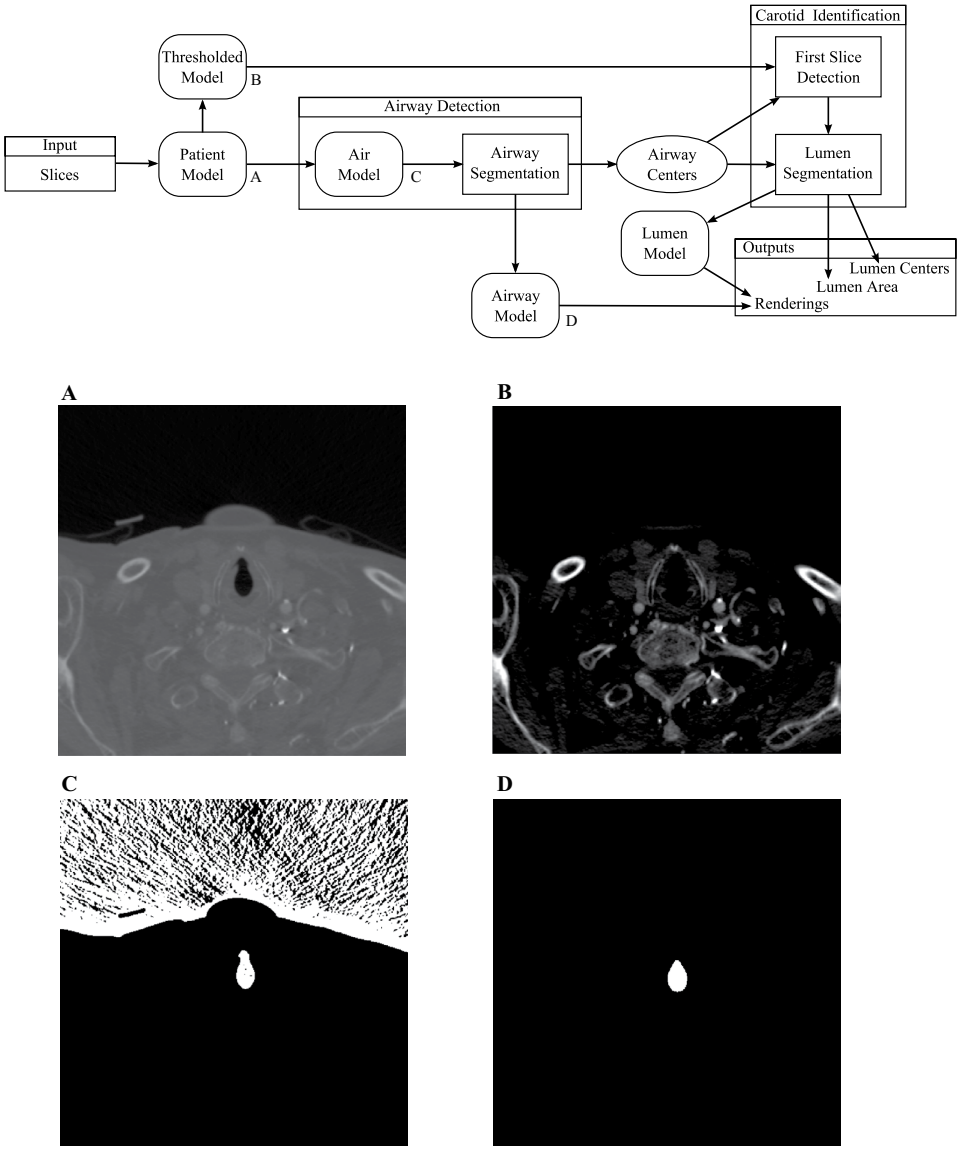

Fig. 1 Two-step (airway detection and carotid identification) analysis scheme for carotid identification in CTA (example intermediate results A, B, C and D)

boundary allows for the clearing of small objects while the uppermost boundary allows for the clearing of objects such as lungs, nasal cavity, sinuses, bed-patient space, and other foreign objects. Since two patients presented with a collapsed trachea or were intubated, the values had to include the endotracheal tube in the final TP model. The criterion for this event was the detection of an abrupt area reduction.

These processing steps produce a volume with only one or a few very specific structures (Fig. 2D). If there is more than one candidate for TP, the distances of each object centroid from the center of the volume (DCV) will be compared. The centrally located object is chosen to represent the real TP.

The floor of the nasal cavity is exploited to limit the carotid detection in the z-axis. The nasal cavity can be

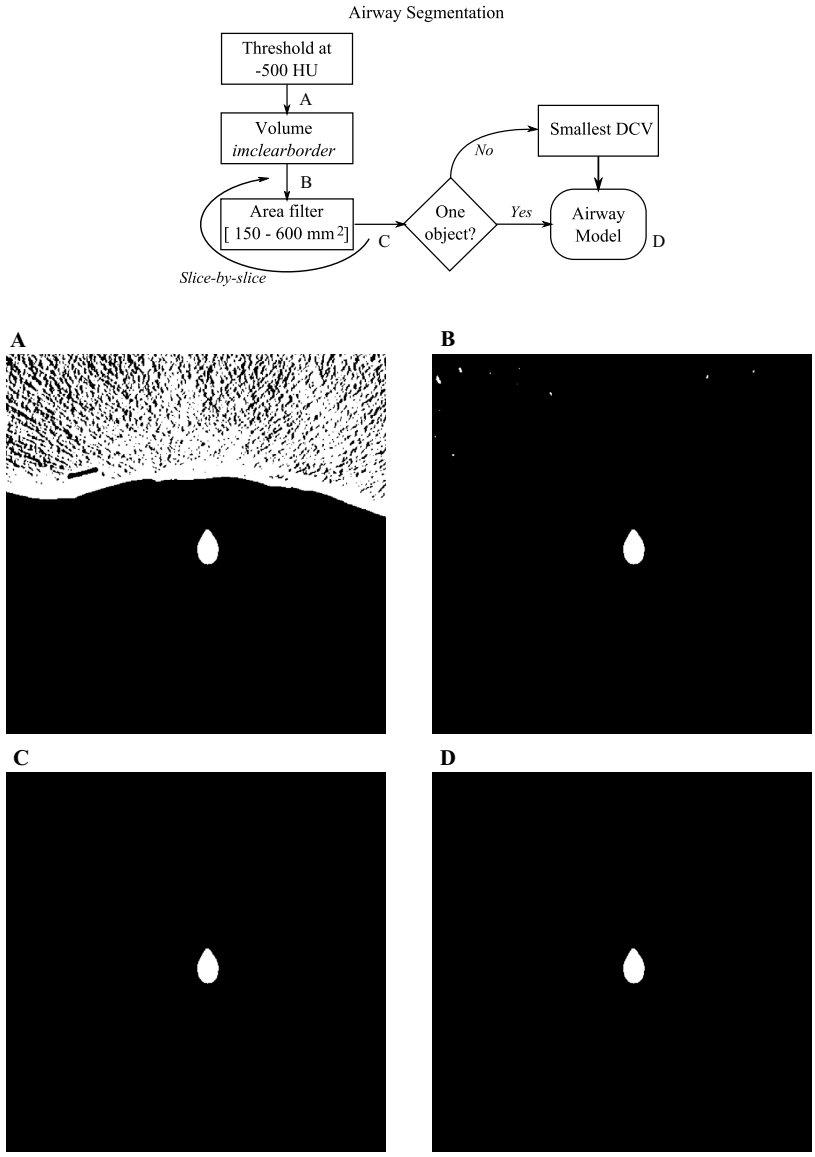

Fig. 2 Airway (TP) detection scheme in CTA (*DCV* distance to the center of volume) (example intermediate results A, B, C and D)

identified in a specific slice through the presence of multiple objects whose areas differ more than 10% from the TP identified object in the previous slice. Thus, the airway volume is restricted between the lowest slice and the slice where the floor of the nasal cavity appears. Depending on the patient's positioning, this subset includes 60–75% of the initial slices. After the TP detection, the coordinates of the trachea centroid are extracted from each slice to be applied in the carotid detection.

The final outputs of the airway detection are (i) the slice-wise centroid coordinates of the TP, (ii) the TP volume for 3D rendering, and (iii) the uppermost slice for the carotid artery detection.

Carotid identification

The detection of the carotids requires morphological operators and a decision process to select the true positives among all the potential candidates. The substeps for carotid identification are presented in Fig. 3.

Due to the contrast concentration of 25–30 HU per mg/mL and the voltage of 100 kV, the lumen has an attenuation

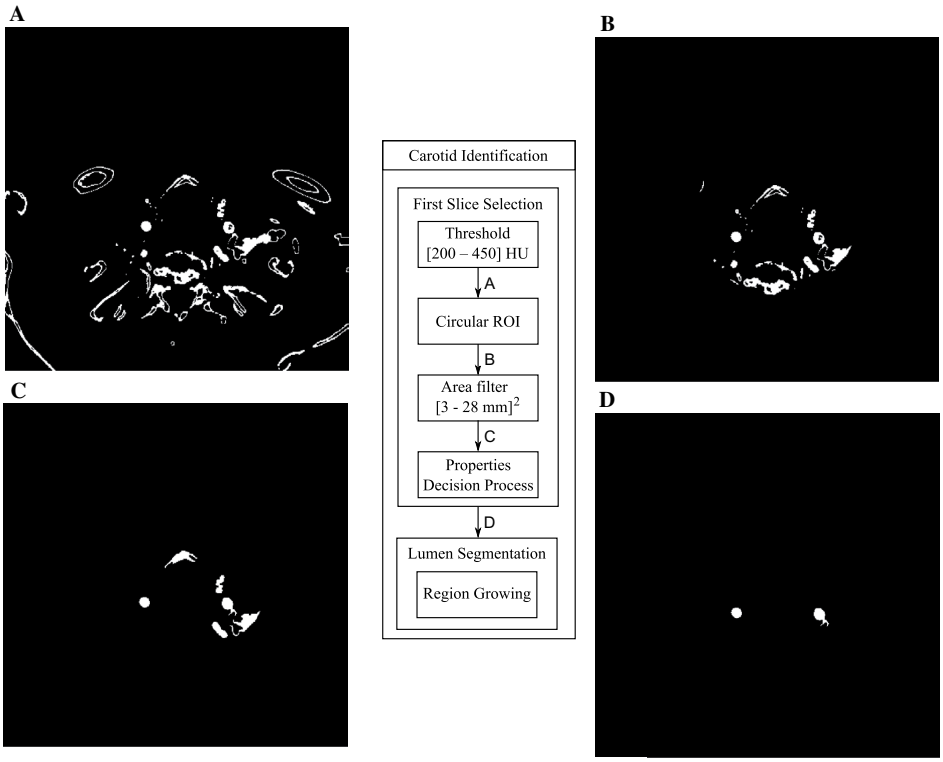

Fig. 3 Carotid identification scheme in CTA (example intermediate results A, B, C and D)

of 340 ± 74 HU [27]. Consequently, the attenuation values are constrained to the range 200–450 HU in order to exclude other tissues, noise and foreign objects (Figs. 1A, B, 3A). Moreover, this attenuation constraint allows for the saving of memory and clears the bolus and washing effect.

The TP center coordinates (as determined in the "Airway Detection" step) are used to create a circular region of interest (ROI) in each slice with a radius of 1/5 (defined empirically) of the total image size. In our dataset, the mean radius is approximately 4 cm. All the objects potentially representing the carotid artery are assumed to be located inside this ROI (Fig. 3B).

The lumen area is defined by an object area filter with the diameter range 2–6 mm (mean: 4 mm and area 13 mm^2) [28]. This represents an area of between 30 and 300 pixels. Such a hard attenuation threshold poses the risk of losing pixels inside the lumen. To reconstruct these pixels, the 3D model is rebuilt, converted to a binary matrix, and the holes filled. The union of this model with the original reconstitutes the empty pixels and so assures a model without holes (Fig. 3C).

The process continues with the identification of the carotid arteries, which should not be primarily based on the attenuation values. The attenuation of the lumen depends on various parameters (contrast agent concentration, acquisition machine, etc.), on patient features (size, weight, fat content), and on the vessel anatomy, complexity, and tortuosity. The object properties (descriptors) chosen for this evaluation were based on the morphology of each object[2] as well as the Euclidean distances[3] (i) from each object to the center of the trachea and (ii) from each object's border element to its center.

The object descriptors comprise: (i) border distance variance (BD^{var}), defined as $BD^{var}_{object} = Var[dist(P_{oc}, P_{ob})]$, where P_{oc} and P_{ob} are the object centroid and each border pixel coordinate, respectively; (ii) distance to trachea (DT), defined as $DT_{object} = dist\left(P_{oc}, P_{traq}\right)$, both the centroid coordinates for the object and for the trachea, respectively; (iii) shape factor [29] (SF), calculated by.

$$SF_{object} = \frac{4 \times \pi \times Area_{object}}{Perimeter_{object}^{\ 2}};$$

[2] Matlab function: *regionprops* (image, properties).

[3] Matlab function: $pdist2(X_1, X_2)$ (expressed as *dist* in this manuscript).

Table 2 Decision descriptor weights (w_p) and thresholds (τ_P) for the detection of the lowest and uppermost slice with carotid arteries

	Lowest slice		Uppermost slice	
	w_p	τ_P	w_p	τ_P
BD^{var}	0.25	$BD^{var} < 1$	0.25	$BD^{var} < 1$
DT	0.19	2 cm ≤ DT < 5 cm	0.19	DT ≤ 7 cm
ECC	0.06	ECC < 0.6	Not used	Not used
SF	0.40	$SF_{obj} \geq$ mean ($SF_{all\ obj}$)	0.46	$SF_{obj} \geq$ mean ($SF_{all\ obj}$)
A	0.10	A ≥ 13 mm^2	0.10	A ≥ 3 mm^2

BD^{var} border distance variance, *DT* distance to trachea, *ECC* eccentricity, *SF* shape factor, *A* area

(iv) area (A); and (v) eccentricity (ECC). ECC is defined as the ratio of the distance between the foci and the major axis of the ellipse fitted on each object. ECC ranges from 0 (for a circle) to 1 (for a segment). As this calculation is based on an elliptic fitting, it is prone to over- or under-estimate the true area and shape of the object.

The aforementioned descriptors are applied to assign a score ($Score_{object}$) to each carotid candidate in the interval [0, 1] (0 noise, 1 perfect candidate) according to

$$Score_{object} = \sum_{P} w_P \times b_P$$

where P represents the pth descriptor, and w_p the weight associated to the pth descriptor, while b_p is attributed according to

$$b_p = \begin{cases} 1, & if\ complies\ with\ \tau_P \\ 0, & otherwise \end{cases}$$

and τ_P is the threshold for the pth descriptor's inclusion in the final score.

The weights, w_p, were hand-tuned based on the acknowledgement that certain descriptors are more representative than others for a carotid artery. ECC has a weight of only 0.06 since an elliptic shape is forced onto the subject, while BD^{var} has a weight of 0.25 considering that a circular carotid artery has a very homogeneous distance between the centroid and all the edge pixels. The inclusion conditions τ_P are represented as threshold or threshold ranges. Table 2 represents w_p and τ_P.

The two objects with the highest scores are chosen as the carotid candidates (Fig. 3D). To finally confirm that they truly represent the carotid arteries, they are evaluated and accepted if (i) the two objects are located on opposite sides with respect to the trachea (symmetry landmark), (ii) the coronal coordinates distance is less than 5 cm, and (iii) their attenuation values differ by less than 100 HU.

The final outputs of the carotid identification step are the lowest slice where the carotid arteries appear (usually above the branching of the right carotid artery from the brachiocephalic artery) and their coordinates.

The same methodology is applied for the detection of the uppermost CTA slice representing the ICAs before the fusion with the circle of Willis. Using the areas and centers obtained during the detection of the airway, the analysis is restrained between the lowest slice and the topmost singular element in the TP model. To reduce the amount of data in the process, only pixels located closer than 7 cm from the trachea are accepted for finding the carotids in each slice. For the area-based filtering, a diameter range of 1–4 mm [6] is applied. The lower range limits are for the low resolution of carotids near the cranium entrance. The eccentricity (ECC) of the carotids is limited to 0.7. This analysis is performed from the top-down, slice-by-slice. For the identification of the ICAs in the uppermost CTA slices, four out of the five descriptors with distinct weights (Table 2) are applied: BD^{var}, DT, SF and Area. As the objects areas are small, the ECC is even further more non-descriptive of the carotid arteries and therefore not used.

To compare the performance of the proposed protocol with that of the manual seed placement, four trained operators identified the location of both carotid arteries between the thorax area and the circle of Willis. The lowest slice is only considered after the branching of the right CCA from the brachiocephalic artery. These seeds were considered the true location of the carotid vessels. A special software program, "SeedsTool", was created for this manual seeding task (Fig. 4).

Presentation of results

The numerical results of this analysis are obtained from the lowest and uppermost slices where both carotid arteries are identified. To evaluate the viability of the methodology, the centroids and slice numbers from the manual and automatic identification are compared using the two-sided Wilcoxon rank sum test. The p-values[4] are calculated and all p-values of less than 0.05 are considered statistically significant.

[4] Matlab function: *ranksum*.

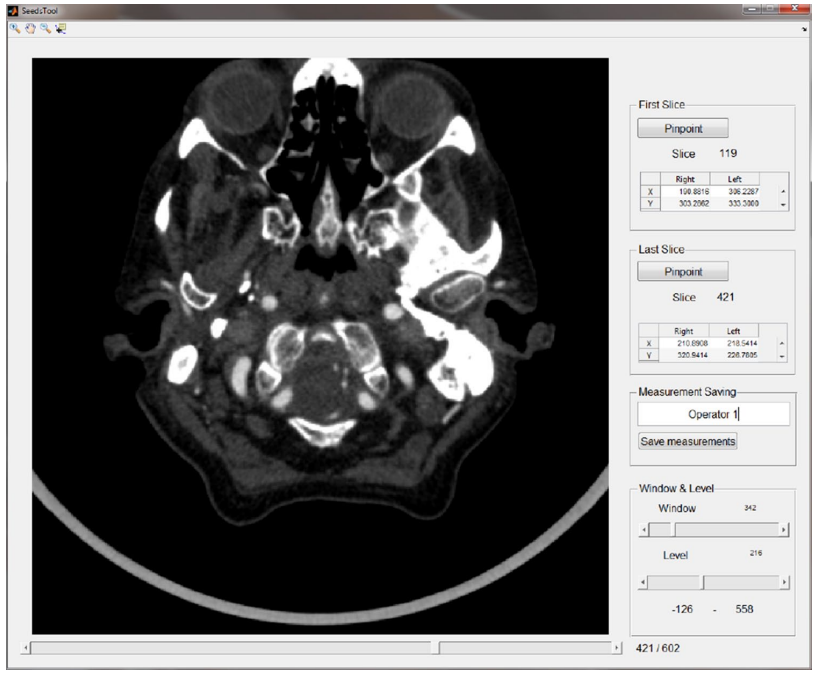

Fig. 4 SeedsTool interface for manual seed positioning

For each carotid location (lowest and uppermost), the carotid side seed point coordinates (x, y and z as slice) are averaged over all operators (Op) and the left and right values concatenated into a single column for the p-value calculation. These values are considered as the base value for the relative error calculation. The percentage coefficient of variation (CV) is the metric used for inter-operator variability and is defined as $CV_{algorithm} = 100 \times \left[STD\left(Op_{1,2,3,4}\right) / Mean\left(Op_{1,2,3,4}\right) \right]$. The 3D lumen renderings are constructed by applying region growing [30]. The maximum difference (threshold) used to prevent the leakage of the growing region is defined as three times the standard deviation of the attenuation values from the calculated carotid seeds and applied in the lumen volume. The regions are grown from both the lowest and uppermost seeds. This prevents a high stenotic plaque from stopping the development of the region.

Results

The proposed protocol was successful in detecting and segmenting the TP volume in all the patients. Specifically, the detection rate was 75 % for the lowest slices and 71 % for the uppermost slices. Table 3 presents the detection performance for each patient.

Figure 5 shows the carotids and the airway centers as pinpointed in two illustrative patients.

Table 4 reports the relative difference between the automatic and manual seeding processes: (i) for the z-coordinate +24 slices (overestimation of the lowest slice) and −70 slices (underestimation of the uppermost slice); and (ii) for

Table 3 Performance matrix for the automatic detection of the carotid arteries

Patient	Lowest slice		Uppermost slice	
	Right	Left	Right	Left
1	X			
2		X		
3	X	X	X	X
4	X	X	X	X
5	X	X	X	X
6	X	X		
7		X	X	X
8	X	X	X	X
9		X	X	X
10	X		X	X
11	X	X	X	X
12		X		
13	X	X	X	X
14		X	X	X
Detection rate (%)	75		71	

X carotid correctly detected

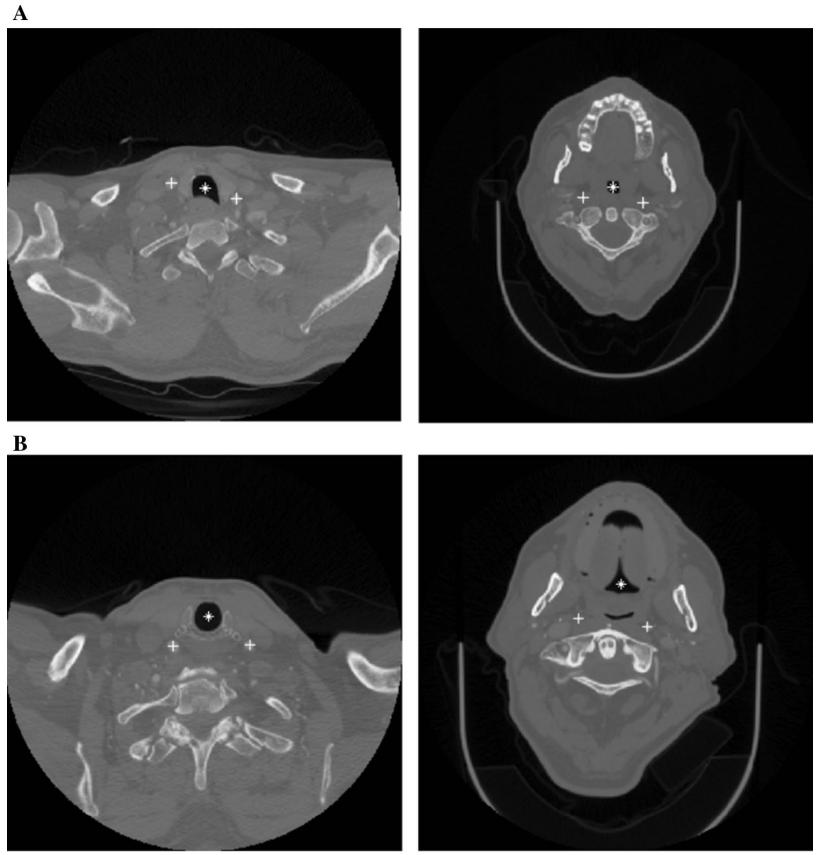

Fig. 5 Lowest and uppermost slice carotid locations (+, carotids; *, airway) detected by the protocol for patients 3 (**A**) and 7 (**B**)

x- and y-coordinates +1 % (lowest seeds) and −1 % (uppermost seeds).

The mean number of slices was 286 for our method, corresponding to 18 cm in the GE LightSpeed scan and 14 cm with the Philips CT scan. The manual identification produced a mean of 380 slices (23 and 20 cm respectively) corresponding to a +35 % difference.

The inter-operator variability expressed by the CV is (MINIMUM, AVERAGE, MAXIMUM): (0, 1, 3 %) for the lowest and (0, 2, 5 %) for the uppermost carotid seeds. The mean *p*-values for the protocol versus operator comparison on the seed coordinates are $p=0.25$ for the lowest seeds and $p=0.33$ for the uppermost seeds (Table 5). For the full analysis, it is $p=0.29$.

Figure 6 depicts the carotids and airway 3D models constructed during the analysis. Patient 3, having a severe stenosis (75 % occlusion in the right carotid artery, no data available for the left stenosis), is illustrated in Fig. 6A with a clearly visible plaque on both sides (sparse points in space). Figure 6B renders patient 7 (85 and 73 % occlusion in the left and right carotid arteries, respectively) where a leakage to the hyoid bone originated from the region growing process. The right carotid artery's lowest seed slice was not identified. In this particular case, the initial seed was identified in a higher slice, thus also providing the necessary data for the reconstruction of the lowest artery volume.

The mean time necessary to process one patient is 167 s for the protocol and 386 s for the operators. Both values encompass (i) patient data loading, (ii) TP detection (only for the protocol), (iii) slice detection, (iv) seed positioning and (v) coordinates saving. The mean time needed by the protocol for the sole identification of the uppermost and lowest slices (and their coordinates) is 12 s (4 s for the lowest and 8 s for the uppermost slice).

Discussion

While the previous work [6] focused in a semi-automatic (manual single seed point) segmentation of the carotid vessels (lumen) and in an automatic segmentation of the carotid

Table 4 Relative difference between automatic and manual seeding for the lowest and uppermost

Patient	Lowest		Uppermost	
	Slice	Coordinates (%)	Slice	Coordinates (%)
1	+8	+2	−35	−3
2	−12	+3	−167	+10
3	+39	+1	−47	−3
4	+36	−4	−115	−4
5	+1	0	−158	−4
6	+28	+2	−83	−6
7	+23	+2	−41	−2
8	+54	−3	−12	−1
9	−8	−1	−50	−2
10	+139	+6	−37	0
11	+60	−1	−55	−1
12	+19	−4	−69	+5
13	−45	+2	−86	+2
14	−12	+4	−32	0
Mean	+24	+1	−70	−1

Table 5 *p*-values for the uppermost and lowest slice seeding

	x	y	Slice (z)	Mean
Lowest	0.47	0.21	0.07	0.25
Uppermost	0.89	0.10	0.00	0.33

vessel wall [22], the present work focuses on the automatic detection of the carotid vessel in CTA images.

Our goal is to apply this method in the anatomical assessment of atherosclerotic lesions in clinic. CTA is mainly used for the functional (blood flow) assessment of atherosclerosis and it is one of the most common imaging modalities. Our protocol was developed using only clinical diagnostic images with their inherent hindering low resolution. The detection method here proposed is another step forward in achieving full automation of the atherosclerotic burden study. The detection pipeline presented here allows for the correct detection (compared with manual seeding) of 75 % of the CCA and 71 % of the ICA.

The method for the detection of the tubular structures is critical for the identification of carotid arteries. We did not follow the procedure suggested by Atherton et al. [12] (Matlab® function *imfindcircles*) for two reasons. First, it does not allow the detection of circles smaller than 5 pixels radius (r_{min}) and, second, its optimal radius range ($r_{max} < 3 \times r_{min}$) is too narrow for the identification of carotid arteries.

The *AnitA* method proposed by Sanderse et al. [16] exploits the shoulder plates as the landmark. We chose to use the TP as the landmark in our approach because this structure is present throughout the studied volume. This allowed the use of the TP volume as a guideline for the ROI

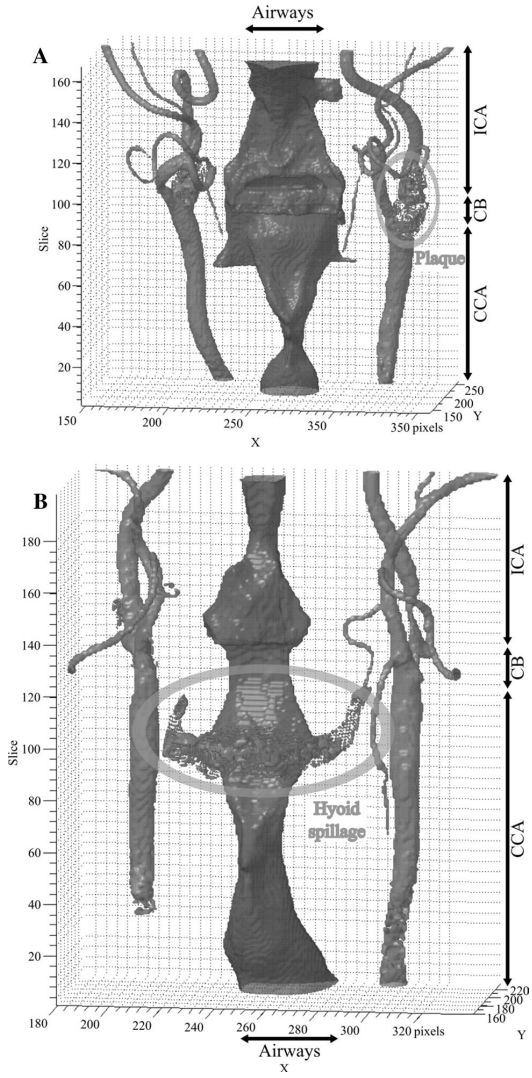

Fig. 6 Carotid and airway renderings for patients 3 (**A**) and 7 (**B**). *CCA* common carotid artery, *CB* carotid bifurcation, *ICA* internal carotid artery). **A** Atherosclerotic plaque volume (marked by *elliptical area*) in the CB and initial ICA region. **B** A spillage of the ICA in the hyoid bone. The right lowest seed was not found and so the volume is determined based on the right uppermost ICA seed

area in the detection of the carotid vessels. The comparison between *AnitA* and our protocol shows that ours obtains a lower performance (75 % vs. 88 %) in terms of the lowest carotid detection. This difference can be explained by multiple factors such as different patient images (quality, resolution, artifacts, etc.) but also by the intrinsic characteristics of the two protocols. *AnitA* not only applies edge enhancing before the Hough transform to improve the image contrast

but also assumes a linear centerline for CCA, ICA and the transition between these and CB. However, as demonstrated in Fig. 6, ICA does not always present such a straightforward morphology. The mean *AnitA* computation time was 120 s while ours was 167 s. This value was higher since it not only includes the loading of the patient's data and lowest slice carotid detection, but also the TP detection and volume construction, the uppermost slice carotid detection, and the carotid region growing.

Kawai et al. successfully implemented a protocol based on support vector machine classifiers to differentiate carotid artery and non-carotid artery images (accuracy between 69 and 100 %) [19]. They applied this promising protocol in the ultrasound (perpendicular to the artery) of healthy arteries, but it has not thus far been applied to atherosclerotic CTA images. For a more representative comparison of the aforementioned protocols, one or more common open-access datasets would be useful.

In some patients, having small-caliber arteries with very similar attenuation to adjacent tissues lead to the region growing algorithm leaking out of the contours and preventing any further analysis. This is more evident in the upper ICA. This can also be a possible explanation for the p-value <0.05 observed in Table 5 for the detection of the uppermost slice. The bolus effect in a very narrow strip of slices presents another problem: the region growing is not able to continue the ascent through the artery. This failure can also occur as a result of a high occlusion. To avoid it, we implemented the top-down and bottom-up region growing procedure. Again, the TP is a crucial landmark in the proposed protocol. Without this landmark, the region growing would not be able to stop before the circle of Willis in the bottom-up growth and would have spread to the aorta and brachiocephalic artery in the top-down growth.

Despite the protocol being able to correctly identify the lowest and uppermost carotid arteries, it may fail in the intermediate slices. In the advanced stages of the disease, the presence of a plaque or of occlusions affects the morphology and therefore the decision process. However, the identification of the carotids in the central slices is outside of the aim of our protocol.

A limitation of the current study is the size of the dataset: in this paper we presented preliminary results, relative to fourteen patients, that will be confirmed when a more extensive dataset will be available. Nonetheless, our actual results show a qualitative and quantitative agreement with the multiple sets of manually chosen seeds, thus confirming the viability of our protocol. Moreover, future improvements, e.g. the optimization of the weights necessary for the carotid arteries identification, will contribute to increase both the accuracy and the speed of this detection system.

We believe that by applying the proposed automatic protocol, the detection, and assessment of atherosclerotic disease in the carotid arteries can be improved.

Conclusion

We have presented a novel, fully automatic, protocol for the detection of the carotid arteries in the thorax and neck area. The performances achieved are 75 and 71 % respectively, with a total processing time of 167 s per patient. Not all the carotid arteries were successfully detected, but compared to the manual method, the reported results are encouraging.

Acknowledgments FS was supported by the CIMO Foundation (Centre for International Mobility; KM-12-8107), Tampere University Hospital and the iBioMEP doctoral scholarship. AJ was supported by the Tampere City Science Fund and by Tampere University Hospital. MP was supported by the Finnish Cultural Foundation (Central Fund). This project was also partly supported by the Competitive State Research Financing of the Expert Responsibility Area of Tampere University Hospital (Grant number R07210/9 K115). The authors would like to thank RN Raija Paalavuo, MD Anna-Kaisa Parkkila, and Lic. Sc., Med. Phys. Ullamari Hakulinen for their help with patient recruitment and management.

Compliance with ethical standards

Conflict of interest The authors declare that they have no conflict of interest.

Ethical approval All procedures performed in studies involving human participants were in accordance with the ethical standards of the institutional and/or national research committee and with the 1964 Helsinki declaration and its later amendments or comparable ethical standards. This research was approved by the Ethics Committee of the Pirkanmaa Hospital District (decision number R07210).

Informed consent Informed consent was obtained from all individual participants included in the study.

References

1. Wittenauer R, Smith L (2012) Priority medicines for Europe and the world: a public health approach to innovation update on 2004 background paper
2. Go AS, Mozaffarian D, Roger VL et al (2013) Heart disease and stroke statistics-2013 update: a report from the American Heart Association. Circulation. doi:10.1161/CIR.0b013e31828124ad
3. Enterline DS, Kapoor G (2006) A practical approach to CT angiography of the neck and brain. Tech Vasc Interv Radiol 9:192–204. doi:10.1053/j.tvir.2007.03.003
4. Vukadinovic D, van Walsum T, Manniesing R et al (2010) Segmentation of the outer vessel wall of the common carotid artery in CTA. IEEE Trans Med Imaging 29:65–76. doi:10.1109/TMI.2009.2025702
5. Augst AD, Ariff B, Thom SAG McG, Xu XY, Hughes AD (2007) Analysis of complex flow and the relationship between blood pressure, wall shear stress, and intima-media thickness

in the human carotid artery. Am J Physiol Heart Circ Physiol 293(2):H1031–H1037. doi:10.1152/ajpheart.00989.2006
6. Santos FLC, Joutsen A, Terada M et al (2014) A semi-automatic segmentation method for the structural analysis of carotid atherosclerotic plaques by computed tomography angiography. J Atheroscler Thromb 21:930–940. doi:10.5551/jat.21279
7. Indes LG, Gates L, Indes J (2014) Evaluation and treatment of carotid artery stenosis, carotid artery disease. In: Rezzani R (ed) Carotid artery disease—from bench to bedside beyond. InTech, Rijeka, pp 1–18
8. Markiewicz T, Dziekiewicz M, Maruszyński M et al (2014) Recognition of atherosclerotic plaques and their extended dimensioning with computerized tomography angiography imaging. Int J Appl Math Comput Sci 24:33–47. doi:10.2478/amcs-2014-0003
9. Bartlett E (2006) Quantification of carotid stenosis on CT angiography. AJR Am J Roentgenol 36:13–19. doi:10.1016/j.ejvs.2008.04.016
10. Renard F, Yang YYY (2008) Image analysis for detection of coronary artery soft plaques in MDCT images. In: 2008 5th IEEE int symp biomed imaging from nano to macro, pp 25–28. doi:10.1109/ISBI.2008.4540923
11. Weert TT, Monyé C, Meijering E et al (2008) Assessment of atherosclerotic carotid plaque volume with multidetector computed tomography angiography. Int J Cardiovasc Imaging 24:751–759. doi:10.1007/s10554-008-9309-1
12. Atherton TJ, Kerbyson DJ (1999) Size invariant circle detection. Image Vis Comput 17:795–803. doi:10.1016/S0262-8856(98)00160-7
13. Yuen H, Princen J, Illingworth J, Kittler J (1990) Comparative study of Hough Transform methods for circle finding. Image Vis Comput 8:71–77. doi:10.1016/0262-8856(90)90059-E
14. Adame IM, Van Der Geest RJ, Wasserman B et al (2004) Automatic segmentation and plaque characterization in atherosclerotic carotid artery MR images. Magn Reson Mater Phys Biol Med 16:227–234. doi:10.1007/s10334-003-0030-8
15. Bogunović H, Pozo JM, Cárdenes R, Frangi AF (2010) Automatic identification of internal carotid artery from 3DRA images. Conf Proc EEE Eng Med Biol Soc 2010:5343–5346. doi:10.1109/IEMBS.2010.5626473
16. Sanderse M, Marquering H, Hendriks E et al (2005) Automatic initialization algorithm for carotid artery segmentation in CTA images. In: Medical image computing and computer-assisted intervention – MICCAI 2005, vol 3750. Springer, Heidelberg, pp 846–853. doi:10.1007/11566489_104
17. Kim J, Srinivasan MA (2005) Characterization of viscoelastic soft tissue properties from in vivo animal experiments and inverse FE parameter estimation. Med Image Comput Comput Assist Interv 8:599–606. doi:10.1007/11566489
18. Hassan M, Chaudhry A, Khan A, Iftikhar MA (2014) Robust information gain based fuzzy c-means clustering and classification of carotid artery ultrasound images. Comput Methods Program Biomed 113:593–609. doi:10.1016/j.cmpb.2013.10.012
19. Kawai F, Hayata K, Ohmiya J et al (2013) Fully automatic detection of the carotid artery from volumetric ultrasound images using anatomical position-dependent LBP features. In: Wu G, Zhang D, Shen D et al (eds) Lecture notes in computer science (including Subser. Lect. Notes Artif. Intell. Lect. Notes Bioinformatics). Springer, Cham, pp 41–48
20. Stoitsis J, Golemati S, Kendros S, Nikita KS (2008) Automated detection of the carotid artery wall in B-mode ultrasound images using active contours initialized by the Hough transform. Conf Proc IEEE Eng Med Biol Soc 2008:3146–3149. doi:10.1109/IEMBS.2008.4649871
21. Acharya UR, Sree SV, Mookiah MR et al (2013) Computed tomography carotid wall plaque characterization using a combination of discrete wavelet transform and texture features: a pilot study. Proc Inst Mech Eng Part H - J Eng Med 227:643–654. doi:10.1177/0954411913480622
22. Santos FLC, Joutsen A, Salenius J, Eskola H (2014) Fusion of edge enhancing algorithms for atherosclerotic carotid wall contour detection in computed tomography angiography. In: Comput. Cardiol. Conf. (CinC), 2014. Cambridge, MA, pp 925–928
23. Ferguson GG, Eliasziw M, Barr HWK et al (1999) The North American symptomatic carotid endarterectomy trial: surgical results in 1415 patients. Stroke 30:1751–1758. doi:10.1161/01.STR.30.9.1751
24. Fox AJ (1993) How to measure carotid stenosis. Radiology 186:316–318. doi:10.1148/radiology.186.2.8421726
25. Griscom NT, Wohl MEB (1986) Dimensions of the growing trachea related to age and gender. Am J Roentgenol 146:233–237. doi:10.2214/ajr.146.2.233
26. Hoffstein V, Fredberg JJ (1991) The acoustic reflection technique for non-invasive assessment of upper airway area. Eur Respir J 4:602–611
27. Eller A, Wuest W, Kramer M et al (2014) Carotid CTA: radiation exposure and image quality with the use of attenuation-based, automated kilovolt selection. AJNR Am J Neuroradiol 35:237–241. doi:10.3174/ajnr.A3659
28. Zhang Z, Berg M, Ikonen A et al (2005) Carotid stenosis degree in CT angiography: assessment based on luminal area versus luminal diameter measurements. Eur Radiol 15:2359–2365. doi:10.1007/s00330-005-2801-2
29. Podczeck F, Newton JM (1994) A shape factor to characterize the quality of spheroids. J Pharm Pharmacol 46:82–85. doi:10.1111/j.2042-7158.1994.tb03745.x
30. Koon D-J Region Growing. http://www.mathworks.com/matlabcentral/fileexchange/19084-region-growing

IV

VASIM: AN AUTOMATIC TOOL FOR QUANTIFYING ATHEROSCLEROSIS IN CAROTID ARTERIES BASED ON COMPUTED TOMOGRAPHY ANGIOGRAPHY

The International Journal of Cardiovascular Imaging
https://doi.org/10.1007/s10554-019-01549-1

ORIGINAL PAPER

VASIM: an automated tool for the quantification of carotid atherosclerosis by computed tomography angiography

Florentino Luciano Caetano dos Santos[1,4,5] · Marcin Kolasa[4] · Mitsugu Terada[2] · Juha Salenius[3] · Hannu Eskola[1,4] · Michelangelo Paci[1]

Received: 24 September 2018 / Accepted: 28 January 2019

Abstract
The diagnostic imaging techniques currently used to evaluate the arterial atherosclerosis hinge on the manual marking and calculation of the stenosis degree. However, the manual assessment is highly dependent on the operator and characterized by low replicability. The study aimed to develop a fully-automated tool for the segmentation and analysis of atherosclerosis in the extracranial carotid arteries. The dataset consisted of 59 randomly-chosen individuals who had undergone head-and-neck computed tomography angiography (CTA), at the Tampere University Hospital, Tampere, Finland. The analysis algorithm was mainly based on the detection of carotid arteries, delineation of the vascular wall, and extraction of the atherosclerotic plaque. To improve the vascular detection rate, the model-based and volume-wide analytical approaches were deployed. A new fully-automated vascular imaging (VASIM) software tool was developed. For stenosis over 50%, the success rate was 83% for the detection and segmentation. Specificity and sensitivity of the algorithm were 25% and 83%, respectively. The overall accuracy was 71%. The VASIM tool is the first published approach for the fully-automated analysis of atherosclerosis in extracranial carotid arteries. The tool provides new outputs, which may help with the quantitative and qualitative, clinical evaluation of the atherosclerosis burden and evolution. The findings from this study provide a basis for the further development of automated atherosclerosis diagnosis and plaque analysis with CTA.

Keywords Carotid atherosclerosis · Angiography · Computer-assisted image analysis · Computer-assisted diagnosis

Abbreviations

CCA	Common carotid artery
CT	Computed tomography
CTA	Computed tomography angiography
CVAs	Cerebrovascular accidents
CVDs	Cardiovascular diseases
ECA	External carotid artery
HU	Hounsfield unit
ICA	Internal carotid artery
MRI	Magnetic resonance imaging
NASCET	North American Symptomatic Carotid Endarterectomy Trial
SD	Standard deviation
TAYS	Tampere University Hospital
VASIM	Vascular imaging

✉ Florentino Luciano Caetano dos Santos
florentino.l.c.santos@ieee.org

[1] BioMediTech, Faculty of Medicine and Health Technology, Tampere University, SM312, Korkeakoulunkatu 3, 33720 Tampere, Finland

[2] Department of Applied Physics, Faculty of Science, Fukuoka University, Fukuoka, Japan

[3] Division of Vascular Surgery, Department of Surgery, Tampere University Hospital and Medical School, Tampere, Finland

[4] Department of Radiology, Medical Imaging Center, Tampere University Hospital, Tampere, Finland

[5] BioMediTech, Faculty of Medicine and Health Technology, Tampere University, P.O. Box 692, Tampere 33014, Finland

Introduction

Cardiovascular diseases (CVDs) are the leading cause of death worldwide. According to the World Health Organization, in 2012, 37% of premature deaths were caused by CVDs. This translated to 17.5 million deaths, of which 6.7 million were due to cerebrovascular accidents (CVAs) [1, 2]. Majority of CVAs are ischemic strokes, caused mainly by atherosclerosis.

Published online: 28 February 2019

Existing research recognizes the critical role of early diagnosis and treatment of atherosclerosis in CVDs mortality prevention [3]. A considerable amount of literature has been published on diagnostic accuracy that has been improved by new imaging techniques, image processing, and image analysis methods [4, 5].

Computed tomography angiography (CTA), is a common modality for imaging the carotid arteries. Currently, evaluating atherosclerotic lesions is based on the degree of maximal luminal stenosis, and the composition and morphology of the plaque [6–8]. However, assessment of these parameters is performed manually.

The manual assessment has several major limitations, including operator dependency, long analysis time, questionable analysis dependability and repeatability [9]. It has been reported that the inter- and intra-operator variability (coefficients of variation) for plaque area measurements were 19% and 8%, respectively [10]. Despite these major limitations, manual stenosis level measurement, e.g., using the North American Symptomatic Carotid Endarterectomy Trial (NASCET) [11] criterion, remains the main accepted metric for determining the urgency of prevention and treatment. There remains a need for a fully-automated method of carotid artery analysis, providing both satisfactory running time and reliability.

The previous research by the authors has established: (i) the initial semi-automated segmentation of the carotid arteries based on manual seeding [6], (ii) the fully automated detection of the carotid arteries allowing to avoid manual seeding [9], and (iii) the automated carotid walls contour segmentation [12].

The main aim of this study was to develop a fully-automated tool for atherosclerosis segmentation and analysis in the carotid arteries. This paper describes the design and implementation of a new vascular imaging (VASIM) software tool, which is a fully-automated and structured integration of all methods previously established by the authors.

Materials and methods

Study population

The source population for this study were patients obtained from the Tampere University Hospital (TAYS), Tampere, Finland, between the January 1st, 2008 and December 31st, 2015. The study population was recruited retrospectively from the TAYS database. All patients were selected randomly.

Inclusion criteria were defined a priori as follows: a patient with at least one head-and-neck CTA scan (i.e., aorta arch to skull apex). The exclusion criteria were defined as: patients with CT scan only (without CTA); patients with incomplete medical records, i.e., without sufficient data on CTA technical information.

From the TAYS patient's population, all were randomly selected and the final study population consisted of 59 patients (N = 59): 34 men (58%) and 25 women (42%). The mean age was 64 years (standard deviation (SD) 14), ranging from 12 to 83 years.

Head-and-neck CTA scans of all 59 individuals were retrospectively reassessed, and the stenosis levels were manually calculated according to the NASCET criteria. Subsequently, based on the level of stenosis, individuals were included in one of the two groups—cases or controls. Cases were defined as individual carotids with stenosis $\geq 50\%$. Controls were all individual carotids with stenosis $< 50\%$.

The study was approved by the Ethical Committee of Pirkanmaa Hospital District, Tampere, Finland (decision number R07210).

Imaging

CTAs were performed using helical, 64-slice, multidetector CT scanners; either a General Electric LightSpeed (slice thickness 1.25 mm; increment 0.5–0.7 mm; pixel size 0.6–0.7 mm; 120 kVp; 130–327 mAs) or a Philips Brilliance CT 64-slice (slice thickness 1 mm; increment 0.5 mm; pixel size 0.42–0.49 mm; 120 kVp; 178–243 mAs). All of the images were exported in DICOM® standard, as a 512×512 matrix.

To improve carotid artery contrast, one of the following CTA contrast media was used: Iomeron® 350 mg/ml, Omnipaque® (350 mg/ml; General Electric), and Xenetix® (350 mg/ml; Guerbet). They were administered intravenously (ulnar or palmar vein), in accordance with the manufacturers' instructions.

Image analysis

VASIM's image analysis algorithm was divided into five consecutive stages: (i) loading of the patient's stack; (ii) carotid arteries detection, subdivided into airways segmentation and carotid segmentation; (iii) vascular wall delineation; (iv) atherosclerotic plaque extraction; (v) metrics, 2D tissue masks, 3D model calculation, and rendering. Figure 1depicts the general analysis diagram followed by VASIM.

Automatic detection of carotid arteries

The detection methodology was explained on an example of the Patient 3 (75 years-old male). This patient had previously suffered a transient ischemic attack, and had arterial hypertension and hyperlipidemia history. Carotid arteries component evaluation detected a plaque of mixed nature

(fibrosis, lipid pool, and calcification) located in the right internal carotid artery (ICA), causing a 75% stenosis.

Airways segmentation As in the previous study of the authors [9], the first step of the carotid arteries detection was creating an anatomical landmark, based on the upper respiratory tract (i.e., above the sternal angle) (Fig. 1a.1). The image analysis was restricted to the level of the auditory tube opening, which approximates the carotid canal level.

Airways provided the axis for a cylindrical volume-of-interest. This enabled the detection of vascular trees rather than slice-wise circular structures. To create the airways models, a hard threshold of −500 Hounsfield units was applied. To exclude the air surrounding a patient, objects connected to the volume borders were discarded. Figure 2 shows an example of airways model for the Patient 3.

Additionally, the airways landmark enabled normalizing the dataset by the patient's body size.

Automatic segmentation of the carotid vessel During the automatic analysis of CTA neck cross-sections, several structures can be misclassified as the carotid arteries, e.g., feeding tubes, needles, and jugular veins.

In the previous study [9], the algorithm identified carotid arteries between two anatomical structures: brachiocephalic artery bifurcation and circle of Willis. However, that method was dependent on manual seeding and parameterization. Therefore, here, a new method based on a fully-automated volume-of-interest analysis is presented.

In the first stage, a tilted cylinder (radius of 5 cm) was created around the airways, on the section between the most proximal and distant CTA slices. Subsequently, the resultant model was cleaned from lower attenuation tissues (e.g., lipid pools), using MATLAB's native *isovalue* function. The airways divided objects into the right and left side. The division enabled estimation of their interconnectivity. Single, uncompromised arteries were accepted as the final model. In the case of completely occluded arteries, their continuity was assessed distantly to the occlusion (Fig. 1a.2).

Sporadically, after thresholding, the algorithm presented objects that crossed the sagittal plane of the airways. Examples of such objects were the mandible and hyoid bone. The contrast between arteries and objects mentioned above may be insufficient to distinguish these structures. Figure 3 presents an example of a horizontal object (thyroid cartilage) connecting both arterial trees into a single volume.

The separation of the carotids and other objects was divided into the following steps: (i) volume skeletonization [13], (ii) skeleton nodes (branching points) location and removal, (iii) vertical degree evaluation of each resultant object, (iv) non-vertical removal, and (v) reconstruction of arterial trees using the acquired volume skeleton and the original 3D model. The bounding box dimension of each object was used to determine the vertical degree. Every object with a z/x-axis or z/y-axis ratio < 1.5 was discarded from the volume.

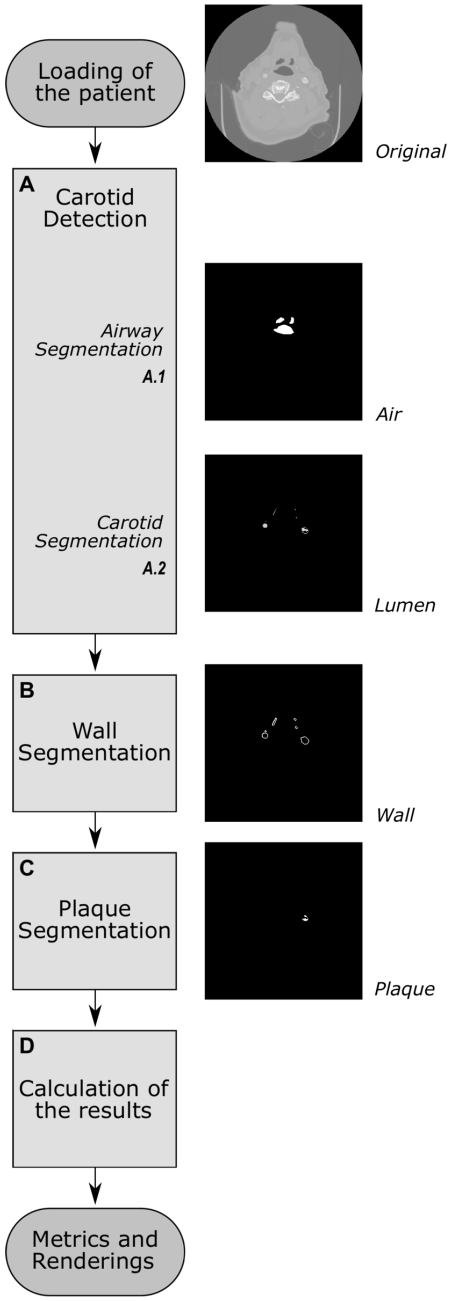

Fig. 1 VASIM protocol diagram

Fig. 2 Segmented airways for Patient 3 (seen from the anterior plane)

The current methodology and handling of possible hindrances resulted in two carotid models. Each artery skeleton was recalculated and used to define the carotid area perpendicularly to the vascular curvature. This prevented incorrect cross-sections, e.g., in horizontal branches of the ICA.

To ensure contradistinction between the common carotid artery (CCA), ICA, and external carotid artery (ECA), the algorithm initially detected the CCA bifurcation. The bifurcation location was defined as the most proximal cross-section where the number of objects increased from one to two, and the distance between their centroids was smaller than < 1 cm. The latter rule prevented potential errors caused by loops in the distant segment of the artery. The separation between ECA and ICA was conducted using the vertical degree threshold as previously used in the separation between arterial tree and surrounding objects.

Segmentation of the outer carotid wall

To calculate the vascular wall thickness the lumen and carotid wall boundaries were delimitated. A method based on morphological operators and edge enhancers/detectors was used (Fig. 1b) to define the boundary of the carotid wall. This method was described in detail in a previous study by the group [12].

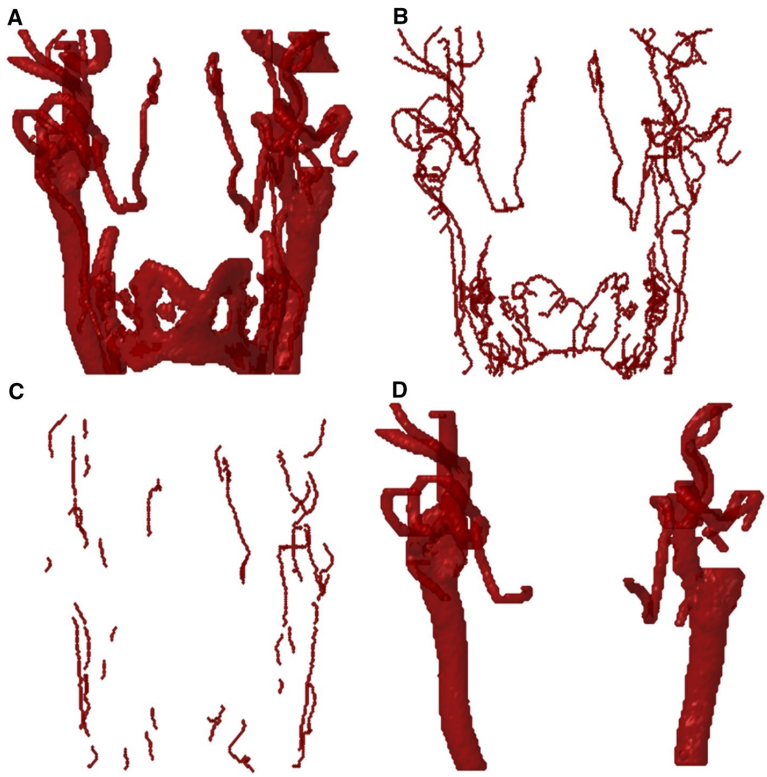

Fig. 3 Example of thyroid region spillage (Patient 3). **a** Two carotids visible with a horizontal structure joining both arteries into the same volume. **b** Model's skeleton. **c** Vertical elements of the skeleton. **d** Resulting model after connecting vertical objects' centroids in the original model

Plaque volume extraction

For segmenting the carotid plaque and assessing its morphology, a new method was developed. This was accomplished similarly to the airways segmentation. However, the threshold value was defined using the histogram of the maximum-intensity projections on the three axes. In each maximum-intensity projection, a threshold value based on the Otsu method [14] was calculated. Subsequently, the three values were averaged and applied to the 3D volume. The automatic threshold was deployed to address high variability in patient atherosclerosis level, which demanded a higher adaptability from the method. This considerably reduced the time required for plaque segmentation compared with the previously deployed algorithm [13] (Fig. 1c). Following this processing, a 3D rendering of the three major components of the carotid was produced. It presented lumen, the vascular wall, and any possible atherosclerotic plaque. Example of such a presentation is shown in Fig. 4. The plaques were poorly visualized as they are always located between the lumen and the outer vascular wall. Therefore, they were modeled in Fig. 4c with the open lumen path.

Metrics evaluated

The current protocol allows side-wise extraction of the following metrics: the minimum lumen area in the region of interest; the maximum area percentage occupied by the arterial wall in a slice; the maximum area percentage occupied by the plaque; and the maximum stenosis of the carotid artery calculated by the algorithm (Fig. 1d). Moreover, location-specific stenosis can be calculated for the CCA, ICA, and ECA. In our study, the region of interest was comprised of the CCA and ICA models, which were used for stenosis calculation. All of the stenosis values are calculated according to the NASCET criteria, i.e., one minus the minimum lumen area in the region of interest divided by the assumed healthy lumen area in the region of interest. Prior to the NASCET stenosis calculation, the equivalent diameter of the perpendicular-corrected section of the vessel model was calculated.

Following the development of the automated stenosis assessment with the VASIM methodology, the data on manually calculated stenosis values were obtained from medical records. The manual assessment was performed by an experienced radiologist beforehand, which ensured blinding to the VASIM results. Subsequently, the absolute difference between the manually and automatically calculated stenosis values was computed. Only arteries with both manually- and automatically-determined stenosis percentages were taken into consideration for the statistical calculations.

The classification as a case or control (binary classification test) was based on the manually assessed level of stenosis. According to the NASCET, the demonstrated, conclusive benefit for carotid endarterectomy is observed in patients with symptomatic 70–99% ICA stenosis [11]. Notwithstanding, in this study, the cut-off point between cases and controls was stenosis of 50%. The justification for this cut-off point was the fact, that according to the European

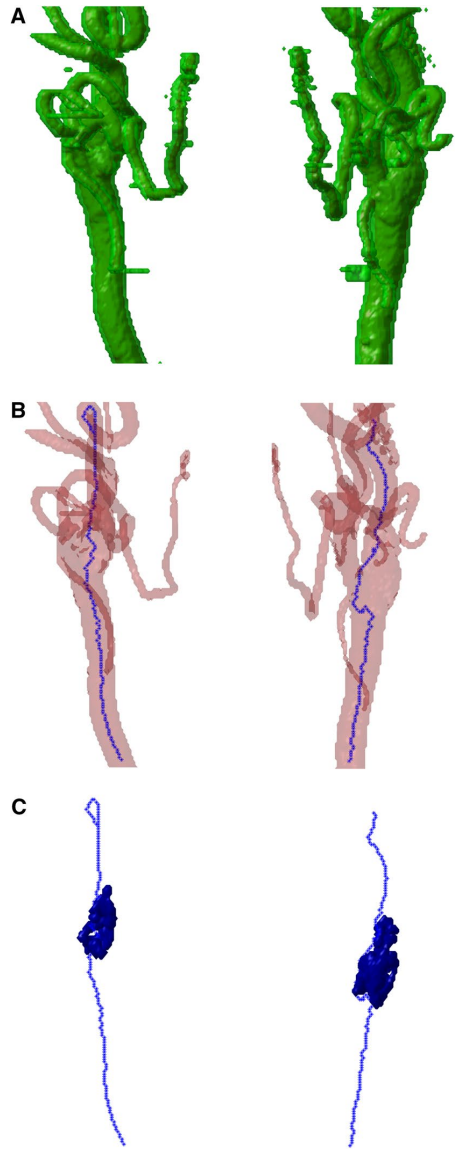

Fig. 4 Full rendering of the carotid structures (Patient 3). **a** Carotid walls (green). **b** Overlay of the semi-transparent lumen (red) and carotid open pathway (dotted blue line). **c** Carotid open lumen pathway (dotted blue line) and calcified plaque elements (blue volumes)

Association of Vascular Surgery endarterectomy is more appropriate for symptomatic 50–99% stenosis patients, and for asymptomatic 70–99% stenosis patients [15].

Furthermore, sensitivity, specificity, and accuracy of our method were assessed. The VASIM performance was evaluated based on the tissue segmentation success rate, variation between manually and automatically calculated stenosis values, and the total analysis time. The Pearson's coefficient was used for hypothesis test evaluation. The success of the segmentation was determined visually by the operator. The assessment was based on volume comparison and segmentation masks with the image stack for the verification of the correct tissue detection and segmentation (airway, lumen, wall, and plaque).

The atherosclerotic plaque accuracy evaluation based on the comparison with histopathology was not performed. It was previously demonstrated, that both endarterectomy procedure and pre-histopathological preparation affect the plaque's morphology. Hence, the comparison between the in-vivo CTA plaque and the ex-vivo sample is impossible [16].

Finally, a user-friendly and intuitive graphical interface was developed.

VASIM and its underlying algorithms were developed and tested on a Lenovo workstation (Lenovo W541, Windows 7 Enterprise, 64 bits, 4 2.80 GHz, 32.0 GB RAM) equipped with the MATLAB (version R2017a, Image Processing Toolbox version 10.0, Signal Processing Toolbox version 7.4, and Statistical Analysis and Machine Learning Toolbox version 11.1).

Results

In this study, a new VASIM software tool was designed, developed, and used to assess atherosclerosis in the CCA and the cervical segment of the ICA.

The overall tissue segmentation (lumen, wall, and plaque) success rate was 83%, equivalent to 49 out of 59 correctly identified carotids. The average absolute difference between the manual and automated stenosis calculations was 37% (95% confidence interval 29–46%) (Tables 1, 2). The *p*-value for the automated and manual analysis was 0.2976.

Forty-two atherosclerotic plaques were identified in the study population (Table 1). Forty of them were located in the ICA, and two in the CCA. Based on the morphology, the plaques mentioned above can be classified into the following categories: 13 of mixed nature, 23 calcified, two ulcerated, two soft tissue, and two irregular.

VASIM's overall accuracy was 71%. The average time for the whole procedure (loading of patient's volume, airways segmentation, carotid detection and segmentation, vascular wall and plaque segmentation, quantitative results, 3D modeling, and saving of results) was 1381 s. The average analysis time was 1.62 s per slice. The number of slices was different for each patient. Table 2 presents the summary statistics for the stenosis metrics.

The detected carotid arteries were subsequently classified into two groups, i.e., stenosis $< 50\%$ and $\geq 50\%$ (Table 3). The 32 manually-detected $\geq 50\%$ stenoses were compared with the automated analysis performed with the VASIM.

In cases of stenosis $\geq 50\%$, the sensitivity and specificity were 83% and 25%, respectively. The confusion matrix used in the metrics calculation is presented in Table 4.

The VASIM interface provided three main functions (Fig. 5a): patient image stack loading, analyzing the data, and creating a 3D model. The facultative "Model" function allowed to obtain a 3D model, based on current window and level values. In Fig. 5a, the "Analyze" button is hidden as the analysis of the image was completed.

The user interface presented information on the patient and imaging parameters (Fig. 5b). Additionally, it showed values of the maximal stenosis for each carotid artery (Fig. 5c). Furthermore, the VASIM interface allowed the user to create an overlay of the segmented structures (wall and plaque) using both 2D and 3D lumen models (Fig. 5d).

The bottom panel of the VASIM interface provided a histogram, and image controls, which allowed to change the 2D image stack visualization (Fig. 5e). The right side of the panel D presented a linearized arterial view (Fig. 5d). The panel F (Fig. 5f) provided multiple color maps options, which enabled tissue contrast regulation.

Discussion

This research aimed to develop a fully-automated tool for the segmentation and analysis of atherosclerosis in the CCA and ICA cervical segments. The main result of the study is a new VASIM software tool. To the authors' knowledge, the VASIM is the first fully-automated, and user-independent tool for carotid arteries CTA images analysis.

In this study, the approaches previously presented by the authors in [6, 9, 12, 16] were revised, improved, and structured. The reliability of the methods mentioned above increased and the computational time for VASIM was reduced.

The new method presented in the study allows skipping the initial and final seed positioning. Unlike in our previous studies, finding two 3D objects in a given volume was unnecessary. This enabled the analysis of images of patients with complete occlusion. Also, the 3D object identification was improved by removing the need to find similar objects bilaterally to the central volume. Contrary to the previous methodology, it was possible to include arteries with loops.

Table 1 Detailed information about age, sex of patients, localization and morphology of atherosclerotic plaque, and VASIM performance compared with manual stenosis calculation

Patient	Age	Sex	Location of the plaque		Composition of the plaque		Stenosis according to VASIM (%)		Stenosis according to the operator (%)		Absolute difference (%)		Plaque volume (mm^3)		Time (s)	
			Left	Right	Left	Right	Left	Right	Left	Right	Left	Right	Left	Right	Total	Per slice
1	–	F					0	71					122	94	1211	2.3
2	83	M	ICA	ICA	C, Irr	C, Irr	83	81	79	76	4	5	2879	1229	2286	3.8
3	75	M	ICA	ICA	C	C	0	92	29	75	29	17		0	867	1.9
4	70	M	ICA	ICA	C	C	96	76	19	79	77	3	806	880	381	0.6
5	54	M	ICA		M		0	87	78		78			662	134	0.3
6	72	F	ICA	ICA	S	M	0	76	90	58	90	18	22	23	787	1.8
7	79	M		ICA		M	100	97		70		27	232	260	426	0.7
8	72	M	ICA	ICA	C	C	34	65	85	73	51	8	0	0	687	2.3
9	73	M														
10	59	M					67	0					707	682	1744	1.8
11	67	F	ICA	ICA	M	C	47	97	69	74	22	23	680	762	2185	2.1
12	34	F					60	89	100		40		185	176	1956	1.7
13	49	F											1063	870		
14	56	M					100	100					274	138	1403	1.5
15	59	F						91		80		11	1085	277	930	0.9
16	78	F												15		
17	50	F					63	89					3926	4048	3133	3.9
18	81	F		ICA		M	71	100	53	72	18	28	272	630	471	0.5
19	78	F	ICA	ICA	C	M			2	36	2	36		261		
20	56	M					0	61					553	651	1977	2.2
21	60	M					0	97					459	1381	588	0.5
22	83	M												8		
23	71	F	ICA	ICA	C	C	99	100	72	74	27	26	2013	1508	948	0.9
24	75	M					65	45							2608	2.9
25	72	M		ICA		C	100	92		16		76	1007	863	785	0.8
26	62	M	CCA	ICA	C	C	96	95		13		82	822	1320	522	0.6
27	77	M	ICA		S		90	100	40		50		395	659	686	0.7
28	72	F					58	0					839	578	2004	2.2
29	12	F					0	0							222	0.5
30	66	F					64	0					1117	926	2126	1.9
31	72	M					52	94						3385	886	0.9
32	69	F	CCA		C		100	86	80		20		620	507	1442	2.9
33	56	M					75	100					44	78	391	0.6
34	69	F														
35	43	F						96						1244	4266	4.6
36	70	F	ICA	ICA	C	C			80	100	80	100				
37	55	M	ICA	ICA	M		95	95	83	77	12	18	183	26	387	0.4
38	77	M						100					1234	1174	699	0.7
39	81	F					84	100					1306	0	305	0.3
40	45	M														
41	66	M	ICA		M		100	100	80		20				604	0.6
42	77	M					87								885	0.8
43	58	F					70	73					245	186	392	0.7
44	37	M											1458	1471		
45	71	M	ICA		M		88	90	80		8		91	93	4630	4.7

Table 1 (continued)

Patient	Age	Sex	Location of the plaque		Composition of the plaque		Stenosis according to VASIM (%)		Stenosis according to the operator (%)		Absolute difference (%)		Plaque volume (mm^3)		Time (s)	
			Left	Right	Left	Right	Left	Right	Left	Right	Left	Right	Left	Right	Total	Per slice
46	73	M	ICA		C		99	90	28		71			393	498	0.5
47	55	M		ICA		U	72	100		42		58	655	565	404	0.4
48	57	M	ICA		M		81	100	60		21		412	92	553	0.6
49	47	F					79	0					816	215	231	0.3
50	77	F					66	81					2088	343	3375	3.5
51	64	M	ICA	ICA	U	M			44	84	44	84		956		
52	57	F	ICA		M		0	30	100		100				1206	1.3
53	73	M		ICA			100	61		50		11	4288	543	3911	4.1
54	54	M					74	68					1072	906	3339	3.3
55	47	M	ICA	ICA	C	C	0	100	38	63	38	37		143	338	0.4
56	48	F					87	60							2237	2.6
57	76	M					0	63					269	835	1510	1.8
58	75	M	ICA		M		63	85	80		17		1953	2404	2314	2.3
59	80	F	ICA	ICA	C	C	100	100	72	73	28	27	3296	3917	1807	2.2

Sex: *M* male, *F* female

Location of the plaque: *ICA* internal carotid artery, *ECA* external carotid artery, *CCA* common carotid artery

Composition of the plaque: *M* mixed plaque, *C* calcified lesion, *U* ulcerated lesion, *S* soft lesion, *Irr* irregular plaques

Table 2 Summary statistics for the stenosis metrics

		Mean	SD
Stenosis	**Manual**	65%	22 %
	Automatic	74 %	33 %
	Absolute Difference	33%	29%

Table 3 Data on the number of detected carotid arteries, classified by stenosis level

	< 50% stenosis	≥ 50% stenosis
Manual	11	32
Automatic	19	75

Table 4 Confusion matrix for stenosis over 50%

		Manual	
		Positive	**Negative**
VASIM	**Positive**	25	6
	Negative	5	2

The presented research adopted a more extensive study population (N = 59). The study population enclosed both healthy and diseased patients. The presence of healthy patients addresses the importance of early diagnosis as a preventive measure. Moreover, the control group enabled for the software adaptation to low stenosis values, allowing analysis among patients with greater differentiation of atherosclerotic lesions. However, higher stenosis levels presented a higher divergence.

In our study, the carotid areas were measured as the perpendicular cross-sections of the lumen to the carotid vessel path. We believe that this gives a more specific indicator than the diameter measured on an individual slice, which is the clinical routine method in the manual analysis. However, this complicates the comparison of the methods, and can partially explain the difference, which is reported in this paper, for manually and automatically calculated stenosis. Other possible reasons are as follows: (i) different locations used for the minimum area and diameter measurements; (ii) the pre-processing of the data before the manual analysis [filtering by radiology workstations and manual improvement performed by an operator (e.g., for partial-volume effect)]; (iii) different measuring vectors used for manual and automatic measurements of the artery diameter.

The algorithm presented in this manuscript is used to assess the severity of atherosclerosis in the CCA and ICA cervical segments, i.e., from the carotid bifurcation until the carotid canal. The anatomical relationship of the ICA to the lateral mass of the atlas (C-1) (the location where ICA is closest to bone tissue) was assessed by Hoh et al.

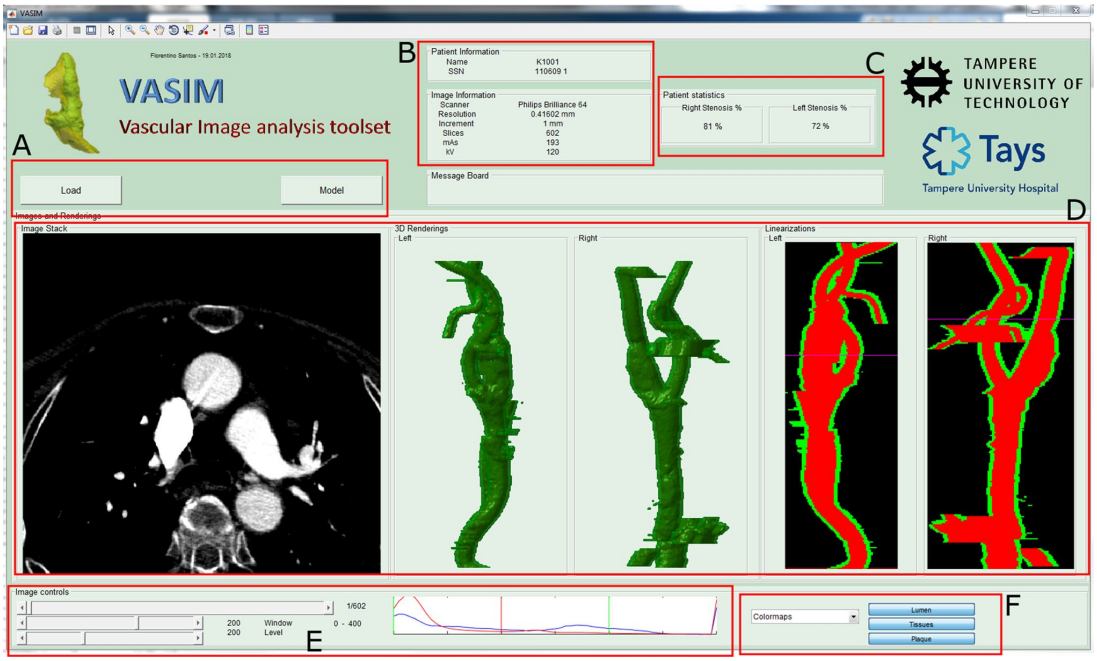

Fig. 5 VASIM interface (example of Patient 3). **a** VASIM controls. **b** Patient's information. **c** Stenosis level. **d** Patient stack, renderings, and linearizations. **e** Histogram-based window and level controls. **f** Overlay masks' control

[17]. The group studied 100 head-and-neck CT scans. The shortest distance between the ICA and lateral mass of C-1 was 3.5 mm (SD 1.5 mm) and 3.9 mm (SD 1.6 mm) for the left and the right ICA, respectively. The minimum size of a single pixel in CTA scans analyzed by VASIM ranged from 0.4 to 0.7 mm, and maximum slice thickness ranged from 1.0 to 1.25 mm. As the scans were analyzed on pixel-basis, no difficulties in distinguishing vertebrae or foreign objects from the calcified plaque were encountered.

The new metrics reflecting flow dynamics [18–20] and plaque stability may be material for both asymptomatic and symptomatic atherosclerosis patients. To date, all studies in carotid artery flow dynamics area have mainly been performed with magnetic resonance [20–24]. Although the presented study focuses only on CT techniques, the findings may well have a bearing on MRI modalities. In the future, the methods used for analysis of CT images with VASIM could be applied to MRI interpretation, subsequently to adapting the software for that modality. One final possible future application of VASIM is the ability to perform patient follow-up, both for disease progression and after-surgery assessment.

The presented methodology could be expanded to automatically classify plaque composition using attenuation discrimination or texture analysis. The composition is usually analyzed by evaluating the plaques' components, such as the lipid pool or the calcified cap. Information on the morphology of the plaque is a factor that modulates urgency for surgical treatment. As MRI techniques provide greater soft tissue contrast, adapting VASIM algorithm to this modality would produce better results in the analysis of the plaque composition. Furthermore, because of the more and more pervasive role of artificial intelligence in medicine, VASIM can have a more prominent role in the fusion of image processing and machine learning in medical imaging reporting [25–29]. Such developments can lead not only to full automation of the analysis but also increasing the feasibility of applying such methods in low resource settings, where specialists are less frequent or even inexistent. The fusion of VASIM with artificial intelligence also has potential in the growing field of telemedicine, where it can be applied as a preliminary assessment before operator evaluation.

The presented study was characterized by the following limitations: dependence on the prior stage of the analysis; possible ICA misclassification in case of its total occlusion; manual assessment performed by only one operator; improvable analysis time; unsatisfactory algorithm specificity.

The main study limitation was dependence on the prior stage of the analysis, e.g., if the carotid model was not properly acquired, accurate vascular wall segmentation was impossible.

Moreover, in the case of total stenosis, the correct determination of the segment distant to the occlusion was challenging. It sometimes resulted in misclassification of the ECA's distant section as the ICA.

Another study limitation was the fact, that the manual stenosis degree evaluation was performed by only one trained radiologist, hindering any inter- and intra-operator variability assessment. In addition, we did not have an actual gold standard to check which measurement (manual vs. automatic) was the most accurate. Therefore, the only feasible comparison was between the manually and automatically measured degrees of stenosis.

The average analysis time of 1381 s per patient (1.62 s per slice) remains still long. The carotid path tracking was the most time-consuming step of the analysis. Moreover, the presented methodology involved saving intermediate results, which was critical to the time efficiency. Designing a more efficient algorithm architecture and coding it in a more efficient programming language is crucial. Nevertheless, usually, the radiological analysis of images is not performed in real-time, allowing the VASIM to be run beforehand.

The VASIM algorithm was somehow oversensitive. Although the algorithm sensitivity was 83%, its specificity was only 25%. A possible explanation of the oversensitivity could be the VASIM's tendency to force the segmentation of full arteries. This might cause occluded arteries to be neglected, or misclassification of fibrosis-calcification plaque tissues as the lumen. Notwithstanding these limitations, the overall VASIM accuracy was 71%.

Despite its limitations, the study certainly adds to the rapidly expanding field of automatic CTA image analysis. The aim of the study, i.e., creating a software tool that could be used for carotid arteries automated analysis, with an emphasis on atherosclerosis, was mostly met.

The present research enhanced our previous efforts and produced higher success rates, both in carotid tree 3D volume detection and segmentation (73% vs. 83%) [9]. Besides, this updated version of VASIM was able to detect single carotid arteries, without the need to detect arteries bilaterally [9]. The software was tested in challenging datasets with different tissues and anomalous structures (e.g., plaques, intima-media thickening, and lipid pools) produced by different CT equipment and imaging parameters. Despite improving these areas, there is a need for further development to ensure robustness for use in patients with a wide range of artifacts, clinical and imaging setups, atherosclerotic burden, and anatomy.

Conclusions

The authors designed and presented the VASIM, a tool for detection, segmentation, and analysis of atherosclerosis in the CCA and the cervical segment of the ICA. The VASIM is the first comprehensive, fully-automated, and user-independent tool for carotid arteries CTA images analysis.

The VASIM achieved a performance of 83%. The average processing time was 1381 s per patient. The accuracy, sensitivity, and specificity values were 71%, 83%, and 25%, respectively.

The findings from this study contribute in several ways to the field of methods for arterial assessment and provide a basis for the further development of automated atherosclerosis diagnosis and plaque analysis with CTA.

Acknowledgements The authors would like to thank Raija Paalavuo RN, Anna-Kaisa Parkkila MD, and Ullamari Hakulinen Lic.Sc., Med. Phys. for their help with patient recruitment and management.

Author contributions All authors declare they have contributed to this article. FLCS was responsible for defining the study objectives and design, data collection, development of the image processing and segmentation algorithms, analysis of the data, and statistical analysis. MK was responsible for data collection from the patients files information and stenosis manual calculation. FLCS wrote the manuscript and the co-authors MK, MT, JS, HE, and MP reviewed, commented, and improved the text.

Funding FLCS was supported by the CIMO Foundation (Centre for International Mobility; KM-12-8107), Tampere University Hospital, and an iBioMEP doctoral scholarship. MP was supported by the Finnish Cultural Foundation (Central Fund, Grant No. 160735) and by the Academy of Finland (decision number 307967). The project was also partly supported by the Competitive State Research Financing of the Expert Responsibility Area of Tampere University Hospital (Grant No. R07210/ 9K115).

Compliance with ethical standards

Conflict of interest The authors declare that they have no conflict of interest.

Ethical approval All procedures performed in studies involving human participants were in accordance with the ethical standards of the institutional and/or national research committee and with the 1964 Helsinki declaration and its later amendments or comparable ethical standards. This research was approved by the Ethics Committee of the Pirkanmaa Hospital District (decision number R07210).

Informed consent Informed consent was obtained from all individual participants included in the study.

References

1. Beevers DG (2005) The atlas of heart disease and stroke. J Hum Hypertens 19(6):505–505
2. Strong K, Mathers C, Bonita R (2007) Preventing stroke: saving lives around the world. Lancet Neurol 6(2):182–187
3. Lusis AJ (2000) Atherosclerosis. Nature 407:233
4. Enterline DS, Kapoor G (2006) A practical approach to CT angiography of the neck and brain. Tech Vasc Interv Radiol 9(4):192–204

5. Vukadinovic D, van Walsum T, Manniesing R, Rozie S, Hameeteman R, de Weert TT, van der Lugt A, Niessen WJ (2010) Segmentation of the outer vessel wall of the common carotid artery in CTA. IEEE Trans Med Imaging 29(1):65–76
6. dos Santos FL, Joutsen A, Terada M, Salenius J, Eskola H (2014) A semi-automatic segmentation method for the structural analysis of carotid atherosclerotic plaques by computed tomography angiography. J Atheroscler Thromb 21(9):930–940
7. Gates L, Indes J (2014) Evaluation and treatment of carotid artery stenosis. In: Gates L, Indes J (eds) Carotid artery disease—from bench to bedside and beyond. IntechOpen, London
8. Markiewicz T, Dziekiewicz M, Maruszyński M, Bogusławska-Walecka R, Kozłowski W (2014) Recognition of atherosclerotic plaques and their extended dimensioning with computerized tomography angiography imaging. Int J Appl Math Comput Sci 24(1):33–47
9. Dos Santos FL, Joutsen A, Paci M, Salenius J, Eskola H (2016) Automatic detection of carotid arteries in computed tomography angiography: a proof of concept protocol. Int J Cardiovasc Imaging 32(8):1299–1310
10. de Weert TT, de Monye C, Meijering E, Booij R, Niessen WJ, Dippel DW, van der Lugt A (2008) Assessment of atherosclerotic carotid plaque volume with multidetector computed tomography angiography. Int J Cardiovasc Imaging 24(7):751–759
11. Ferguson GG, Eliasziw M, Barr HW, Clagett GP, Barnes RW, Wallace MC, Taylor DW, Haynes RB, Finan JW, Hachinski VC et al (1999) The North American symptomatic carotid endarterectomy trial: surgical results in 1415 patients. Stroke 30(9):1751–1758
12. Dos Santos FLC, Joutsen A, Salenius J, Eskola H (2014) Fusion of edge enhancing algorithms for atherosclerotic carotid wall contour detection in computed tomography angiography. Comput Cardiol 41:925–928
13. Lee TC, Kashyap RL, Chu CN (1994) Building skeleton models via 3-D medial surface axis thinning algorithms. CVGIP: Gr Models Image Process 56(6):462–478
14. Otsu N (1979) A threshold selection method from gray-level histograms. IEEE Trans Syst Man Cybern 9(1):62–66
15. Aboyans V, Ricco JB, Bartelink MEL, Bjorck M, Brodmann M, Cohnert T, Collet JP, Czerny M, De Carlo M, Debus S et al (2018) Editor's Choice—2017 ESC guidelines on the diagnosis and treatment of peripheral arterial diseases, in collaboration with the European Society for vascular surgery (ESVS). Eur J Vasc Endovasc Surg 55(3):305–368
16. Santos F, Joutsen A, Salenius J, Eskola H (2011) Carotid artery atherosclerosis plaque analysis using ct and histology. In: Computational vision and medical image processing VIPIMAGE 2011—III ECCOMAS thematic conference on computational vision and medical image processing, Olhao, Algarve, Portugal, 12–14 October, 2011, CRS Press, Boca Raton pp 1–5
17. Hoh DJ, Maya M, Jung A, Ponrartana S, Lauryssen CL (2008) Anatomical relationship of the internal carotid artery to C-1: clinical implications for screw fixation of the atlas. J Neurosurg Spine 8(4):335–340
18. Zarins CK, Giddens DP, Bharadvaj BK, Sottiurai VS, Mabon RF, Glagov S (1983) Carotid bifurcation atherosclerosis. Quantitative correlation of plaque localization with flow velocity profiles and wall shear stress. Circ Res 53(4):502–514
19. Kwak HS, Yang HJ, Hwang SB, Chung GH (2017) Carotid wall imaging with routine brain MRI to facilitate early detection of carotid plaque and intraplaque hemorrhage. J Stroke 19(1):107–108
20. van Hoof RHM, Voo SA, Sluimer JC, Wijnen NJA, Hermeling E, Schreuder F, Truijman MTB, Cleutjens JPM, Daemen M, Daemen JH et al (2017) Vessel wall and adventitial DCE-MRI parameters demonstrate similar correlations with carotid plaque microvasculature on histology. J Magn Reson Imaging 46(4):1053–1059
21. Randoux B, Marro B, Koskas F, Duyme M, Sahel M, Zouaoui A, Marsault C (2001) Carotid artery stenosis: prospective comparison of CT, three-dimensional gadolinium-enhanced MR, and conventional angiography. Radiology 220(1):179–185
22. Jodas DS, Pereira AS, JM RST (2016) Lumen segmentation in magnetic resonance images of the carotid artery. Comput Biol Med 79:233–242
23. Augst AD, Ariff B, Mc GTSA, Xu XY, Hughes AD (2007) Analysis of complex flow and the relationship between blood pressure, wall shear stress, and intima-media thickness in the human carotid artery. Am J Physiol Heart Circ Physiol 293(2):H1031–H1037
24. Cheng DC, Billich C, Liu SH, Brunner H, Qiu YC, Shen YL, Brambs HJ, Schmidt-Trucksass A, Schutz UH (2011) Automatic detection of the carotid artery boundary on cross-sectional MR image sequences using a circle model guided dynamic programming. Biomed Eng Online 10(1):26
25. Acharya UR, Sree SV, Mookiah MR, Saba L, Gao H, Mallarini G, Suri JS (2013) Computed tomography carotid wall plaque characterization using a combination of discrete wavelet transform and texture features: a pilot study. Proc Inst Mech Eng H 227(6):643–654
26. Ambale-Venkatesh B, Yang X, Wu Colin O, Liu K, Hundley WG, McClelland R, Gomes Antoinette S, Folsom Aaron R, Shea S, Guallar E et al (2017) Cardiovascular event prediction by machine learning. Circ Res 121(9):1092–1101
27. Menchón-Lara R-M, Sancho-Gómez J-L (2015) Fully automatic segmentation of ultrasound common carotid artery images based on machine learning. Neurocomputing 151:161–167
28. Menchón-Lara R-M, Sancho-Gómez J-L, Bueno-Crespo A (2016) Early-stage atherosclerosis detection using deep learning over carotid ultrasound images. Appl Soft Comput 49:616–628
29. Nikan S, Gwadry-Sridhar F, Bauer M (2016) Machine learning application to predict the risk of coronary artery atherosclerosis. In: 2016 International conference on computational science and computational intelligence (CSCI): 15–17 Dec. 2016, pp 34–39

Tampereen teknillinen yliopisto
PL 527
33101 Tampere

Tampere University of Technology
P.O.B. 527
FI-33101 Tampere, Finland

ISBN 978-952-15-4196-4
ISSN 1459-2045